UNIVERSITY OF CALIFORNIA
RIVERSIDE

Mechanisms of Division Plane Establishment and Maintenance During Plant Cell Division

A Dissertation submitted in partial satisfaction
of the requirements for the degree of

Doctor of Philosophy

in

Biochemistry and Molecular Biology

by

Pablo Martinez

June 2019

Dissertation Committee:
Dr. Carolyn Rasmussen, Chairperson
Dr. Meng Chen
Dr. Julia Bailey-Serres

The Dissertation of Pablo Martinez is approved:

Committee Chairperson

University of California, Riverside

ACKNOWLEDGEMENTS

In accordance with graduate program guidelines, Chapter 2, in full, is a reprint of a published article in The Plant Cell (www.theplantcell.org): Martinez P, Allsman LA, Brakke KA, Hoyt C, Hayes J, Liang H, Neher W, Rui Y, Roberts AM, Moradifam A, et al (2018) Predicting Division Planes of Three-Dimensional Cells by Soap-Film Minimization. Plant Cell 30: 2255–2266 DOI: 10.1105/tpc.18.00401, Copyright American Society of Plant Biologists. Chapter 3, in full, is a reprint of a published article in Proceedings of the National Academy of Sciences of the United States of America (www.pnas.org): Martinez P, Luo A, Sylvester A, Rasmussen CG (2017) Proper division plane orientation and mitotic progression together allow normal growth of maize. Proc Natl Acad Sci 114: 2759–2764 (DOI: 10.1073/pnas.1619252114). This article is licensed under an Open Access (CC BY-NC-ND) license. To view a copy of this license, visit https://creativecommons.org/licenses/by-nc-nd/4.0/.

Initial Research Evaluation Committee:

Carolyn G. Rasmussen

Daniel R. Gallie

Julia Bailey-Serres

Kathryn DeFea

Qualifying Exam Committee:

Carolyn G. Rasmussen

Paul B. Larsen

Patricia S. Springer

Thomas A. Eulgem

Meng Chen

Dissertation Committee:

Carolyn G. Rasmussen

Meng Chen

Julia Bailey-Serres

Funding:

- Ford Foundation Dissertation Year Fellowship
- NSF 1505848, Division Plane Orientation in Plant Cells
- NSF 1716972, Division plane orientation in plant cells.

AUTHOR CONTRIBUTIONS

CHAPTER 1

Pablo Martinez wrote chapter with comments and edits from Carolyn G. Rasmussen.

CHAPTER 2

Pablo Martinez and Carolyn G. Rasmussen designed research; Pablo Martinez and Carolyn G. Rasmussen performed research; Anding Luo, Anne Sylvester, and Carolyn G. Rasmussen contributed new reagents/analytic tools; Pablo Martinez and Carolyn G. Rasmussen created the figures; Anding Luo produced the TAN1-YFP construct and sequenced the upstream regulatory region of the TAN1 gene to ensure normal regulatory functions and produced the CFP-TUB construct; Pablo Martinez and Carolyn G. Rasmussen analyzed data; and Pablo Martinez and Carolyn G. Rasmussen wrote the manuscript with comments from all authors.

CHAPTER 3

Pablo Martinez, Lindy A. Allsman, Wesley Neher, Hong Liang, Yue Rui, Allyson M Roberts, Christopher Hoyt, and Carolyn G. Rasmussen performed experiments. Jordan Hayes and Christopher Hoyt contributed new methods and tools. Amir Moradifam identified Surface Evolver as a method for soap-film approximations. Kenneth A. Brakke developed Surface Evolver and contributed new methods and tools. Allyson M. Roberts and Bob Goldstein generated and provided *C. elegans* time-lapse images. Yue Rui and Charles T. Anderson provided *Arabidopsis* time-lapse images. Carolyn G. Rasmussen supervised experiments. Pablo Martinez assembled figures. Pablo Martinez and Carolyn G. Rasmussen wrote the article with comments from all authors.

CHAPTER 4

Carolyn G. Rasmussen, Ram Dixit, Seán E. O'Leary, Kenneth A. Brakke provided equipment, reagents and experimental guidance. Pablo Martinez performed *in vitro* experiments with Rachappa Balkunde offering assistance on microtubule co-sedimentation. Pablo Martinez, Christopher Hoyt, Jocelyne Aranda, Sukhmani Sidhu capture images used for modeling. Pablo Martinez and Marschal Bellinger performed live cell time-lapse presented in chapter. Carolyn G. Rasmussen and Ram Dixit supervised experiments. Pablo Martinez analyzed data, made figures and wrote the chapter with comments and edits from Carolyn Rasmussen.

CHAPTER 5

Lab of Dr. Bing Yang created CRISPR-CAS9 gRNA plasmids targeting TAN1 and TAN2, transformed construct into maize callus, and regenerated transgenic plants. Pablo Martinez assembled figures and wrote chapter with comments and edits from Carolyn G. Rasmussen.

ABSTRACT OF THE DISSERTATION

Mechanisms of Division Plane Establishment and Maintenance During Plant Cell Division

by

Pablo Martinez

Doctor of Philosophy, Graduate Program in Biochemistry and Molecular Biology
University of California, Riverside, June 2019
Dr. Carolyn G. Rasmussen, Chairperson

Proper development of a tissue or organism occurs through the growth, division, and differentiation of individual cells. The plane in which these divisions occur can control many developmental processes and changes to this division plane can alter growth and development. Specification of the division site may also depend of factors such as mechanical tissue stress, individual cell shape, and cytoskeletal dynamics. The maize *tangled1* (*tan1*) mutant displays shorter overall growth, delayed mitotic timing, and altered cell patterning. TAN1-YFP localizes to the cortical division site throughout mitosis as well as mitotic microtubule structures. Altered cell shapes in the *tan1* mutant make it difficult to assess the accuracy of the symmetric divisions. A computational approach was taken to determine symmetric division planes by modeling cell shapes as soap-films. This model quantitatively determined that symmetric division planes can be accurately determined by minimization of soap-film surface areas and highlighted cases

where a cell deviates from the geometrically determined optimal plane. When applied to *tan1* mutant cells we see that cells on average have slightly misplaced future division sites compared to wild-type, however these differences are due to the abundant proportion of altered cell shapes in the mutant. A live-cell imaging approach was taken to better characterize the *tan1* mutant phenotype in later stages of mitosis and we determined that 37% of symmetric divisions in maize epidermal leaf cells were misplaced during telophase according to the initial placement of the division site. Mitotic progression was also delayed particularly during metaphase and telophase. Recombinantly expressed HIS-TAN1 was tested for its ability to bind to microtubules using a microtubule co-sedimentation assay. We determined that HIS-TAN1 can bind to *in vitro* taxol stabilized microtubules with an affinity similar to other microtubule associated proteins. Addition of HIS-TAN1 to dynamically unstable microtubules displayed a microtubule crosslinking activity. Microtubules that encounter each other at low angles (below 35 °) are likely to be "zippered" together whereas microtubules that encounter each other at large crossover angles (above 55 °) are linked at a single crossover point leading to a "pulling" effect. These data indicate that TAN1 is a microtubule bundling protein which helps generate proper cell shape by maintaining division site information throughout mitosis.

TABLE OF CONTENTS

LIST OF FIGURES

LIST OF TABLES

LIST OF SUPPLEMENTAL VIDEOS

CHAPTER 1: Division plane orientation in plant cells

Abstract

Given the presence of the plant cell wall, plant cells must undergo oriented cell divisions and controlled cell expansion for the proper development of tissues and the plant body. The orientation of a cell's division plane results from the coordination between individual cell shapes, cytoskeletal processes, tissue level geometry, mechanical stress and developmental programs. This vast network of inputs ultimately shapes and divides individual cells in a tissue to ensure proper growth and development. Computational models, mutant analysis, and developmental approaches have been used to understand this process at the protein, cell, tissue, and organismal level.

Introduction

Cell geometry, tissue level stress and the importance of division plane orientation

Multicellular organisms are composed of many cell types with specialized functions and tend to form cells with specific shapes. Given the diversity in cells shapes, general rules for division of individual cells have been proposed over a century ago. Hofmeister (Hofmeister, 1863) postulated that the cell wall which separates two daughter cells forms perpendicular to the main axis of growth of the dividing cell while Sachs (Sachs, 1878) suggested that new cell walls are inserted perpendicular to existing cell walls. Errera (Errera, 1888) compared the division patterns of cells as mimicking the behavior of soap-films so that the new cell wall occupies a confirmation with minimal surface energy. Analysis of cell shapes in two and three dimensions has been used to accurately

determine division plane positioning within an individual cell across many organisms (Besson and Dumais, 2011; Martinez et al., 2017; Moukhtar et al., 2019). Computational approaches have also revealed mechanisms for orienting microtubules prior to the start of mitosis for proper division plane orientation which coincide with *in vivo* results. (Chakrabortty et al., 2018a; Chakrabortty et al., 2018b). Interpretations of the rules proposed long ago therefore have helped guide the field. However, we still lack the ability to fully explain the generation of complex observed division patterns across many tissues and species (Dupuy et al., 2010; Besson and Dumais, 2011; Martinez et al., 2018; Moukhtar et al., 2019).

While a cell's shape may dictate the exact position of a division or types of divisions which are available to it, these cells exist in an interconnected network to form a tissue which might influence division plane positioning. Tissue level influence on division plane positioning however does not necessarily need to occur at a large scale. Evidence for local fine tuning can be seen in cases where cells avoid the formation of a four-way junction by displacing their divisions away from an existing cell wall or neighboring dividing cell even if this act increases the surface energy of the future division (Flanders et al., 1990; Martinez et al., 2018). Local disruption of mechanics by physical means such as wounding also can alter the division planes of locally surrounding cells which begin as a response by actin and the cortical microtubule array (Lintilhac and Vesecky, 1981; Hush and Overall, 1992, Panteris et al., 2004). Mechanical modeling of *Arabidopsis* sepals revealed that proper organ development was determined to be generated from local developmental variations which are temporally averaged (Hong et al., 2016). Local rules

considered through space and time may therefore provide the building blocks for complex tissue level patterning observed in nature (Long and Boudaoud, 2019). Conversely, studying the local topography of a tissue may suggest what types of cues dominate division plane positioning at the tissue level. The readout of large-scale tissue level developmental changes can be manifested as a change in the cell shape populations and division planes within the tissue. In the developing maize leaf, growth is asymmetric with much more tissue expansion occurring in the base to tip orientation compared to across its width. Developmentally young maize leaf shapes which are more isotropic and undergo tip-ward growth display high proportions of longitudinal divisions while at the same time display the presence of geometrically favorable cell shapes for that type of division (Martinez et al., 2018). As the leaf develops and tissue geometry is more anisotropic, less of these longitudinal cell shapes and divisions are observed in the tissue (Martinez et al., 2018). Observable cell shape and division plane outcomes can therefore act as a readout of tissue level alterations through development. This phenomenon has been observed in the cortical microtubule arrays which appear to align along areas of maximal tension across the *Arabidopsis* sepal (Hervieux et al., 2016). An individual cell with a specific cell shape therefore may execute a distinct type of division given its positional context within the tissue.

Tissue stress can also alter division planes without the need for altered cell shapes as shown by division patterns in the *Arabidopsis* meristem across areas of maximal tension (Louveaux and Hamant, 2013). These tissue level influences therefore can shape the cytoskeleton across supra-cellular levels which can cause changes which persist long after a stimulus is removed (Jacques et al., 2013). Alignment of microtubules into

specific organized arrays do not always have to lead to changes in division plane positioning. In non-dividing *Arabidopsis* hypocotyl cell, the cytoskeleton is aligned in a transverse orientation to expand tip-ward under dark grown conditions compared to light growth conditions (Le et al., 2005). Responses like these are not limited to mechanical stimuli, as shown by the longitudinal rearrangement of cortical microtubules in response to blue light (Lindeboom et al., 2013).

Two conflicting ideas on the importance of proper plane division plane maintenance exist. One suggests that the organismal body is specified at the tissue level and cells fill in the space, while a cell centric theory suggest that cell division patterning is important for tissue level development and growth. A study in *Drosophila* suggested that the orientation of division planes in wing development are not required for proper organ shape (Zhou et al., 2019). In the *Drosophila mud* mutant, spindle orientations which dictate the division plane are distributed randomly instead of lining up preferentially across the proximal-distal axis (Zhou et al., 2019). Given the altered division planes present, cellular rearrangements within the tissue still are able to compensate and lead to proper wing shape formation (Zhou et al., 2019). In maize, altered orientations of division planes in the *tan1* mutant do not change leaf organ shape however overall organismal size is diminished (Smith et al., 1996). Partial restoration of mitotic delays and division plane defects can lead to proper organ shape and size (Martinez et al., 2017). These results suggest that organ shape is not necessarily only dictated by the proper orientation of division planes and that compensatory mechanisms both at the cell and tissue level are in place to ensure proper organ shape and development.

The role of the cytoskeleton during plant cell division

After the culmination of all available inputs, a cell will eventually divide into two daughter cells unless an endoreduplication program is initiated (Joubès and Chevalier, 2000). During interphase, microtubule arrays form a complex arrangement at the cortex of the cell (Dixit, 2004). The microtubule cytoskeleton responds to and controls many important cellular processes such as providing a large part of the machinery necessary for executing a division. In preparation for a future division, the microtubules of the cytoskeleton are aligned at the cortex parallel to the division axis. During this time a ring-shaped structure, the pre-prophase band (PPB) is formed from microtubules, microfilaments, and other microtubule associated proteins at the cortex of the cell, usually encircling the nucleus (Van Damme, 2009). The location of the plasma membrane just subtending PPB is now termed the cortical division zone and predicts or marks the site of future cell wall insertion (Smertenko et al., 2017; Rasmussen and Bellinger, 2018). The PPB is disassembled after prophase; however some PPB co-localized proteins are retained and help keep the spatial information of the cortical division zone throughout mitosis (Walker et al., 2007; Xu et al., 2008; Lipka et al., 2014; Buschmann et al., 2015; Li et al., 2017; Martinez et al., 2017). Mutants which lack the ability to form complete PPBs often display division plane defects (Azimzadeh et al., 2008; Wright et al., 2009; Komis et al., 2017). The metaphase spindle may be organized and possibly oriented by the PPB leading to the generation of robust division patterns (Ambrose and Cyr, 2008; Schaefer et al., 2017). In animal systems spindle centering is a critical factor in maintaining division plane orientation but generally plant cells are able to correct for this in later stages of mitosis (Rasmussen et al., 2013; Schaefer et al., 2017;

Zhou et al., 2019). Interestingly the spindles in plants are constructed without the use of centrioles, so the use of acentrosomal microtubule organizing centers and γ-tubulin becomes important for their structural organization (Brown and Lemmon, 2011). During cytokinesis, the phragmoplast is formed from microtubules, microfilaments and endomembrane and helps build and guide the cell plate while centrifugally expanding outwards toward the division site until cell plane fusion and completion of the division (Smertenko et al., 2018). The phragmoplast is able to move across a cell volume by the action of continuous new polymerization of microtubules nucleated from pre-existing microtubules. Phragmoplast microtubules are organized into an antiparallel array with a small overlap region at the leading edge of the structure while microtubules at the lagging edge of the phragmoplast are undergoing catastrophe, leading to a net movement forward (Murata et al., 2013; Smertenko, 2018). While it is clear in a general sense how the phragmoplast is able to traverse through a cell; how it is able to find the correct division site is still a mystery. At the leading edge of the phragmoplast, peripheral microtubules along with actin may provide some guiding cues as they contact the division site slightly ahead of the main body of the phragmoplast (Wu and Bezanilla, 2014). PHRAGMOPLAST ORIENTING KINESIN 2 (POK2) protein which localizes to the cortical division site (Lipka et al., 2014) and MICROTUBULE ASSOCIATED PROTEIN 65-3 (MAP65-3) which aids in bundling phragmoplast microtubules (Ho et al., 2012) interact suggesting that this protein complex may also be used to connect phragmoplast microtubules to the cortical division site as the phragmoplast approaches the cortex. These models however do not completely explain how a phragmoplast can be

guided in divisions which may be tens of microns in length or how a phragmoplast may be curved to generate an asymmetric division.

Mutant analysis of cortical division site localized proteins such as in the maize *tangled1* (*tan1)* mutant reveal it as a necessary factor for division site maintenance due to the widespread division plane defects observed (Smith et al., 1996; Martinez et al., 2017). *phragmoplast orienting kinesin 1,2* (*pok1 pok2)* double mutants in *Arabidopsis* display a similar cell patterning defect; additionally, POK1 protein is an interactor of TAN1 (Müller et al., 2006; Rasmussen et al., 2011; Lipka et al., 2014). These results suggest that interactions between cortical division site localized proteins, microtubule binding proteins and the phragmoplast microtubules are important factors in maintaining phragmoplast guidance.

Research Outline

In this thesis work I aim to understand the influence of cell shape on division plane establishment, and the function of a protein TAN1 in maintaining division site information throughout mitosis until cell plate fusion. In Chapter 2 we describe a computational modeling approach which was employed to determine the contribution of three dimensional cell shape in positioning a cell's division plane by comparing *in vivo* divisions to *in silico* predictions. The universality of this model to predict divisions was shown using several maize cell types, *Arabidopsis* guard cells, as well as *C. elegans* embryo cells. In Chapter 3 we describe the maize *tangled1* (*tan1)* mutant which displays altered cell patterning in all tissue types observed as well as stunted growth. TAN1 protein is a microtubule binding protein which colocalizes with the PPB and is retained at the division site throughout mitosis. In Chapter 4, I assess the consequence of altered cell

shapes in the *tan1* mutant using our previous modeling approach as well as describe the function of TAN1 as a microtubule binding protein *in vitro* and *in vivo*. In Chapter 5, I will summarize the research presented and suggest future work and experiments.

References

Ambrose JC, Cyr R (2008) Mitotic spindle organization by the preprophase band. Mol Plant **1**: 950–60

Azimzadeh J, Nacry P, Christodoulidou A, Drevensek S, Camilleri C, Amiour N, Parcy F, Pastuglia M, Bouchez D (2008) Arabidopsis TONNEAU1 proteins are essential for preprophase band formation and interact with centrin. Plant Cell **20**: 2146–59

Besson S, Dumais J (2011) Universal rule for the symmetric division of plant cells. Proc Natl Acad Sci **108**: 6294–6299

Brown RC, Lemmon BE (2011) Dividing without centrioles: innovative plant microtubule organizing centres organize mitotic spindles in bryophytes, the earliest extant lineages of land plants. AoB PLANTS. doi: 10.1093/aobpla/plr028

Buschmann H, Dols J, Kopischke S, Pena EJ, Andrade-Navarro MA, Heinlein M, Szymanski DB, Zachgo S, Doonan JH, Lloyd CW (2015) Arabidopsis KCBP interacts with AIR9 but stays in the cortical division zone throughout mitosis via its MyTH4-FERM domain. J Cell Sci **128**: 2033–2046

Chakrabortty B, Blilou I, Scheres B, Mulder BM (2018a) A computational framework for cortical microtubule dynamics in realistically shaped plant cells. PLOS Comput Biol **14**: e1005959

Chakrabortty B, Willemsen V, de Zeeuw T, Liao C-Y, Weijers D, Mulder B, Scheres B (2018b) A Plausible Microtubule-Based Mechanism for Cell Division Orientation in Plant Embryogenesis. Curr Biol **28**: 3031-3043.e2

Dixit R (2004) The Cortical Microtubule Array: From Dynamics to Organization. PLANT CELL ONLINE **16**: 2546–2552

Dupuy L, Mackenzie J, Haseloff J (2010) Coordination of plant cell division and expansion in a simple morphogenetic system. Proc Natl Acad Sci **107**: 2711–2716

Errera L (1888) Über Zellformen und Siefenblasen. Bot Cent 395–399

Flanders DJ, Rawlins DJ, Shaw PJ, Lloyd CW (1990) Nucleus-associated microtubules help determine the division plane of plant epidermal cells: avoidance of four-way junctions and the role of cell geometry. J Cell Biol **110**: 1111–1122

Hervieux N, Dumond M, Sapala A, Routier-Kierzkowska A-L, Kierzkowski D, Roeder AHK, Smith RS, Boudaoud A, Hamant O (2016) A Mechanical Feedback Restricts Sepal Growth and Shape in Arabidopsis. Curr Biol **26**: 1019–1028

Ho C-MK, Lee Y-RJ, Kiyama LD, Dinesh-Kumar SP, Liu B (2012) Arabidopsis Microtubule-Associated Protein MAP65-3 Cross-Links Antiparallel Microtubules toward Their Plus Ends in the Phragmoplast via Its Distinct C-Terminal Microtubule Binding Domain. Plant Cell **24**: 2071–2085

Hofmeister W (1863) Zusatze und Berichtigungen zu den 1851 veroffentlichen Untersuchungengen der Entwicklung hoherer Kryptogamen. Jahrbucher Wiss Bot 259–293

Hong L, Dumond M, Tsugawa S, Sapala A, Routier-Kierzkowska A-L, Zhou Y, Chen C, Kiss A, Zhu M, Hamant O, et al (2016) Variable Cell Growth Yields Reproducible Organ Development through Spatiotemporal Averaging. Dev Cell **38**: 15–32

Hush JM, Overall RL (1992) Re-orientation of cortical F-actin is not necessary for wound-induced microtubule re-orientation and cell polarity establishment. Protoplasma **169**: 97–106

Jacques E, Verbelen J-P, Vissenberg K (2013) Mechanical stress in Arabidopsis leaves orients microtubules in a 'continuous' supracellular pattern. BMC Plant Biol **13**: 163

Joubès J, Chevalier C (2000) Endoreduplication in higher plants. Plant Mol Biol **43**: 735–745

Komis G, Luptovčiak I, Ovečka M, Samakovli D, Šamajová O, \v Samaj J (2017) Katanin Effects on Dynamics of Cortical Microtubules and Mitotic Arrays in Arabidopsis thaliana Revealed by Advanced Live-Cell Imaging. Front Plant Sci **8**: 866

Le J, Vandenbussche F, De Cnodder T, Van Der Straeten D, Verbelen J-P (2005) Cell Elongation and Microtubule Behavior in the Arabidopsis Hypocotyl: Responses to Ethylene and Auxin. J Plant Growth Regul **24**: 166–178

Li H, Sun B, Sasabe M, Deng X, Machida Y, Lin H, Julie Lee Y-R, Liu B (2017) Arabidopsis MAP65-4 plays a role in phragmoplast microtubule organization and marks the cortical cell division site. New Phytol **215**: 187–201

Lindeboom JJ, Nakamura M, Hibbel A, Shundyak K, Gutierrez R, Ketelaar T, Emons AMC, Mulder BM, Kirik V, Ehrhardt DW (2013) A Mechanism for Reorientation of Cortical Microtubule Arrays Driven by Microtubule Severing. Science **342**: 1245533–1245533

Lintilhac PM, Vesecky TB (1981) Mechanical Stress and Cell Wall Orientation in Plants. II. The Application of Controlled Directional Stress to Growing Plants; with a Discussion on the Nature of the Wound Reaction. Am J Bot **68**: 1222

Lipka E, Gadeyne A, Stöckle D, Zimmermann S, De Jaeger G, Ehrhardt DW, Kirik V, Van Damme D, Müller S (2014) The Phragmoplast-Orienting Kinesin-12 Class Proteins Translate the Positional Information of the Preprophase Band to Establish the Cortical Division Zone in Arabidopsis thaliana. Plant Cell **26**: 2617–2632

Long Y, Boudaoud A (2019) Emergence of robust patterns from local rules during plant development. Curr Opin Plant Biol **47**: 127–137

Louveaux M, Hamant O (2013) The mechanics behind cell division. Curr Opin Plant Biol **16**: 774–779

Martinez P, Allsman LA, Brakke KA, Hoyt C, Hayes J, Liang H, Neher W, Rui Y, Roberts AM, Moradifam A, et al (2018) Predicting Division Planes of Three-Dimensional Cells by Soap-Film Minimization. Plant Cell **30**: 2255–2266

Martinez P, Luo A, Sylvester A, Rasmussen CG (2017) Proper division plane orientation and mitotic progression together allow normal growth of maize. Proc Natl Acad Sci **114**: 2759–2764

Moukhtar J, Trubuil A, Belcram K, Legland D, Khadir Z, Urbain A, Palauqui J-C, Andrey P (2019) Cell geometry determines symmetric and asymmetric division plane selection in Arabidopsis early embryos. PLOS Comput Biol **15**: e1006771

Müller S, Han S, Smith LG (2006) Two Kinesins Are Involved in the Spatial Control of Cytokinesis in Arabidopsis thaliana. Curr Biol **16**: 888–894

Murata T, Sano T, Sasabe M, Nonaka S, Higashiyama T, Hasezawa S, Machida Y, Hasebe M (2013) Mechanism of microtubule array expansion in the cytokinetic phragmoplast. Nat Commun. doi: 10.1038/ncomms2967

Panteris E, Apostolakos P, Quader H, Galatis B (2004) A cortical cytoplasmic ring predicts the division plane in vacuolated cells of Coleus: the role of actomyosin and microtubules in the establishment and function of the division site. New Phytol **163**: 271–286

Rasmussen CG, Bellinger M (2018) An overview of plant division-plane orientation. New Phytol

Rasmussen CG, Sun B, Smith LG (2011) Tangled localization at the cortical division site of plant cells occurs by several mechanisms. J Cell Sci **124**: 270–9

Rasmussen CG, Wright AJ, Müller S (2013) The role of the cytoskeleton and associated proteins in determination of the plant cell division plane. Plant J Cell Mol Biol **75**: 258–269

Sachs J (1878) Uber die Anordnung der Zellen in jungsten Pflanzentheilen. Arb Bot Inst Wurzburg 46–104

Schaefer E, Belcram K, Uyttewaal M, Duroc Y, Goussot M, Legland D, Laruelle E, de Tauzia-Moreau M-L, Pastuglia M, Bouchez D (2017) The preprophase band of microtubules controls the robustness of division orientation in plants. Science **356**: 186–189

Smertenko A (2018) Phragmoplast expansion: the four-stroke engine that powers plant cytokinesis. Curr Opin Plant Biol **46**: 130–137

Smertenko A, Assaad F, Baluška F, Bezanilla M, Buschmann H, Drakakaki G, Hauser M-T, Janson M, Mineyuki Y, Moore I, et al (2017) Plant Cytokinesis: Terminology for Structures and Processes. Trends Cell Biol **27**: 885–894

Smertenko A, Hewitt SL, Jacques CN, Kacprzyk R, Liu Y, Marcec MJ, Moyo L, Ogden A, Oung HM, Schmidt S, et al (2018) Phragmoplast microtubule dynamics – a game of zones. J Cell Sci **131**: jcs203331

Smith LG, Hake S, Sylvester AW (1996) The tangled-1 mutation alters cell division orientations throughout maize leaf development without altering leaf shape. Development **122**: 481–9

Van Damme D (2009) Division plane determination during plant somatic cytokinesis. Curr Opin Plant Biol **12**: 745–51

Walker KL, Müller S, Moss D, Ehrhardt DW, Smith LG (2007) Arabidopsis Tangled Identifies the Division Plane Throughout Mitosis and Cytokinesis. Curr Biol CB **17**: 1827–1836

Wright AJ, Gallagher K, Smith LG (2009) discordia1 and alternative discordia1 function redundantly at the cortical division site to promote preprophase band formation and orient division planes in maize. Plant Cell **21**: 234–47

Wu S-Z, Bezanilla M (2014) Myosin VIII associates with microtubule ends and together with actin plays a role in guiding plant cell division. eLife. doi: 10.7554/eLife.03498

Xu XM, Zhao Q, Rodrigo-Peiris T, Brkljacic J, He CS, Muller S, Meier I (2008) RanGAP1 is a continuous marker of the Arabidopsis cell division plane. Proc Natl Acad Sci **105**: 18637–18642

Zhou Z, Alégot H, Irvine KD (2019) Oriented Cell Divisions Are Not Required for Drosophila Wing Shape. Curr Biol **29**: 856-864.e3

CHAPTER 2: Predicting Division Planes of Three-Dimensional Cells by Soap-Film Minimization

Abstract

One key aspect of cell division in multicellular organisms is the orientation of the division plane. Proper division plane establishment contributes to normal plant body organization. To determine the importance of cell geometry in division plane orientation, we designed a three-dimensional probabilistic mathematical model to directly test the century-old hypothesis that cell divisions mimic soap-film minima. According to this hypothesis, daughter cells have equal volume and the division plane occurs where the surface area is at a minimum. We compared predicted division planes to a plant microtubule array that marks the division site, the preprophase band (PPB). PPB location typically matched one of the predicted divisions. Predicted divisions offset from the PPB occurred when a neighboring cell wall or PPB was directly adjacent to the predicted division site to avoid creating a potentially structurally unfavorable four-way junction. By comparing divisions of differently shaped plant cells (maize [*Zea mays*] epidermal cells and developing ligule cells and *Arabidopsis thaliana* guard cells) and animal cells (*Caenorhabditis elegans* embryonic cells) to divisions simulated *in silico*, we demonstrate the generality of this model to accurately predict *in vivo* division. This powerful model can be used to separate the contribution of geometry from mechanical stresses or developmental regulation in predicting division plane orientation.

Introduction

Cell division planes are dictated by geometric, mechanical, and polarity cues in plants, animals, bacteria, and fungi (Minc and Piel, 2012). A challenging problem in understanding division plane orientation lies in separating the effects of cell polarity or mechanical cues from the effects of cell shape-mediated cues. In plant and animal cells, the absence of external polarity or mechanical cues often leads to a division plane that bisects the long axis of the cell (Errera, 1888; Minc and Piel, 2012; Besson and Dumais, 2014). In zebrafish embryos, the placement of future divisions can be predicted by cell shapes (Xiong et al., 2014). In the late 1800s, biologists identified basic patterns of plant cell division. The plane of division is typically perpendicular to the primary growth axis of the tissue (Hofmeister, 1863). The new cell wall often forms at a 90 degree angle to the mother cell wall (Sachs, 1878). Plant cell divisions appear to mimic soap-films (which are made by dipping a wire frame into a soap solution), often dividing along the smallest local plane to minimize the surface area of the division (Errera, 1888; Besson and Dumais, 2014). Later, oversimplification from multiple planes to a single global minimum division plane significantly limited the ability to account for the observed variability in division plane orientation, leading biologists to ignore this problem for decades (Besson and Dumais, 2014).

Recently, researchers have used computational or mathematical approaches to understand division plane orientation in plant cells in two dimensions (Dupuy et al., 2010; Sahlin and Jönsson, 2010; Besson and Dumais, 2011). In several studies, empirically derived factors were added to account for the stochasticity of the observed division orientations (Dupuy et al., 2010; Besson and Dumais, 2011). The length difference between two predicted

divisions, with the addition of an empirically defined stochasticity factor, was sufficient to describe the relative proportions of population level divisions in cells from several plant species (Besson and Dumais, 2011). Other 2D approaches modeled different division plane preferences without using stochasticity in the Arabidopsis thaliana shoot apical meristem. The shortest path through the center of mass of the cell best fit the observations, although it incompletely captured *in vivo* size variability (Sahlin and Jönsson, 2010). A fitness function that combined length minima for new cell walls with daughter cells of equal areas accurately predicted division planes and functioned similarly to "modern" Errera predictions (Shapiro et al., 2015).

An interest in 3D modeling of cell division led to division plane analysis in the *Arabidopsis thaliana* embryo (Yoshida et al., 2014). The center of mass for each cell was used as a point to sample 2000 different planes to identify the lowest flat surface area. Some embryonic cells did not divide according to the shortest plane, but instead divided asymmetrically to produce unequal daughter cell volumes. Asymmetric divisions in the embryo were driven by the response to auxin and associated with alterations in both gene expression and differentiation. Mutants that do not respond to auxin lost division asymmetry in these cells (Yoshida et al., 2014). While this approach did not minimize surface areas locally or provide a probabilistic prediction of division plane orientation, it was successfully used to predict a potential global minimum in 3D.

Computational approaches have begun modeling the dynamics of interphase microtubule arrays using 3D shapes with a potential long-term application of predicting division plane orientation. Modeling microtubule properties such as directionality, interactions via cross-linking proteins or interactions with the cell wall, were sufficient to promote *in*

silico localization of microtubules to the cortex of a 3D simulated plant cell (Mirabet et al., 2018). The calculated microtubule array depended on cell shape cues but could also be modulated by external forces (Mirabet et al., 2018). Changing either microtubule dynamics or specific face or edge properties generated cortical microtubule arrays in realistically shaped cells (Chakrabortty et al., 2018a). Understanding how the cortical microtubule array may be oriented by cell shape and other parameters might help predict the orientation of the future division plane. This model of cortical microtubule arrays in Arabidopsis embryo cells was applied to generate cortical microtubule arrays aligned with division planes, but they were not compared with *in vivo* divisions (Chakrabortty et al., 2018b).

Accurate division plane prediction provides a mechanism to weigh relative contributions of multiple, potentially developmentally or mechanically regulated, drivers of plant growth. Here, we used a 3D mathematical modeling approach to generate multiple division-plane predictions for any cell. This 3D model explicitly tests the long-held hypothesis that plant cell divisions mimic soap-film minimum surfaces (Errera, 1888). This model depends only on the shape of the cell: Division predictions are performed by initiating soap-film-like, area-minimizing, descending gradients from starting planes designed to fully and evenly sample the volume of the cell. This geometry-based model identifies cases when plant cells divide according to their geometry and highlights when they do not. The location of preprophase band (PPBs), microtubule and microfilament structures that accurately predict the future division plane in typical land plant cells (PICKETT-HEAPS and NORTHCOTE, 1966; Camilleri, 2002; Van Damme et al., 2007; Martinez et al., 2017; Smertenko et al., 2017), most often closely match one class of the

predicted division planes. Discrepancies in PPB location compared with predicted divisions were sometimes due to PPB shifting in response to an adjacent cell wall. Finally, we demonstrate that the model provides accurate predictions for the location of the future division of diverse symmetrically dividing cells including maize (*Zea mays*) epidermal cells and developing ligule cells, *Arabidopsis* guard cells, and nematode (*Caenorhabditis elegans*) embryonic cells.

Results

We established a geometry-based model to generate local minimum (soap-film) predicted divisions for any cell shape using Surface Evolver (Brakke, 1992). First, confocal micrographs of maize cells with PPBs were taken with 0.2- or 0.4-μm-interval Z-stacks (Figures 2.1A-2.1C show a single Z-plane). The images were semiautomatically thresholded and their 3D surfaces were extracted using FIJI (Figure 2.1D see Methods). The surfaces were imported into Surface Evolver. The surfaces were smoothed using 30th degree spherical harmonics, a method that approximates the cell outline as a function of polar coordinate angles, analogous to Fourier transformation approximations of 2D shapes (Figures 2.1F, 2.1J, and 2.1K; Supplemental Figure 2.1; see Methods) (Givoli, 2004) and commonly used in 3D rendering (Shen et al., 2009). Next, mathematically predicted divisions were generated for each of the cells using a set of 241 starting planes that evenly sampled the entire cell volume (Methods). These starting planes were used to initiate a process known as gradient descent (Supplemental Movie 2.1). Gradient descent iteratively minimized the initial surface area until the lowest local surface area (soap-film minimum) was reached to divide the mother cell into two daughter cells of equal volume (Figure 2.1G).

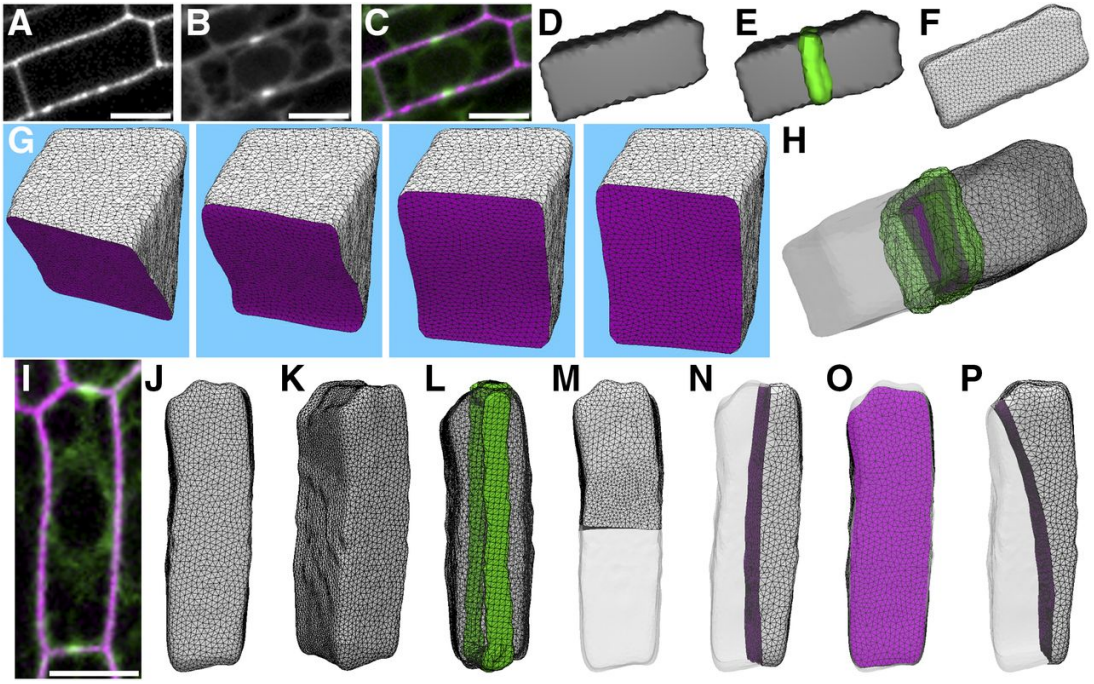

Figure 2.1: Division Plane Predictions and Their Comparison to *in Vivo* Divisions. A) Maize adaxial epidermal cell wall stained with propidium iodide. (B) Same cell expressing YFP-TUBULIN to identify the PPB. (C) Merced image of the cell wall (magenta) and PPB (green). (D) Reconstruction of the 3D surface. (E) The 3D surface overlayed with the 3D PPB. (F) Surface generated in Surface Evolver after 30th degree spherical harmonics. (G) An example of gradient descent identifying the soap-film local minimum from an initial starting position (left panel) to an anticlinal transverse division plane. (H) The PPB (green) colocalized with one of the final predicted divisions (magenta). (I) Maize leaf epidermal cell wall stained with propidium iodide (magenta) and expressing YFP-TUBULIN (green) with a longitudinally oriented PPB. (J) to (L) 3D cell surface of example shown in (I). (J) cell oriented as shown in (I). (K) Cell oriented to show surface along the z axis. (L) Cell surface with PPB (green). (M) to (P) Examples of each predicted division class generated by identification of local minimum surfaces. (M) Transverse division pane, the global minimum division surface. (N) Longitudinal division. (O) Periclinal division. (P) “other” division. Bars = 10 µm.

The local minima identified from 241 independent soap-film minimizations tended to coalesce on discrete locations within the cell. The final predicted surface areas of division planes were closely matched in size and location. Soap-film minimization of rectangular prism-shaped epidermal cells from two different maize leaf developmental stages generated between one and four local minima. Based on the location of the predicted division and its location within the cell relative to the tissue, these local minima were classified as transverse (Figure 2.1M), longitudinal (Figure 2.1N), periclinal (Figure 2.1O), and other (Figure 2.1P). The most common predicted division was a transverse, anticlinal division, which was predicted for all cells (*n* = 181), followed by periclinal divisions (98%, 178/181) and longitudinal anticlinal divisions (63%, 114/181). The majority of maize epidermal cells (78%, *n* = 141/181) displayed a PPB that closely spatially matched one of the predicted divisions. A small number of cells did not have any predicted division that matched the orientation of the PPB even broadly (2%, *n* = 4/181), while 20% (*n* = 36/181) had small spatial discrepancies, which are discussed in detail in two paragraphs.

For the majority of maize epidermal cells (78%, *n* = 141/181), the PPB closely spatially matched one of the predicted divisions. YFP-TUBULIN signal was used to reconstruct the PPB in 3D (Figures 2.1E and 2.1L). Next, the PPB was aligned with the predicted surface closest to the PPB (Figure 2.1H). To quantitatively assess PPB and predicted division overlap, we measured the distance in μm^2 between the midplane of the PPB and the cortical region of the predicted division. As the distance reaches 0, the predicted division more closely aligns with the PPB midplane. The average distance or offset between the PPB and the closest predicted division was $0.492 \pm 1.156\ \mu m^2$; mean

± sd, n = 141/177 (the four cells where the PPB and prediction had no overlap were not included; Figure 2.2J). These data indicate that the predicted division typically localized within the boundary of the PPB.

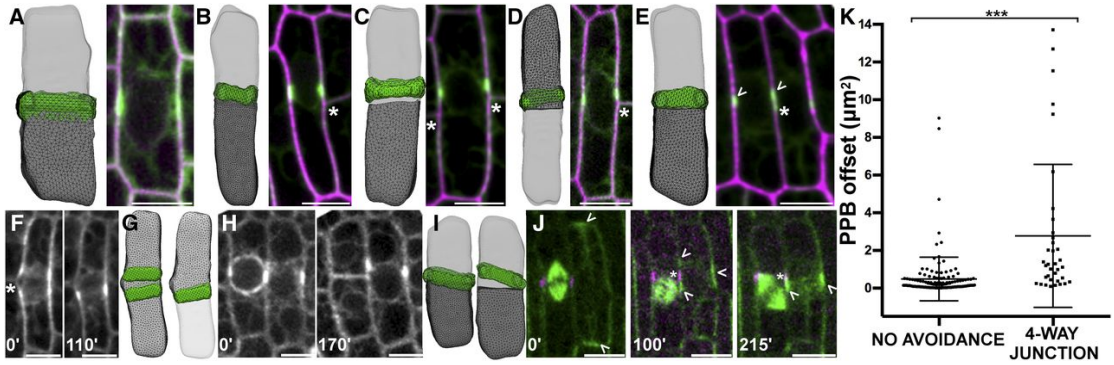
A
B
C
D
E
F
G
H
I
J
K
0'
110'
0'
170'
0'
100'
215'
***
PPB offset (µm²)
0
2
4
6
8
10
12
14
NO AVOIDANCE
4-WAY JUNCTION

Figure 2.2: Comparison between Predicted Divisions and Location of the PPB: Identification of Four-Way Junction Avoidance. (A) to (E) Best-fit predicted divisions overlaid with *in vivo* PPB location compared with *in vivo* maize epidermal cells expressing YFP-TUBULIN (green) and either expressing membrane marker PIP2-CFP ([A], [C], and [D]; magenta) or stained with propidium iodide to outline the cell wall ([B] and [E]; magenta). Neighboring cell wall or PPB indicated with an asterisk. (A) Cell with low PPB offset, 0.04 μm^2. (B) Cell where the predicted division and the PPB are slightly offset at 0.54 μm^2. (C) Example of cell with two neighboring cell walls and a high offset between the PPB and the predicted division (12.69 μm2). (D) Cell with neighboring cell wall with high PPB offset in one direction (13.72 μm^2). (E) Cell that has an offset PPB caused by a neighboring PPB (0.10 μm^2). PPB marked by arrowheads. (F) to (H) Time lapse of cells expressing YFP-TUBULIN where neighboring cells potentially influence PPB location. (F) Cell with a split PPB (left) that collapsed into one PPB before entering mitosis (time in minutes on the lower left). (G) Reconstruction of cell surface with both possible PPBs next to best fit predicted division to the PPB that was chosen (offset = 0.13 μm^2). (H) Cell (left) with a PPB that initiated mitosis next to a neighboring cell still in pre-prophase with an offset PPB. (I) Reconstruction of both cell surfaces with the best fit predicted division overlaid onto each respective PPB, offset for cell on left is 0.13 μm^2, while the offset for the cell on the right is 5.59 μm^2. (J) Time lapse of cell expressing CFP-TUBULIN (green) and TAN1-YFP, which labels the division site (magenta). The cell on the right had a longitudinal PPB that switched to a split transverse PPB without signal directly adjacent to the division site of the neighboring cell. (K) PPB offset (distance from the midplane of the PPB to the closest predicted division surface) was 0.49 ± 1.16 μm^2 sd (n = 136/177) for cells with PPBs without neighbor cell walls or PPBs near the predicted *in silico* division plane. Cells with predicted divisions that would form a four-way junction (due to an adjacent neighbor wall or PPB) had significantly higher offset between the predicted division and the PPB location (average 2.78 ± 3.79 μm^2 sd, n = 36/177, Mann-Whitney $P < 0.0001$). Bars = 10 μm

In a subset of the cells (~20%, n = 36/181), small but noticeable deviations between PPB location and predicted divisions were observed, likely due to neighboring cell influence. The PPB was visibly and significantly offset from the *in silico* predicted division plane to avoid creating a four-way junction with an already established adjacent cell wall next to the predicted division plane (offset = 2.778 ± 3.793 μm^2; mean ± sd; Figure 2.2K). PPBs adjacent to sites that influenced neighboring cells, including either an adjacent cell wall (Figures 2.2B to 2.2D; n = 34) or an adjacent PPB (Figure 2.2E; n = 2), were shifted from the mathematically optimal division plane on average five times further than PPBs without obvious neighboring cell influence. Avoidance of four-way junctions is a recognized feature of plant cells thought to increase structural stability (Flanders et al., 1990). In vacuolate cells, dense rings of cytoplasm, called phragmosomes, accumulate at the division site. Neither phragmosomes in vacuolate plant cells (Sinnott and Bloch, 1941) nor PPBs (Gunning et al., 1978) in adjacent cells overlap, but in this study, we demonstrated that cells with neighboring cell walls shift the PPB away from a soap-film minimum predicted division plane. It is not currently known how four-way-junction avoidance occurs.

We used time-lapse imaging to analyze PPB movement and avoidance in live cells, revealing the dynamic nature of PPBs and their interaction with neighboring cells. Dynamic PPB events such as avoidance of adjacent cell PPBs or cells were rare (n = 6, <1% of forming PPBs observed during time-lapse imaging), limiting the sample size. Time-lapse imaging revealed a PPB split into two microtubule accumulations across an adjacent cell wall (Figure 2.2F, time 0) that later coalesced into one location (Figures 2.2F and 2.2G, time 110'). Time-lapse images showed two nonoverlapping but adjacent

PPBs. One PPB closely matched the soap-film minimum, while the other had high offset that was maintained as one neighboring cell completed mitosis (Figures 2.2H and 2.2I). Finally, we observed a PPB shifting from longitudinal (Figure 2.2J, time 0') to transverse, while splitting into two segments to avoid an adjacent cell division site indicated by TANGLED1 (TAN1)-YFP localization (Figure 2.2J, time 100'), then finally coalescing on one position (Figure 2.2J, time 215'). These data demonstrated that PPB shifting occurred *in vivo* when some interaction with an adjacent cell promoted PPB offset.

Longitudinal and transverse symmetric divisions were observed *in vivo* during two distinct maize leaf developmental stages (described below) via PPB location. Cells with longitudinal PPBs (n = 36) had significantly higher proportions of predicted longitudinal divisions after soap-film minimization (predicted longitudinal division frequency = 5.05% ± 3.61; mean ± sd) compared with cells with transverse PPBs (n = 145, predicted longitudinal division frequency 1.85% ± 2.60; mean ± sd, Mann-Whitney $P < 0.0001$; Figure 2.3A). To determine whether there was a characteristic feature of longitudinally or transversely dividing cell shapes, we used a metric independent of cell size called the eigenvalue ratio (described in Methods) to evaluate shape features. As the eigenvalue ratio approaches one, the cell appears less prolate, or more cube shaped. Longitudinally dividing cells had significantly lower eigenvalue ratios than transversely dividing cells (Figure 2.3B). Cells with lower eigenvalue ratios were more cube-shaped, while cells with higher ratios tended to be long and thin, i.e., more prolate (Figure 2.3C). Calculated eigenvalue ratios for each cell were plotted as a function of percent transverse predicted divisions: As cells become more cube-shaped, less transverse division predictions and

more longitudinal and periclinal divisions were predicted (Figure 2.3D). Although a direct comparison cannot be made, this result is similar to the elegant cell-shape-based division predictions made for 2D cells in which the probability of the predicted division was more equally shared if the division lengths were similar in size (Besson and Dumais, 2011). This result suggests that cells that will divide longitudinally tend to be less prolate or more cube-shaped.

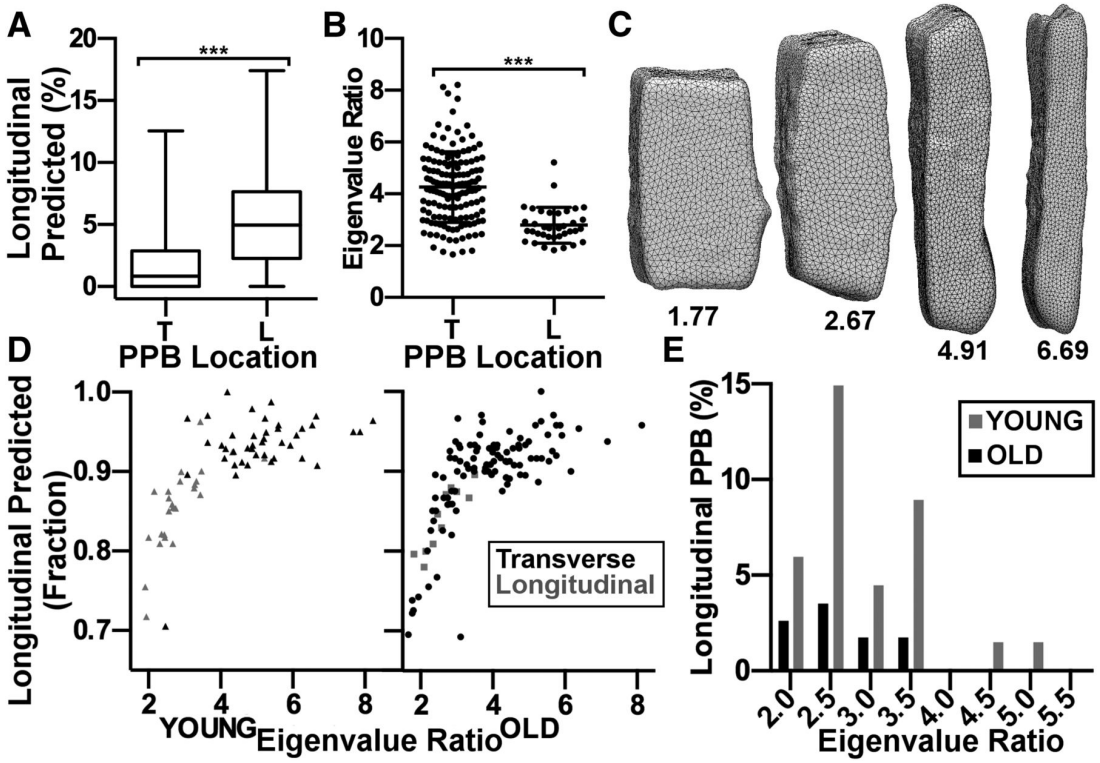

Figure 2.3: Cells with Longitudinal PPBs Were More Cube Shaped and Had More Longitudinal Predictions *in Silico* Than Cells with Transverse PPBs. (A) Box and whisker plot of the percent longitudinal divisions predicted between transverse or longitudinal PPBs. Cells with longitudinal PPBs (n = 36) predicted significantly (mean = 5.1% ± 3.6 sd) more longitudinal divisions than those with transverse PPBs (n = 145, mean = 1.9% ± 2.6 sd, Mann-Whitney, $P < 0.0001$). **(B)** Dot plot of eigenvalue ratios of cells with a transverse (n = 145, mean = 4.3 ± 1.4 sd) or longitudinal PPB (n = 36, mean = 2.8 ± 0.7 sd). Cells with transverse PPBs had higher eigenvalue ratios (Mann-Whitney, $P < 0.0001$). **(C)** Cells with varying eigenvalue ratios. Larger eigenvalue ratios reflected longer and thinner cells (cells not displayed to scale). **(D)** Eigenvalue ratio versus fraction transverse division predicted. Cells with higher eigenvalue ratios ended up having higher proportions of transverse divisions predicted, a relationship with significant correlation ($P < 0.0001$ for both leaves; young leaf Pearson $R^2 = 0.46$; old leaf Pearson $R^2 = 0.49$). **(E)** Histogram of cells that display longitudinal PPB binned by eigenvalue ratio for both maize leaf data sets. The young leaf sample had higher proportions of cells with longitudinal PPBs across all eigenvalue ratios.

Two different developmental stages of the maize leaf were analyzed. As the maize leaf develops, the proportions of symmetric division classes change. Developmentally younger leaf epidermal cells have higher proportions of longitudinal divisions that decrease in frequency as the leaf grows (Sylvester, 2000). Adaxial epidermal cells from a single developmentally younger leaf (leaf L14, leaf height 15.58 mm from a 28-d-old maize plant) and a single developmentally older leaf (L9 or L10, ligule height ~2 mm from a 28-d-old maize plant) were analyzed. Cells with transverse anticlinal divisions were the most common in both maize epidermal cell developmental stages. While the younger leaf had 37% longitudinal and 63% transverse PPBs (n = 67), the developmentally older leaf had ~10% longitudinal and ~90% transverse PPBs (n = 114; Table 2.1). In both samples, cells with longitudinal PPBs had more predicted longitudinal divisions *in silico* (previous paragraph and Figure 2.3B). However, *in vivo* longitudinal divisions occurred significantly more often than predicted by Surface Evolver soap-film minimization (2.6% total longitudinal predictions in young leaf cells versus 37% *in vivo* and 2.3% longitudinal predictions in old leaf cells versus 10%; Table 2.1), indicating that soap-film minimization under predicts longitudinal divisions *in vivo*. The young leaf cells had proportionally more longitudinal PPBs across all eigenvalue ratios, potentially suggesting developmentally regulated shifts in the probabilities of division plane positioning in response to shape (Figure 2.3E). Our data indicate that *in vivo* population-level division plane orientations of cells with the same shape do not occur with the same frequencies in different developmental contexts nor can they be fully predicted using a geometry-based soap-film model. This suggests that developmental or mechanical forces also play a role orienting the final division plane (Figure 2.3D).

	Tissue	Old leaf	Young leaf	Ligule region[a]
	n (Cells)	114	67	34
***In Vivo* (%)**	Transverse	90.3	62.7	N/A
	Longitudinal	9.7	37.3	N/A
	Periclinal	0	0	100
***In Silico* (%) (Mean ± sd)**	Transverse	89.1 ± 6.1	90.5 ± 6.0	17.5 ± 17.4
	Longitudinal	2.6 ± 3.0	2.3 ± 3.3	11.9 ± 17.5
	Periclinal	8.0 ± 3.9	6.8 ± 3.4	68.8 ± 22.9
	Other	0.3 ± 1.9	0.5 ± 2.5	1.8 ± 5.2

[a] Only perclinally dividing cells in the developing ligule were chosen for analysis.

Table 2.1: *In Vivo* Division Class Percents and *in Silico* Division Predictions

Periclinal divisions occur rarely in the maize epidermis (Sharman, 1942; Poethig, 1984), although they accounted for ~7% of *in silico* predicted divisions. We therefore examined cells from the developing ligule, an epidermally derived structure found in grass leaves, which contains a high proportion of periclinally dividing cells during specific developmental stages (Becraft et al., 1990; Sylvester et al., 1990). Micrographs of cells undergoing periclinal divisions within the developing ligule were selected for soap-film minimization predictions using Surface Evolver (n = 34 cells; Figure 2.4A). While transverse divisions represented the global minimum division and also the most predicted division plane in leaf epidermal cells, the predicted periclinal divisions represented the global minimum in 97% of the cells in the developing ligule (n = 33/34). Cells in this tissue expanded in the Z-plane before the periclinal division was initiated (Figures 2.4B and 2.4C), suggesting that directional cell expansion rather than division plane

specification may the driving force behind the eventual periclinal division in the developing ligule.

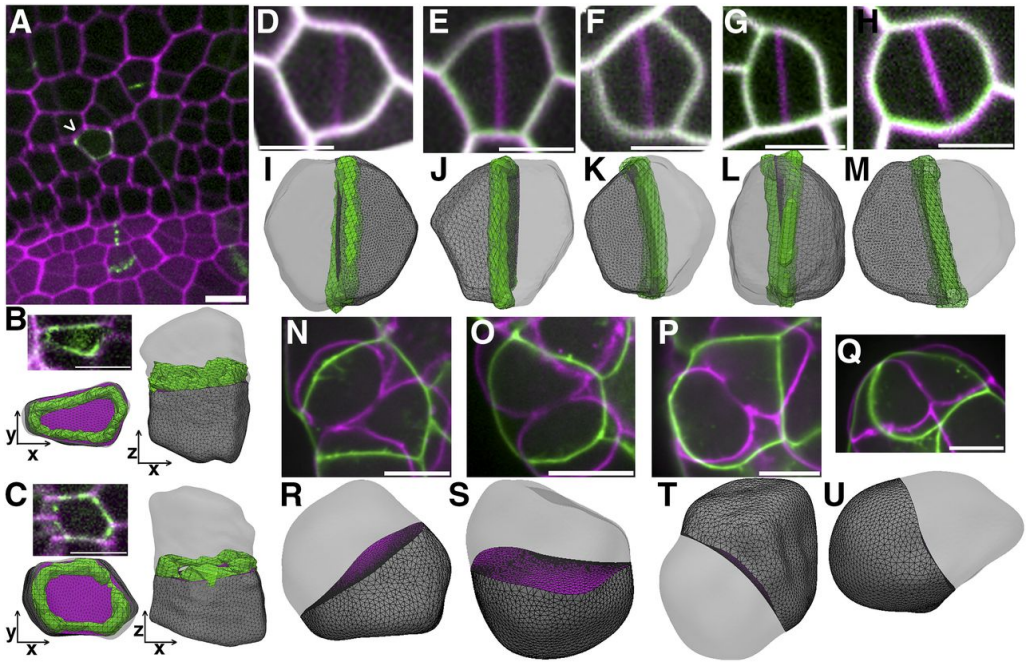

Figure 2.4: Division Plane Prediction in Plant and Animal Cells. (A) Micrograph of maize developing ligule. Cell walls are stained with PI (magenta) and division sites are marked by TAN1-YFP (green). Arrowhead indicates periclinal division. (B) and (C) Micrographs of cells from the developing ligule expressing PIP2-CFP (magenta) for identification of cell outlines and TAN1-YFP (green) for division site location. The PPB and 3D reconstruction in both the XY (bottom left) and XZ plane (right) show the periclinal division plane. (D) to (H) Time-lapse imaging of *Arabidopsis* guard cell division. The time point before the start of cytokinesis (green) overlaid with the completed division location (magenta). (I) to (M) 3D reconstruction of cells in (D) to (H) with the corresponding predicted division plane by Surface Evolver. The final division site was the newly formed cell wall (green) for comparison to the predicted division. (N) to (Q) Predicted division planes of cells in early gastrulation-stage *C. elegans* embryos. The cell shape prior to furrow ingression (green) was used for division predictions and overlaid with the dividing cell (magenta). (R) to (U) 3D reconstruction of cells in (N) to (Q) along with the corresponding predicted division plane by Surface Evolver. Bars = 10 μm.

To test the generality of this method of division plane prediction, soap-film minima were predicted for *Arabidopsis* symmetric guard mother cells and *C. elegans* embryonic cells. Time-lapse imaging of dividing guard mother cells in the Arabidopsis epidermis was used to identify local minimum surface division planes. The final division plane was used as a marker for the division site to calculate offset between the predicted and *in vivo* divisions. Guard mother cell divisions that generated a guard cell pair were accurately represented by a soap film minimum predictions, with an average offset of 1.04 μm^2 ± 0.95 sd (Figures 2.4D to 2.4M), similar to offset observed in maize epidermal cells. Interestingly, the predicted division that matched the future *in vivo* location typically did not occupy the global minimum (n = 7/8) but instead trended toward an anticlinal division plane with a larger surface area (Figures 2.4D to 2.4M). The cell that did not match this trend only had one anticlinal division class predicted, which was closely matched by the *in vivo* division. The eigenvalue ratio of these cells on average was 1.5 ± 0.3 sd, similar to (or even lower than) longitudinally dividing maize epidermal cells. Whether developmentally regulated cell shape parameters or mechanical cues promote long anticlinal divisions instead of the global minimum division is still unknown, although there are correlations between PPB location and local thickening of cell walls during guard cell division (Zhao and Sack, 1999). The close correspondence between a predicted division plane and the *in vivo* division indicates that soap film minimization accurately predicts the possible placement of divisions in flat, cylindrically shaped cells in addition to rectangular prism-shaped cells.

Finally, *C. elegans* developing embryo cells were used to determine whether soap-film minima can be used to predict future division planes in symmetrically dividing animal

cells. Time-lapse imaging was performed on dividing cells, and the cell shape immediately before furrow ingression was used for soap film minimization. While we could not accurately measure division plane offset in these cells due to their dynamic shape changes, the surface for one of the predicted division classes was approximately in the same location as the final division plane for the *C. elegans* cells (Figures 2.4N to 2.4U). The division class that matched the location of the *in vivo* division accounted for 75.8% ± 28.4%; mean ± sd of the surfaces generated by gradient descent surface minimization. These cells divided along the shortest division plane: The predicted division that matched the *in vivo* division was typically the global minimum for the cell (n = 7/8). These data provide evidence that the geometric cues contributed by premitotic cell shapes can be used to predict the final division plane.

Discussion

Much progress has been made recently on geometry-based modeling in 2D (Dupuy et al., 2010; Sahlin and Jönsson, 2010; Besson and Dumais, 2011; Minc and Piel, 2012; Yoshida et al., 2014; Shapiro et al., 2015), but the transition to 3D plant cell modeling is essential to understanding the fundamental mechanisms of division plane orientation (Yoshida et al., 2014; Chakrabortty et al., 2018a). Symmetric division planes can be predicted by importing any 3D cell shape into Surface Evolver (Brakke, 1992) and performing iterative gradient descent from multiple starting planes to generate local soap-film minima. We demonstrated that this model generates reasonable predictions for three different maize cell types, as well as *Arabidopsis* and *C. elegans* cell divisions. Modeling each cell produced one or more local minima that when compared with *in vivo* division, typically produced a close match.

In addition to predicting multiple potential division plane orientations, the predicted divisions were directly compared with the location of the PPB, a structure known to predict the future division site (Rasmussen et al., 2013; Smertenko et al., 2017; Rasmussen and Bellinger, 2018). Several elegant studies have used time-lapse imaging to compare cells before and after division (Shapiro et al., 2015; Louveaux et al., 2016; von Wangenheim et al., 2016), but they did not directly assess PPB location in comparison to predicted divisions. This step allowed us to identify alterations in PPB location compared with the mathematically optimal division. When PPB locations shifted, it was due to coordination between cells to prevent the formation of a four-way-junction. Four-way junction avoidance is a well-known feature of plant cells (Sinnott and Bloch, 1941; Gunning et al., 1978; Flanders et al., 1990), but whether PPB localization was driven by

cell shape or interactions between cells had been unclear. Although previously suspected, we demonstrated that the PPB is offset from the soap-film predicted division site during four-way junction avoidance. The alterations in PPB location to avoid an adjacent wall or another PPB strongly suggest that a signal, whether chemical, mechanical, or both, is actively communicated between cells. Therefore, PPB dynamics and positioning are likely modulated by cell-cell interactions.

It is not surprising that the overall probabilities predicted by our model, which are generated via unbiased soap-film minimization by sampling the entire cell shape, do not describe *in vivo* proportions of division planes observed in maize epidermal cells, particularly the underprediction of longitudinal divisions and overprediction of periclinal divisions. During symmetric cell division, cells can divide with an increased probability along a longer plane rather than the shortest plane, such as when they are under mechanical stress (Lintilhac and Vesecky, 1984; Landrein and Hamant, 2013; Louveaux et al., 2016). In addition, the division axis of asymmetrically dividing cells can be influenced by the growth axis of the tissue and accompanying mechanical stresses (Bringmann and Bergmann, 2017). The cortical microtubule array interacts with and helps direct formation of the cell wall polymers such as cellulose, leading long-term to alterations in cell shape (Paredez et al., 2008; Wasteneys and Ambrose, 2009; Li et al., 2012; Zhu et al., 2015). Cortical microtubule arrays and sometimes subsequent division planes align parallel to plane of stress (Lintilhac and Vesecky, 1984; Lynch and Lintilhac, 1997; Asada, 2013; Landrein and Hamant, 2013) and after wounding or neighbor cell ablation (Sinnott and Bloch, 1941; Lintilhac and Vesecky, 1981; Hush and Overall, 1996; Heisler et al., 2010). In the vast majority of divisions we observed, cell

shape predicts all potential division planes, but local and tissue level stresses likely alter the final location, similar to microtubule array realignment after mechanical perturbation (Sampathkumar et al., 2014).

Epidermal cells divide almost exclusively along an anticlinal plane (Poethig, 1984; Galletti et al., 2016), even though soap-film predictions indicate that periclinal divisions are possible, suggesting that molecular or mechanical mechanisms inhibit periclinal divisions in the epidermis. Epidermal cell fate is specified early, and multiple gene regulatory networks uniquely define and specify the epidermal cell layer (Takada and Iida, 2014). In addition, the outer epidermal wall is both covered in cuticle and typically much thicker than interior walls in maize (Carpita et al., 2001) and tomato *Solanum lycopersicum*; (Kierzkowski et al., 2012). The epidermis is thought of as a load-bearing layer under tension: Its growth influences the overall size of the tissue (Marcotrigiano, 2010) and it acts as a shell resisting MPa turgor pressure (Beauzamy et al., 2015). Although epidermal cells do not typically divide along a periclinal plane, the mechanisms that normally prevent periclinal divisions are still unknown.

Periclinal divisions tend to occur during developmental processes such as formation of the vasculature, root, anther, and ligule (Lang Selker and Green, 1984; Poethig, 1984; Sylvester et al., 1990; Sakaguchi and Fukuda, 2008; Wachsman et al., 2015; Van Norman, 2016; Walbot and Egger, 2016). Therefore, we chose to analyze cells undergoing periclinal divisions during ligule development in maize. During ligule development, the periclinal division is the global minimum prediction, suggesting that these cells expanded before the division plane was established. The potential coordination between expansion and division plane orientation was previously revealed by analyzing

the Arabidopsis BREAKING ASYMMETRY IN THE STOMATAL LINEAGE (BASL) protein, which localizes to one edge of the cell to promote an asymmetric division during stomatal development. Interestingly, ectopic BASL expression promotes localized and directional expansion, a process dependent on Rho of Plants (ROP) monomeric GTPase function (Dong et al., 2009). Directional cell expansion may be a general mechanism to promote division plane orientation along a specific plane.

Our model has the potential to identify the correct placement of the symmetric division plane in cells with any shape. Defects in cortical microtubule organization or other defects can lead to aberrantly shaped daughter cells (Kirik et al., 2012; Pietra et al., 2013; Hashimoto, 2015; Komis et al., 2017; Martinez et al., 2017). In mutants with aberrant cell shapes, it can be difficult to determine whether the symmetric division plane specified by the PPB follows the geometry of the cell (Pietra et al., 2013; Lipka et al., 2014; Martinez et al., 2017; Mir et al., 2018). Potentially "misplaced" PPBs may arise either as a direct consequence of altered cell shape, the absence of protein function or indirectly through alterations in stress or tension on the cell (Willis et al., 2016). This model may be useful in uncoupling cell shape defects from division plane specification defects.

Cell shape changes during animal cell mitosis make it difficult to assess whether factors such as geometric cues before mitosis are used to orient the division or if the division plane is specified by other interactions as the cell is dividing (Minc and Piel, 2012). Surface area minimization (akin to soap bubbles) along with cell-cell contacts or adhesion have been used to describe the patterning and division plane orientation of animal cells (Goldstein, 1995; Hayashi and Carthew, 2004; Kafer et al., 2007; Gibson et al., 2011; Pierre et al., 2016). Landmark cues, including tricellular junctions during

mitotic rounding and contacts with the extracellular matrix, can be maintained to properly orient animal cell division planes (Théry et al., 2005; Bosveld et al., 2016). While geometric cues are only one of several factors promoting division plane orientation in plant and animal cells, soap-film surface area minimization accurately predicts *in vivo* symmetric division planes regardless of specific, and as yet still mostly unknown, mechanisms.

Materials and Methods

Imaging of Maize Tissue

Maize (*Zea mays*) leaves from a 28-d-old plant grown in standard greenhouse conditions with temperature setpoint at 32°C and expressing a live cell marker for microtubules were dissected to reveal symmetrically dividing cells (Sylvester et al., 1990). YFP-TUBULIN (YFP-variant Citrine fused to α-TUBULIN originally created by (Mohanty et al., 2009) was used to identify PPB location. Cell walls were stained with 0.1 mM propidium iodide (Fisher) or plasma membranes were identified using PIP2-1-CFP PLASMA MEMBRANE INTRINSIC PROTEIN2-1 fused to cerulean fluorescent protein (Mohanty et al., 2009). Two distinct leaf developmental stages were chosen for analysis, a young leaf, L14, and an older leaf, L9 or L10. Leaf 14 (total blade height = 15.6 mm) from a 28-d-old plant was dissected and the abaxial side was imaged near the leaf margin. Leaf 9 or 10 (ligule height ~2 mm) was imaged directly above the ligule near the margin. They were loaded into a Rose chamber for imaging on an inverted Nikon Ti stand with Yokogawa spinning disk and a motorized stage (ASI Piezo) run with Micromanager software (micromanager.org) and built by Solamere Technology. Solid-state lasers (Obis) and emission filters (Chroma Technology) used excitation, 445; emission, 480/40 (for CFP-TUBULIN and PIP2-1-CFP); excitation, 561; emission, 620/60 (for propidium iodide); and excitation, 514; emission, 540/30 (for YFP-TUBULIN and TAN1-YFP). Perfluorocarbon immersion liquid (RIAAA-678; Cargille) was used for 40× or 60× water-immersion objectives with 1.15 and 1.2 numerical aperture, respectively. Micrographs of transverse or longitudinal PPBs and cell wall or membranes in 0.2- or

0.4-μm Z-stack increments. The Z-stack images were opened in FIJI (http://fiji.sc/) and then cropped to one cell. The cell wall or plasma membrane outline was extracted using the following process in FIJI: segmentation, find maxima, and make binary (Schindelin et al., 2012). The PPB was extracted using trainable Weka segmentation in FIJI (Arganda-Carreras et al., 2017). After manual correction of cell wall outlines and PPB binary files, the cell wall and PPBs were converted into a 3D surface using Plug-in >> 3D Viewer with a resampling factor of 2. Then, the 3D surface was exported using the options File >> Export As >> STL (ASCII). Maize leaves were dissected to reveal preligule bands where periclinal divisions were frequent (L10 PLB height ~2 mm). Propidium iodide, PIP2-CFP, YFP-TUBULIN, and TAN1-YFP were used identify cell outlines and division site locations.

Time-Lapse Imaging of Maize Tissue

The adaxial side of the maize leaf blade near the margin was imaged at 21°C. For time-lapse experiments, leaf samples were mounted on a cover slip within a Rose chamber, surrounded by vacuum grease, and covered with another cover slip inside the chamber (Rasmussen, 2016). Maize epidermal cells expressing YFP-TUBULIN were imaged at 1-μm Z-intervals every 5 min for up to 6 h, and viability was assessed by presence of actively dividing cells. Cell outlines and PPBs were extracted using the YFP-TUBULIN signal and segmented using Weka Trainable Segmentation algorithm (Arganda-Carreras et al., 2017). Time-lapse imaging was also conducted using maize expressing TAN1-YFP and CFP-TUBULIN (CFP fused to β-TUBULIN) to identify mitotic stages.

Imaging of Arabidopsis Guard Cell Divisions

Confocal imaging of 4-d-old light-grown *Arabidopsis thaliana* seedlings of the Col-2 ecotype, expressing LTI6b-GFP (Cutler et al., 2000) was performed on a Zeiss Axio Observer microscope with a Yokogawa CSU-X1 spinning disk head and a 63× oil immersion objective, and a 488-nm excitation laser and a 525/50-nm emission filter. Z-stack time-lapse (stacklapse) imaging was performed as by (Peterson and Torii, 2012): A cotyledon was cut from a seedling and placed under a 0.5% agar pad in a NuncTM Lab-Tek coverglass chamber (Thermo Fisher; catalog no. 155360). The edge between the agar pad and the chamber was sealed by adding additional melted agar. The abaxial side of the cotyledon was oriented facing the cover glass. The chamber was mounted on the microscope stage with the lid on to minimize evaporation. Stacklapse images were collected with an interval of 0.5 h, up to 48 h, and a step size of 0.5 µm using 2% 488-nm laser power and 200-ms exposures.

Imaging of *Caenorhabditis elegans* Embryo Cell Divisions

C. elegans animals were cultured on Normal Growth Medium plates, fed *Escherichia coli* (OP50 strain), and grown at 20°C. The strain used is LP733 *cpIs131* [*Pmex-5*>mScarlet-I-C1::PH::*tbb-2*3′UTR lox N ttTi5605] II. Embryos were imaged using methods described by (Heppert et al., 2018). In brief, embryos were mounted at approximately the 24-cell stage and imaged on a spinning disk confocal microscope. mScarlet was excited using a 561-nm solid state laser with a 568LP emission filter set. Single-channel embryo samples were filmed at 30-s intervals. Images were cropped and rotated, and brightness and contrast were adjusted using FIJI.

Sample Size

Two individual maize leaves from two separate plants were carefully imaged to capture developmental "snapshots" of all the cell divisions within those tissues. The purpose of this experiment was to capture enough cell shape and division plane data to compare these two different developmental stages. Sixty-seven cells were captured from a developmentally younger leaf (leaf L14, leaf height 16 mm from a 28-d-old maize plant) and 114 cells were captured from a developmentally older leaf were used (L9 or L10, ligule height ~2 mm from a 28-d-old maize plant). For time-lapse imaging data, maize leaf epidermal cells from three individual maize plants were analyzed. Cells from maize ligule cells (n = 34) were captured from more than three individual ligules from three separate 28-d-old maize plants (L10 preligular band height ~2 mm). Arabidopsis guard cell divisions (n = 8) were captured from six individual cotyledons of different plants 4-d-old light-grown seedlings (Col-2 ecotype). *C. elegans* cell divisions (n = 8) were captured from two individual *C. elegans* embryos (at ~24-cell stage).

Surface Evolver

The 3D surfaces were imported into Surface Evolver. Spherical harmonics, a common 3D rendering technique used to generate a formula to describe complex cell shapes, were generated in Surface Evolver. Spherical harmonics approximate the cell outline as a function of spherical coordinate angles (Givoli, 2004). A Github workflow diagram for the Surface Evolver can be found at https://github.com/jdhayes/predictive_division/blob/master/doc/predictive_division.svg . Cells from maize leaf and ligule and Arabidopsis guard mother cells were smoothed

using 30th degree spherical harmonics. For modeled *C. elegans* embryo cells, 10th degree spherical harmonics were used to approximate the cell shapes. Spherical harmonics code in Surface Evolver https://github.com/jdhayes/predictive_division/blob/master/etc/SphericalHarmonics.cmd. Next, soap-film minimization was performed using 241 initial planes (https://raw.githubusercontent.com/jdhayes/predictive_division/master/etc/241points.txt) with normals uniformly distributed over a sphere (https://github.com/jdhayes/predictive_division/blob/master/etc/trailer.inc). Gradient descent, a computational method to generate a soap-film minimum surface, generated surface areas reflecting predicted divisions. Predicted divisions with similar surface areas were grouped together and categorized by their location in the cell relative to the tissue as transverse, longitudinal, periclinal, and other. To determine the PPB offset for each cell, the midplane of the PPB was aligned to the predicted division. The surface with the lowest offset from the *in vivo* location of the PPB was used in Figure 3 (code at https://github.com/jdhayes/predictive_division/blob/master/etc/PPB_OFFSET.txt). This measurement indicates how closely the PPB and the predicted division align. Cell shape was described using eigenvalue ratios. Eigenvalue ratios were calculated using the following steps. First, using Surface Evolver, three eigenvectors were calculated from the moment of inertia matrix for each cell. Second, the square root was taken of the largest eigenvector divided by the smallest eigenvector to generate the final eigenvalue ratio. Third, the square root was taken of the largest eigenvector divided by the smallest eigenvector to generate the final eigenvalue ratio (https://raw.githubusercontent.com/jdhayes/predictive_division/master/etc/inertia.txt).

Spherical Harmonics

The 3D surfaces generated from FIJI were imported into Surface Evolver. Since Surface Evolver input files need to be represented by a formula, surfaces were defined using 30th degree spherical harmonics. Increasing spherical harmonic degrees increased cell shape accuracy, but also increased computational time. The 30th degree spherical harmonics provided accurate cell shape while minimizing computational time. Using 10th degree spherical harmonics led to inaccurate cell shapes that lacked many of the distinguishing geometric features of cells (Supplemental Figures 2.1A to 2.1E), resulting in overprediction of transverse divisions for the cells (Supplemental Table 2.1). The 20th degree spherical harmonics did not properly model the corners and some features of the cell shape (Supplemental Figures 2.1A to 2.1E). The 30th degree spherical harmonics more accurately represented the original cell shape and allowed for efficient and complete calculation of gradient descent (Supplemental Figures 2.1A to 2.1E). Results for predicted divisions of different spherical harmonic degrees for each cell are summarized in Supplemental Table 2.1.

Surface Evolver

Surface Evolver code can be found on github. The workflow is outlined here: https://github.com/jdhayes/predictive_division/blob/master/doc/predictive_division.svg; 241 initial planes used for initiating gradient descent soap-film minimization (https://raw.githubusercontent.com/jdhayes/predictive_division/master/etc/241points.txt) with normals uniformly distributed over a sphere (https://github.com/jdhayes/predictive_division/blob/master/etc/trailer.inc). To determine

the PPB offset for each cell, the midplane of the PPB was aligned to the predicted division https://github.com/jdhayes/predictive_division/blob/master/etc/PPB_OFFSET.txt). Eigenvalue ratio (https://raw.githubusercontent.com/jdhayes/predictive_division/master/etc/inertia.txt).

Accession Numbers

Sequence data from this article can be found in the GenBank/EMBL libraries under accession numbers NM_001308507.1 (α-TUBULIN GRMZM2G153292), NM_001111554.2 (PLASMA MEMBRANE INTRINSIC PROTEIN2-1 GRMZM2G014914), AF305892.1 (TANGLED1), and NM_001348079.1 (β-TUBULIN, GRMZM2G164696).

Supplementary Figures and Tables

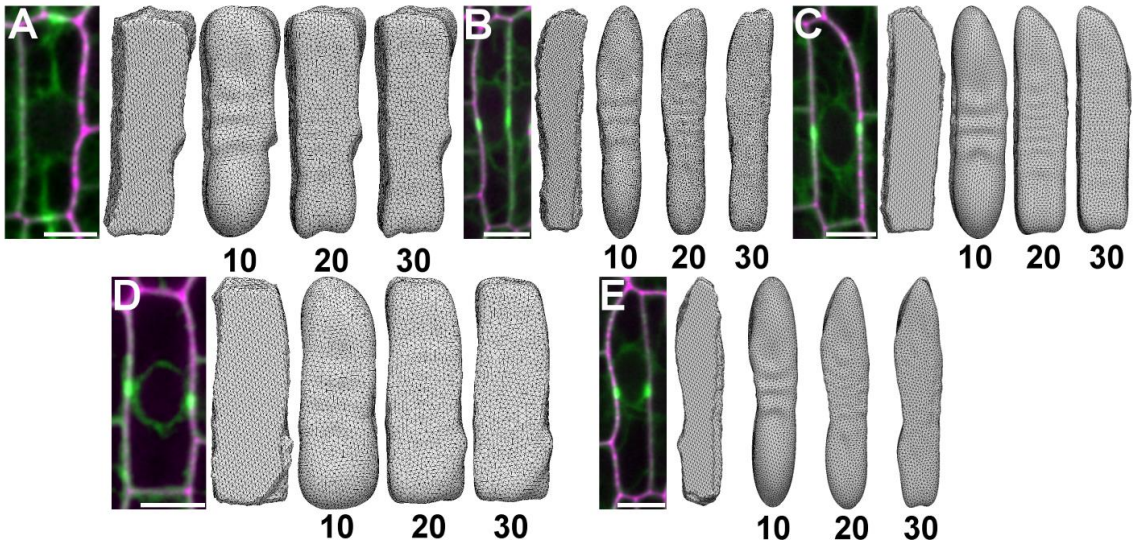

Supplemental Figure 2.1: Spherical Harmonics: different degrees. (A-E) Micrograph of maize epidermal cells expressing YFP-TUBULIN (green) and stained with propidium iodide (magenta). Left-most 3D representation is the original cell threshold without spherical harmonics applied. Proceeding from left to right 10th, 20th and 30th degree spherical harmonics (labeled below). Scale bar is 10μm.

Cell	Degree of SH	Transverse (%)	Longitudinal (%)	Periclinal (%)	Other (%)
Supplemental Figure 1A	10	92.1	0	7.9	0
	20	88.8	2.5	8.7	0
	30	86.7	3.7	9.6	0
Supplemental Figure 1B	10	100	0	0	0
	20	90	0	10	0
	30	91.3	0	8.6	0
Supplemental Figure 1C	10	100	0	0	0
	20	92	0	8	0
	30	91.2	0	8.7	0
Supplemental Figure 1D	10	100	0	0	0
	20	91.3	5	3.7	0
	30	90	4.2	5.8	0
Supplemental Figure 1E	10	100	0	0	0
	20	94.6	0	5.4	0
	30	92	0	8	0

Supplemental Table 2.1: Analysis of Cells at different Degrees of Spherical Harmonics. Gradient descent was performed using the 241 initial planes for each cell shown in Supplemental Figure 1. The type of predicted division generated with 10, 20 and 30 degrees Spherical Harmonics are shown.

Supplementary Movie

Supplemental Movie 2.1: Gradient Descent. A three-dimensional plant cell undergoing gradient descent, or soap-film minimization, starting from a specified plane and moving towards the local minimum division prediction. The cell mesh is outlined in grey, while the predicted division surface is shown in magenta. The final location of the division surface (in magenta) at the end of the movie represents the local minimum division plane.

References

Arganda-Carreras I, Kaynig V, Rueden C, Eliceiri KW, Schindelin J, Cardona A, Sebastian Seung H (2017) Trainable Weka Segmentation: a machine learning tool for microscopy pixel classification. Bioinformatics **33**: 2424–2426

Asada T (2013) Division of Shape-Standardized Tobacco Cells Reveals a Limit to the Occurrence of Single-Criterion-Based Selection of the Plane of Symmetric Division. Plant Cell Physiol **54**: 827–837

Beauzamy L, Louveaux M, Hamant O, Boudaoud A (2015) Mechanically, the Shoot Apical Meristem of Arabidopsis Behaves like a Shell Inflated by a Pressure of About 1 MPa. Front Plant Sci. doi: 10.3389/fpls.2015.01038

Becraft PW, Bongard-Pierce DK, Sylvester AW, Poethig RS, Freeling M (1990) The liguleless-1 gene acts tissue specifically in maize leaf development. Dev Biol **141**: 220–232

Besson S, Dumais J (2011) Universal rule for the symmetric division of plant cells. Proc Natl Acad Sci **108**: 6294–6299

Besson S, Dumais J (2014) Stochasticity in the symmetric division of plant cells: when the exceptions are the rule. Front Plant Sci. doi: 10.3389/fpls.2014.00538

Bosveld F, Markova O, Guirao B, Martin C, Wang Z, Pierre A, Balakireva M, Gaugue I, Ainslie A, Christophorou N, et al (2016) Epithelial tricellular junctions act as interphase cell shape sensors to orient mitosis. Nature **530**: 495–498

Brakke K (1992) The Surface Evolver. Exp Math **1**: 141–165

Bringmann M, Bergmann DC (2017) Tissue-wide Mechanical Forces Influence the Polarity of Stomatal Stem Cells in Arabidopsis. Curr Biol **27**: 877–883

Camilleri C (2002) The Arabidopsis TONNEAU2 Gene Encodes a Putative Novel Protein Phosphatase 2A Regulatory Subunit Essential for the Control of the Cortical Cytoskeleton. PLANT CELL ONLINE **14**: 833–845

Carpita NC, Defernez M, Findlay K, Wells B, Shoue DA, Catchpole G, Wilson RH, McCann MC (2001) Cell wall architecture of the elongating maize coleoptile. Plant Physiol **127**: 551–565

Chakrabortty B, Blilou I, Scheres B, Mulder BM (2018a) A computational framework for cortical microtubule dynamics in realistically shaped plant cells. PLOS Comput Biol **14**: e1005959

Chakrabortty B, Willemsen V, Zeeuw T de, Liao C-Y, Weijers D, Mulder B, Scheres B (2018b) A microtubule-based mechanism predicts cell division orientation in plant embryogenesis. bioRxiv. doi: 10.1101/270793

Cutler SR, Ehrhardt DW, Griffitts JS, Somerville CR (2000) Random GFP::cDNA fusions enable visualization of subcellular structures in cells of Arabidopsis at a high frequency. Proc Natl Acad Sci **97**: 3718–3723

Dong J, MacAlister CA, Bergmann DC (2009) BASL controls asymmetric cell division in Arabidopsis. Cell **137**: 1320–1330

Dupuy L, Mackenzie J, Haseloff J (2010) Coordination of plant cell division and expansion in a simple morphogenetic system. Proc Natl Acad Sci **107**: 2711–2716

Errera L (1888) Über Zellformen und Siefenblasen. Bot Cent 395–399

Flanders DJ, Rawlins DJ, Shaw PJ, Lloyd CW (1990) Nucleus-associated microtubules help determine the division plane of plant epidermal cells: avoidance of four-way junctions and the role of cell geometry. J Cell Biol **110**: 1111–1122

Galletti R, Verger S, Hamant O, Ingram GC (2016) Developing a "thick skin": a paradoxical role for mechanical tension in maintaining epidermal integrity? Development **143**: 3249–3258

Gibson WT, Veldhuis JH, Rubinstein B, Cartwright HN, Perrimon N, Brodland GW, Nagpal R, Gibson MC (2011) Control of the mitotic cleavage plane by local epithelial topology. Cell **144**: 427–438

Givoli D (2004) High-order local non-reflecting boundary conditions: a review. Wave Motion **39**: 319–326

Goldstein B (1995) Cell contacts orient some cell division axes in the Caenorhabditis elegans embryo. J Cell Biol **129**: 1071–1080

Gunning BE, Hardham AR, Hughes JE (1978) Evidence for initiation of microtubules in discrete regions of the cell cortex in Azolla root-tip cells, and an hypothesis on the development of cortical arrays of microtubules. Planta **143**: 161–179

Hashimoto T (2015) Microtubules in plants. Arab Book **13**: e0179

Hayashi T, Carthew RW (2004) Surface mechanics mediate pattern formation in the developing retina. Nature **431**: 647–652

Heisler MG, Hamant O, Krupinski P, Uyttewaal M, Ohno C, Jönsson H, Traas J, Meyerowitz EM (2010) Alignment between PIN1 Polarity and Microtubule

Orientation in the Shoot Apical Meristem Reveals a Tight Coupling between Morphogenesis and Auxin Transport. PLoS Biol **8**: e1000516

Heppert JK, Pani AM, Roberts AM, Dickinson DJ, Goldstein B (2018) A CRISPR Tagging-Based Screen Reveals Localized Players in Wnt-Directed Asymmetric Cell Division. Genetics

Hofmeister W (1863) Zusatze und Berichtigungen zu den 1851 veroffentlichen Untersuchungengen der Entwicklung hoherer Kryptogamen. Jahrbucher Wiss Bot 259–293

Hush JM, Overall RL (1996) Cortical microtubule reorientation in higher plants: dynamics and regulation. J Microsc **181**: 129–139

Kafer J, Hayashi T, Maree AFM, Carthew RW, Graner F (2007) Cell adhesion and cortex contractility determine cell patterning in the Drosophilaretina. Proc Natl Acad Sci **104**: 18549–18554

Kierzkowski D, Nakayama N, Routier-Kierzkowska A-L, Weber A, Bayer E, Schorderet M, Reinhardt D, Kuhlemeier C, Smith RS (2012) Elastic domains regulate growth and organogenesis in the plant shoot apical meristem. Science **335**: 1096–1099

Kirik A, Ehrhardt DW, Kirik V (2012) TONNEAU2/FASS regulates the geometry of microtubule nucleation and cortical array organization in interphase Arabidopsis cells. Plant Cell **24**: 1158–1170

Komis G, Luptovčiak I, Ovečka M, Samakovli D, Šamajová O, \v Samaj J (2017) Katanin Effects on Dynamics of Cortical Microtubules and Mitotic Arrays in Arabidopsis thaliana Revealed by Advanced Live-Cell Imaging. Front Plant Sci **8**: 866

Landrein B, Hamant O (2013) How mechanical stress controls microtubule behavior and morphogenesis in plants: history, experiments and revisited theories. Plant J **75**: 324–338

Lang Selker JM, Green PB (1984) Organogenesis in Graptopetalum paraguayense E. Walther: shifts in orientation of cortical microtubule arrays are associated with periclinal divisions. Planta **160**: 289–297

Li S, Lei L, Somerville CR, Gu Y (2012) Cellulose synthase interactive protein 1 (CSI1) links microtubules and cellulose synthase complexes. Proc Natl Acad Sci U A **109**: 185–190

Lintilhac PM, Vesecky TB (1984) Stress-induced alignment of division plane in plant tissues grown in vitro. Nature **307**: 363–364

Lintilhac PM, Vesecky TB (1981) Mechanical Stress and Cell Wall Orientation in Plants. II. The Application of Controlled Directional Stress to Growing Plants; with a Discussion on the Nature of the Wound Reaction. Am J Bot **68**: 1222

Lipka E, Gadeyne A, Stöckle D, Zimmermann S, De Jaeger G, Ehrhardt DW, Kirik V, Van Damme D, Müller S (2014) The Phragmoplast-Orienting Kinesin-12 Class Proteins Translate the Positional Information of the Preprophase Band to Establish the Cortical Division Zone in Arabidopsis thaliana. Plant Cell **26**: 2617–2632

Louveaux M, Julien J-D, Mirabet V, Boudaoud A, Hamant O (2016) Cell division plane orientation based on tensile stress in Arabidopsis thaliana. Proc Natl Acad Sci U A **113**: E4294–303

Lynch TM, Lintilhac PM (1997) Mechanical signals in plant development: a new method for single cell studies. Dev Biol **181**: 246–256

Marcotrigiano M (2010) A role for leaf epidermis in the control of leaf size and the rate and extent of mesophyll cell division. Am J Bot **97**: 224–233

Martinez P, Luo A, Sylvester A, Rasmussen CG (2017) Proper division plane orientation and mitotic progression together allow normal growth of maize. Proc Natl Acad Sci **114**: 2759–2764

Minc N, Piel M (2012) Predicting division plane position and orientation. Trends Cell Biol **22**: 193–200

Mir R, Morris VH, Buschmann H, Rasmussen CG (2018) Division Plane Orientation Defects Revealed by a Synthetic Double Mutant Phenotype. Plant Physiol **176**: 418–431

Mirabet V, Krupinski P, Hamant O, Meyerowitz EM, Jönsson H, Boudaoud A (2018) The self-organization of plant microtubules inside the cell volume yields their cortical localization, stable alignment, and sensitivity to external cues. PLOS Comput Biol **14**: e1006011

Mohanty A, Luo A, DeBlasio S, Ling X, Yang Y, Tuthill DE, Williams KE, Hill D, Zadrozny T, Chan A, et al (2009) Advancing cell biology and functional genomics in maize using fluorescent protein-tagged lines. Plant Physiol **149**: 601–605

Paredez AR, Persson S, Ehrhardt DW, Somerville CR (2008) Genetic evidence that cellulose synthase activity influences microtubule cortical array organization. Plant Physiol **147**: 1723–1734

Peterson KM, Torii KU (2012) Long-term, High-resolution Confocal Time Lapse Imaging of Arabidopsis Cotyledon Epidermis during Germination. J Vis Exp. doi: 10.3791/4426

PICKETT-HEAPS JD, NORTHCOTE DH (1966) Organization of Microtubules and Endoplasmic Reticulum During Mitosis and Cytokinesis in Wheat Meristems. J Cell Sci **1**: 109

Pierre A, Sallé J, Wühr M, Minc N (2016) Generic Theoretical Models to Predict Division Patterns of Cleaving Embryos. Dev Cell **39**: 667–682

Pietra S, Gustavsson A, Kiefer C, Kalmbach L, Hörstedt P, Ikeda Y, Stepanova AN, Alonso JM, Grebe M (2013) Arabidopsis SABRE and CLASP interact to stabilize cell division plane orientation and planar polarity. Nat Commun **4**: 2779

Poethig S (1984) CELLULAR PARAMETERS OF LEAF MORPHOGENESIS IN MAIZE AND TOBACCO. *In* RA White, WC Dickison, eds, Contemp. Probl. Plant Anat. Academic Press, pp 235–259

Rasmussen CG (2016) Using Live-Cell Markers in Maize to Analyze Cell Division Orientation and Timing. *In* M-C Caillaud, ed, Plant Cell Div. Springer New York, New York, NY, pp 209–225

Rasmussen CG, Bellinger M (2018) An overview of plant division-plane orientation. New Phytol

Rasmussen CG, Wright AJ, Müller S (2013) The role of the cytoskeleton and associated proteins in determination of the plant cell division plane. Plant J Cell Mol Biol **75**: 258–269

Sachs J (1878) Uber die Anordnung der Zellen in jungsten Pflanzentheilen. Arb Bot Inst Wurzburg 46–104

Sahlin P, Jönsson H (2010) A Modeling Study on How Cell Division Affects Properties of Epithelial Tissues Under Isotropic Growth. PLoS ONE **5**: e11750

Sakaguchi J, Fukuda H (2008) Cell differentiation in the longitudinal veins and formation of commissural veins in rice (Oryza sativa) and maize (Zea mays). J Plant Res **121**: 593–602

Sampathkumar A, Krupinski P, Wightman R, Milani P, Berquand A, Boudaoud A, Hamant O, Jönsson H, Meyerowitz EM (2014) Subcellular and supracellular mechanical stress prescribes cytoskeleton behavior in Arabidopsis cotyledon pavement cells. Elife **3**: e01967

Schindelin J, Arganda-Carreras I, Frise E, Kaynig V, Longair M, Pietzsch T, Preibisch S, Rueden C, Saalfeld S, Schmid B, et al (2012) Fiji: an open-source platform for biological-image analysis. Nat Methods **9**: 676–682

Shapiro BE, Tobin C, Mjolsness E, Meyerowitz EM (2015) Analysis of cell division patterns in the *Arabidopsis* shoot apical meristem. Proc Natl Acad Sci **112**: 4815–4820

Sharman BC (1942) Developmental Anatomy of the Shoot of Zea mays L. Ann Bot **6**: 245–282

Shen L, Farid H, McPeek MA (2009) Modeling three-dimensional morphological structures using spherical harmonics. Evolution **63**: 1003–1016

Sinnott EW, Bloch R (1941) Division in Vacuolate Plant Cells. Am J Bot **28**: 225–232

Smertenko A, Assaad F, Baluška F, Bezanilla M, Buschmann H, Drakakaki G, Hauser M-T, Janson M, Mineyuki Y, Moore I, et al (2017) Plant Cytokinesis: Terminology for Structures and Processes. Trends Cell Biol **27**: 885–894

Sylvester AW (2000) Division decisions and the spatial regulation of cytokinesis. Curr Opin Plant Biol **3**: 58–66

Sylvester AW, Cande WZ, Freeling M (1990) Division and differentiation during normal and liguleless-1 maize leaf development. Development **110**: 985–1000

Takada S, Iida H (2014) Specification of epidermal cell fate in plant shoots. Front Plant Sci **5**: 49

Théry M, Racine V, Pépin A, Piel M, Chen Y, Sibarita J-B, Bornens M (2005) The extracellular matrix guides the orientation of the cell division axis. Nat Cell Biol **7**: 947–953

Van Damme D, Vanstraelen M, Geelen D (2007) Cortical division zone establishment in plant cells. Trends Plant Sci **12**: 458–464

Van Norman JM (2016) Asymmetry and cell polarity in root development. Dev Biol **419**: 165–174

Wachsman G, Sparks EE, Benfey PN (2015) Genes and networks regulating root anatomy and architecture. New Phytol **208**: 26–38

Walbot V, Egger RL (2016) Pre-Meiotic Anther Development: Cell Fate Specification and Differentiation. Annu Rev Plant Biol **67**: 365–395

von Wangenheim D, Fangerau J, Schmitz A, Smith RS, Leitte H, Stelzer EHK, Maizel A (2016) Rules and Self-Organizing Properties of Post-embryonic Plant Organ Cell Division Patterns. Curr Biol **26**: 439–449

Wasteneys GO, Ambrose JC (2009) Spatial organization of plant cortical microtubules: close encounters of the 2D kind. Trends Cell Biol **19**: 62–71

Willis L, Refahi Y, Wightman R, Landrein B, Teles J, Huang KC, Meyerowitz EM, Jönsson H (2016) Cell size and growth regulation in the Arabidopsis thaliana apical stem cell niche. Proc Natl Acad Sci U A **113**: E8238–E8246

Xiong F, Ma W, Hiscock TW, Mosaliganti KR, Tentner AR, Brakke KA, Rannou N, Gelas A, Souhait L, Swinburne IA, et al (2014) Interplay of Cell Shape and Division Orientation Promotes Robust Morphogenesis of Developing Epithelia. Cell **159**: 415–427

Yoshida S, Barbier de Reuille P, Lane B, Bassel GW, Prusinkiewicz P, Smith RS, Weijers D (2014) Genetic Control of Plant Development by Overriding a Geometric Division Rule. Dev Cell **29**: 75–87

Zhao L, Sack FD (1999) ULTRASTRUCTURE OF STOMATAL DEVELOPMENT IN ARABIDOPSIS (BRASSICACEAE) LEAVES1. Am J Bot **86**: 929–939

Zhu C, Ganguly A, Baskin TI, McClosky DD, Anderson CT, Foster C, Meunier KA, Okamoto R, Berg H, Dixit R (2015) The fragile Fiber1 kinesin contributes to cortical microtubule-mediated trafficking of cell wall components. Plant Physiol **167**: 780–792

CHAPTER 3: Proper division plane orientation and mitotic progression together allow normal growth of maize

Abstract

How growth, microtubule dynamics, and cell-cycle progression are coordinated is one of the unsolved mysteries of cell biology. A maize mutant, *tangled1*, with known defects in growth and proper division plane orientation, and a recently characterized cell-cycle delay identified by time-lapse imaging, was used to clarify the relationship between growth, cell cycle, and proper division plane orientation. The *tangled1* mutant was fully rescued by introduction of cortical division site localized TANGLED1-YFP. A CYCLIN1B destruction box was fused to TANGLED1-YFP to generate a line that mostly rescued the division plane defect but still showed cell-cycle delays when expressed in the *tangled1* mutant. Although an intermediate growth phenotype between wild-type and the *tangled1* mutant was expected, these partially rescued plants grew as well as wild-type siblings, indicating that mitotic progression delays alone do not alter overall growth. These data indicate that division plane orientation, together with proper cell-cycle progression, is critical for plant growth.

Introduction

Plant cells are surrounded by a cell wall that together with other cellular factors, controls cell growth and restricts cell movement. According to cell theory, the orientation of the division plane sets the ultimate placement of cells and is therefore key for the overall organization of the plant body. Alternately, according to organismal theory, cell partitioning merely fills in space, and therefore division plane orientation plays no role in overall plant organization (Kaplan and Hagemann, 1991). Multiple examples exist that support one theory or the other, but a combined theory whereby overall growth is regulated at the organ level, but executed by cells, may be the most accurate (Beemster et al., 2003). Cell walls are positioned during the cell cycle with the involvement of characteristic microtubule arrays: a preprophase band (PPB), which assembles in late interphase (G2) and predicts the future division site (Rasmussen et al., 2013); a spindle in metaphase and anaphase; and a phragmoplast during telophase and cytokinesis that directs the formation of the new cell wall to the cortical division site (Jurgens, 2005; Van Damme, 2009; Murata et al., 2013). The PPB is not required for cytokinesis but is critical for division plane orientation and may be required for timely cell-cycle progression (Chan et al., 2005; Ambrose and Cyr, 2008). The PPB disassembles before cytokinesis, raising the fundamental question of how the premitotic location of the PPB specifies the position of the future new wall (Buschmann et al., 2006).

Mutants with general division plane defects often have significant alterations in both microtubule organization and overall growth (Camilleri, 2002; Azimzadeh et al., 2008; Wright et al., 2009). Alternatively, mutants may have defective specific asymmetric

divisions leading to developmental defects (De Smet and Beeckman, 2011; Facette and Smith, 2012; Kajala et al., 2014; van Dop et al., 2015; Fisher and Sozzani, 2016; Han and Torii, 2016; Shao and Dong, 2016). Many mutants with general division plane defects have mutations in genes that encode microtubule-associated proteins that disrupt both mitotic and interphase microtubule dynamics. In these cases, it is difficult to separate the relative contribution of mitotic versus interphase functions in wall placement. The division plane mutant *tangled1* (*tan1*) is particularly informative because the TAN1 protein is observed only in mitotic cells (Walker et al., 2007; Rasmussen et al., 2011) and binds microtubules *in vitro* (Smith et al., 2001). Analysis of the *tan1* mutant is therefore used here to elucidate the specific contribution of microtubule dynamics during mitosis. Similar to mutants with defects in both interphase and mitotic microtubule dynamics, maize *tan1* mutants have short stature and misoriented cell patterns (Smith et al., 1996), as do mutants of TAN1-interacting partners *phragmoplast orienting kinesin-1;2* (Lipka et al., 2014). TAN1 is similar to the microtubule binding domain of adenomapolyposis coli (Smith et al., 2001), a multifunctional protein that promotes proper division orientation in animal cells (Yamashita et al., 2003; Feng et al., 2013; Poulton et al., 2013).

In *Arabidopsis thaliana,* AtTAN1 fused to yellow fluorescent protein (YFP) was the first identified positive marker of the cortical division site, remaining at the site after PPB disassembly (Walker et al., 2007). AtTAN1-YFP division site recruitment occurs via several independent mechanisms during different cell-cycle stages (Rasmussen et al., 2011), but AtTAN1 function is still unclear. Because of the mild *tan* mutant phenotype in *A. thaliana* (Walker et al., 2007), it was impossible to determine whether AtTAN-YFP could rescue the *tan* mutant phenotype.

Fully functional maize TAN1 fused to YFP (TAN1–YFP) and TAN1–YFP lines described below were examined using live-cell imaging to assess TAN1 function. One TAN1–YFP line with the destruction box from CYCLIN1B fused to TAN1–YFP (D-TAN1-13–YFP), showed partial rescue of the *tan1* mutant. D-TAN1-13–YFP in the *tan1* mutant background exhibited significant delays in mitotic progression, but only minor defects in division plane orientation. Analysis of this variant allowed us to assess the relative importance of mitotic delays and phragmoplast guidance to the division site. D-TAN1-13–YFP in the *tan1* mutant background grew to the same size as wild-type, suggesting that compensatory mechanisms could rescue growth impacted by mitotic delays but not a combination of mitotic delays and division plane orientation defects.

Results and Discussion

Maize *tan1* mutants have short stature and rough textured leaves with disordered cell patterning and shapes (Mitkovski and Sylvester, 2003) (Figure S3.1 A–C) but did not have cytokinesis defects, such as incomplete cell-wall stubs or multinucleate cells (Figure S1E) (Smith et al., 1996). Moreover, cells derived from both symmetric and asymmetric divisions were abnormally shaped (Figure S3.1E), indicating that TAN1 function is required for proper division plane orientation in symmetrically and asymmetrically dividing cells.

Previous studies suggested that *tan1* mutants have division plane defects caused by the inability of phragmoplasts to track back to the division site (Cleary and Smith, 1998). However, these experiments were conducted with fixed cells: it was not possible to compare the location of the PPB to the final orientation of the completed division. YFP-TUBULIN (Mohanty et al., 2009) was crossed into *tan1* mutants to directly test the hypothesis that *tan1* mutants had a phragmoplast guidance defect using time-lapse imaging. Wild-type and *tan1* mutant cells expressing YFP-TUBULIN were imaged from prophase until the end of cytokinesis and compiled into a single time-lapse to compare PPB location to the final division plane (Figure 3.1A, six other examples in Figure 3.1B, and Movie S3.1). In wild- type cells all completed divisions displayed normal division orientation: the new cell wall aligned with the former location of the PPB (n = 87). When *tan1* mutant cells were observed 62.5% (n = 30 of 48) of new cell walls returned to the division site previously occupied by the PPB (Figure 3.1C and Movie S3.2), whereas 37.5% of new cell walls displayed an aberrant location (Figure 3.1 D and E and Movie

S3.3). These data provide direct evidence that *tan1* mutant cells have defects in division plane orientation because of a phragmoplast guidance defect.

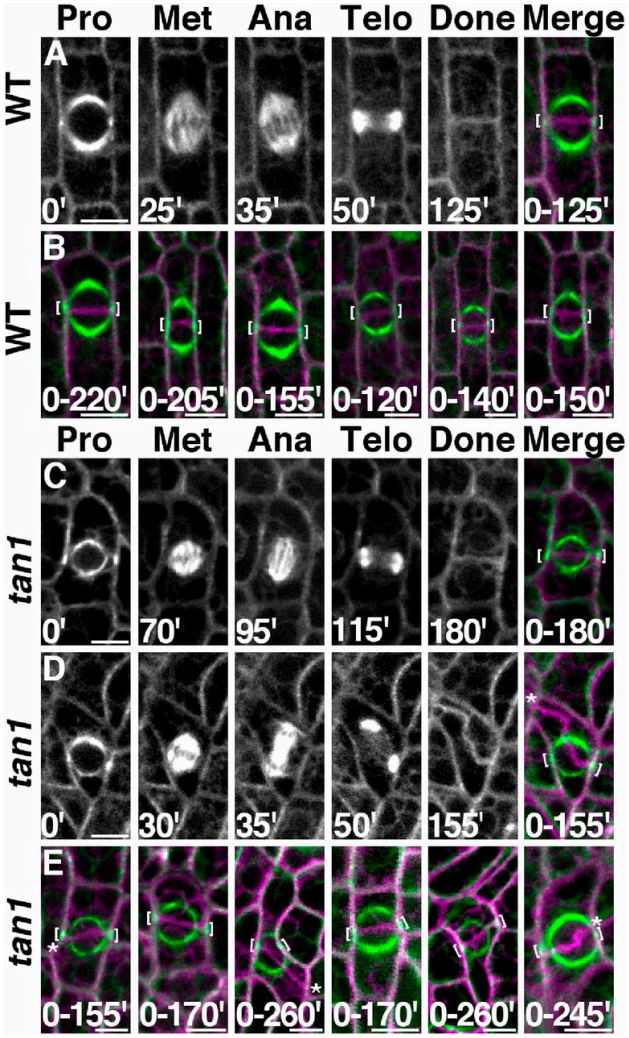

Figure 3.1: Time-lapse and division-time quantification. Merged images show before (green) and after (magenta) division. (A) Wild-type cell division. (B) Six representative wild-type cells. (C) Correctly oriented *tan1* cell division. (D) Misoriented *tan1* division. (E) Six representative *tan1* cells. Brackets mark PPB location. Misplaced cell walls indicated by asterisks. Time (minutes) at the bottom of the image. (Scale bars, 10 μm.)

While performing temperature controlled time-lapse imaging (Rasmussen, 2016), we observed that *tan1* mutant cells were delayed in both metaphase (Figure 3.2A) and telophase (Figure 2B), but not anaphase compared with wild-type siblings (Figure S3.2). Time-lapse imaging was performed by taking a Z-stack every 5 min and assessing at each time the morphology of the mitotic structure. The start of metaphase was counted from the first time the spindle was observed until the anaphase spindle was observed. This time-point became the first time-point for anaphase. Telophase timing was measured from the first time-point a phragmoplast was observed until the phragmoplast was completely disassembled (Rasmussen, 2016). There was no correlation between metaphase delay and defects in phragmoplast guidance to the division site (Figure S3.3A), and no correlation between metaphase and telophase delays (Figure S3.3B). Next, phragmoplast dynamics were analyzed during telophase to determine whether delays in telophase were a result of slower phragmoplast expansion rates in addition to failure to return to the division site. Phragmoplast expansion (Figure 3.2C) and disassembly (Figure 3.2D) were slower in *tan1* mutant cells versus wild-type, but there was no correlation between slow phragmoplast expansion and misoriented phragmoplast orientation (Figure S3.3C) [Kolmogorov–Smirnov (KS) test, $P > 0.1$]. The delays in metaphase and telophase suggest that TAN1 may alter microtubule stability or dynamics in mitotic microtubule arrays. Lack of correlation between mitotic delays and misguided phragmoplast orientation suggest that mitotic progression and proper division plane orientation may be separate.

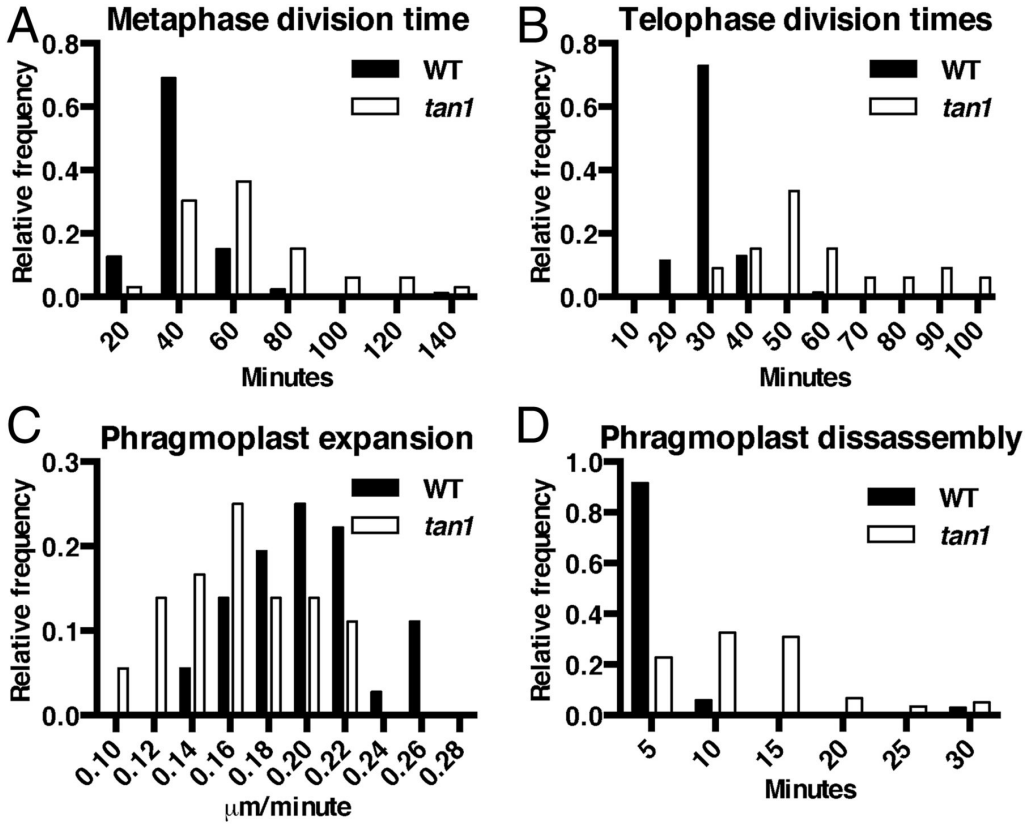

Figure 3.2: Histograms of time required to complete mitotic stages of wild-type and *tan1* mutant cells. (A) Metaphase times: wild-type (39 min, n = 87) and *tan1* (61 min, n = 33), KS test $P < 0.0001$. (B) Transverse telophase times: wild- type (29 min, n = 70) and *tan1* (56 min, n = 33), KS test, $P < 0.0001$. (C) Phragmoplast expansion rates of wild-type (0.20 ± 0.01 μm/min, n = 18 cells) and *tan1* (0.16 ± 0.01 μm/min, n = 18 cells, KS test, $P < 0.001$). (D) Phragmoplast disassembly times for wild-type (6 min, n = 70) and *tan1* (12.5 min, n = 31), KS test, $P < 0.0001$.

TAN1 driven by its own promoter was fused to YFP and transformed into maize (Wu et al., 2013): TAN1–YFP fully rescued the mutant phenotype (Figure 3.3N) and was observed only in mitotic or late G2 cells. TAN1–YFP localized to the cortical division site in symmetrically (Figure 3.3 A–D) and asymmetrically (Figure S3.4) dividing cells. Low TAN1–YFP fluorescence intensity was often observed during G2 (Figure 3.3I),

suggesting that TAN1-YFP was recruited to the division site after PPB formation. After prophase, TAN1-YFP accumulated at the cortical division site and stayed at the same level until the end of telophase (Figure 3.3 A–D and I). In addition to cortical division site localization, TAN1–YFP faintly colocalized with the metaphase spindle (Figure 3.3B) (~23% fluorescence intensity compared with TAN1–YFP at the cortical division site, n = 25), anaphase spindle (Figure 3.3C) (~10% fluorescence intensity compared with TAN1–YFP at cortical division site, n = 6), and phragmoplast microtubules (Figure 3.3D) (~15% fluorescence intensity compared with TAN1–YFP at the cortical division site, n = 21). Spindle and phragmoplast localization of TAN1–YFP together with *in vitro* TAN1–microtubule interaction (Smith et al., 2001) is consistent with the hypothesis that TAN1 directly alters microtubule dynamics in these structures. *At*TAN–YFP did not appear to colocalize with the spindle or phragmoplast in *A. thaliana* (Walker et al., 2007; Rasmussen et al., 2011). The faint nucleolar localization of TAN1–YFP (Figure 3.3A) was similar to that observed in AtTAN–YFP cells (Rasmussen et al., 2011). TAN1–YFP was crossed into the *tan1* mutant to determine if it rescued the mutant phenotype. A population segregating for *tan1*/+ (Figure 3.3L), *tan1/tan1* (Figure 3.3M), and the TAN1–YFP transgene (Figure 3.3N) was assessed for growth by measuring the area of several leaf blades (leaf 7 in Figure 3.3K and leaves 5 and 8 in Figure S3.5). TAN1–YFP; *tan1/tan1* displayed both wild-type growth (Figure 3.3K) (KS test, P = 0.16) and cell-wall patterning similar to wild-type (Figure 3.3N) (n = 13 individual plants), indicating that TAN1–YFP fully rescued the mutant phenotype.

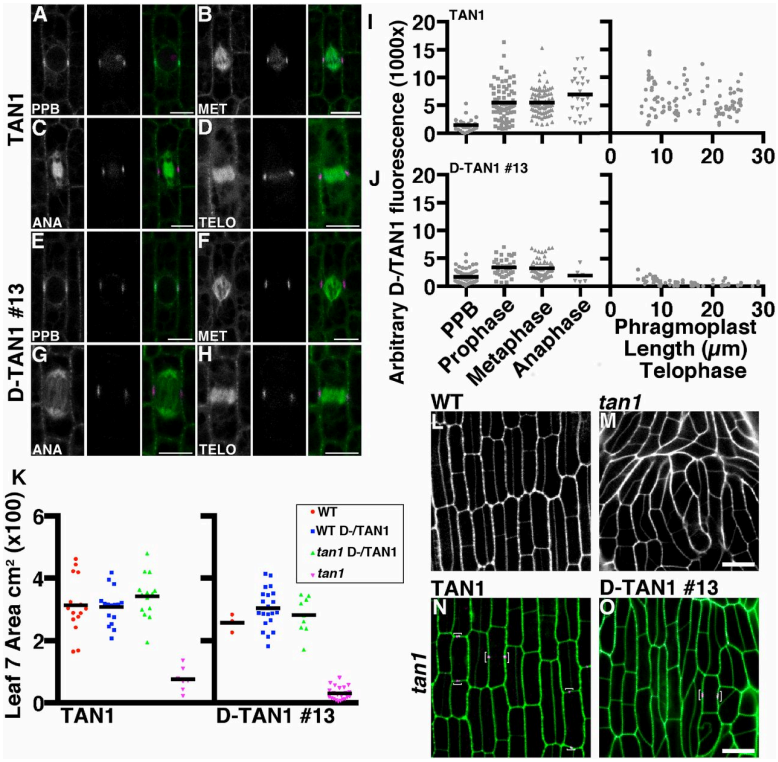

Figure 3.3: Localization and rescue of TAN1–YFP and D-TAN1-13–YFP during mitosis and cytokinesis. TAN1–YFP (magenta) localization during prophase (A), metaphase (B), anaphase (C), and telophase (D) indicated by CFP–TUBULIN (green). Channels are separated CFP–TUBULIN followed by TAN1–YFP and then merged. D-TAN1-13–YFP (magenta) localization during prophase (E), metaphase (F), anaphase (G), and telophase (H) indicated by CFP–TUBULIN (green). Channels are separated CFP–TUBULIN followed by TAN1–YFP and then merged. Arbitrary fluorescence intensities measured at the division site for TAN1–YFP (I) and D-TAN1 (J) using identical imaging conditions. (K) Leaf 7 area measurements of wild-type and *tan1* segregating with TAN1–YFP and D-TAN1-13–YFP. Leaf areas between wild-type and *tan1* TAN1–YFP are not statistically different (KS test, P = 0.1994) and are not different between wild-type and *tan1* D-TAN1-13–YFP (KS test, P = 0.7091). (L) Wild-type and (M) *tan1* epidermal cells stained with propidium iodide (green). (N) TAN1–YFP (magenta) expressed in *tan1* mutant background stained with propidium iodide (green). (O) D-TAN1-13–YFP (magenta) in the *tan1* mutant background stained with propidium iodide (green). (Scale bars, 10 μm.)

The phragmoplast guidance defect observed in the *tan1* mutant (Figure 2.1), together with temporally separate *At*TAN recruitment to the division site during both prophase and telophase (Rasmussen et al., 2011), suggested that TAN1 has a critical function during telophase. We used a TAN1–YFP fusion containing the CYCLIN1B (GRMZM2G034647) destruction box (D-TAN1–YFP) to assess the function of TAN1 after anaphase. Maize CYCLIN1B is degraded in anaphase (33) and *A. thaliana* CYCLIN1B homolog has been used to degrade proteins during anaphase (Krupnova et al., 2009; Van Damme et al., 2011). A negative control with a mutated destruction box was also created (mD- TAN1–YFP). Three independently transformed D-TAN1–YFP and mD-TAN1–YFP lines were crossed into lines expressing cyan-fluorescent protein (CFP)–TUBULIN and the *tan1* mutant to assess localization and rescue. mD-TAN1–YFP localized to the division site similar to TAN1–YFP and had similar fluorescent intensities (Figure S3.6 A–F), indicating that adding a sequence to the N terminus does not alter division site localization or relative fluorescence intensities. All mD-TAN1 lines completely rescued the short stature of the *tan1* mutant and had leaves with the same size quantified through measurement of leaf areas (Figure S3.7 D–F). D-TAN1–YFP also localized to the division site, but fluorescence signal significantly decreased at the division site as telophase progressed (D-TAN1-13–YFP in Figure 3.3 E–H, and J and D-TAN1-3–YFP and D-TAN1-21–YFP in Figure S3.6 G–J). Quantification of fluorescence intensities at the division site indicated that D-TAN1–YFP from three independently transformed lines was eliminated in telophase only when the phragmoplast >10 μm and after the majority of transverse divisions were completed (D-TAN1-13–YFP in Figure 3.3J D-TAN1-3–YFP and D-TAN1-21– YFP in Figure S3.6 H and J). Therefore, the

destruction box, although it eventually led to D-TAN1–YFP elimination from the division site, did not eliminate D-TAN1–YFP completely before the majority of cells finished cytokinesis.

One line containing the D-box-TAN1–YFP fusion, D-TAN1– YFP-13 (Figure 3.3 E–H), had low fluorescent intensity at the division site during all mitotic stages, but had exceptionally low intensity during telophase (quantified in Figure 3.3J) and had no detectable signal in spindles (Figure 3.3 F and G) or phragmoplasts (Figure 3.3H). Although all of the mD-TAN1–YFP and two other D-TAN1–YFP transgenes fully rescued the *tan1* mutant division plane defects (mD-TAN1–YFP in Figure S3.7 A–C and D-TAN1– YFP in Figure S3.8 A and B), D-TAN1-13–YFP *tan1/tan1*, had minor division plane defects first observed by cell-wall staining (Figure 3.3O) and then quantified by time-lapse imaging of D-TAN1-13– YFP *tan1/tan1* dividing cells (described below). All three of the D-TAN1 lines completely rescued the growth defect of the *tan1* mutant quantified via multiple leaf area measurements made at 28 d after planting (D-TAN1 lines #3 and #21 in Figure S3.8 C–E). D-TAN1-13–YFP plant development was additionally compared with wild-type siblings at 1 wk (Figure S3.9), 2 wk (Figure S3.10), and 3 wk (Figure S3.11) after planting.

Two hypotheses could explain the division plane defects in D-TAN1-13–YFP *tan1/tan1* line: (i) overall low expression of D-TAN1-13–YFP provided insufficient protein to fully rescue the mutant phenotype during all stages; or (ii) low levels of D-TAN1-13–YFP during telophase caused the division plane defect observed. If loss of TAN1 exclusively during telophase caused division plane defects, metaphase division times would be the same as wild-type, whereas telophase times would be longer. In contrast, live-cell

imaging indicated that both metaphase and telophase times in D-TAN1-13–YFP *tan1/tan1* cells were intermediate between wild-type and *tan1* mutants (Figure 3.4). During this time-lapse analysis, one aberrant division was observed (n = 1 of 106, < 1%) indicating that D-TAN1-13–YFP *tan1/tan1* cells have minor defects in division plane orientation (Movie S3.4). Phragmoplast expansion rates of *tan1* D-TAN1-13 were significantly slower than wild-type, and similar to phragmoplast expansion rates observed in the *tan1* mutant (Figure S3.12). Total division time of measured mitotic stages (metaphase, anaphase, telophase) for *tan1* (average 123 min, n = 33 from Figure 3.2 dataset) are delayed by 66% compared with wild-type (average 74 min, n = 70), whereas the D-TAN1-13–YFP *tan1/tan1* partial rescue plants (average 94 min, n = 90) have 40% of the mitotic delay seen in the *tan1* mutant. Minor division plane orientation defects were observed in D-TAN1-13–YFP *tan1/tan1* lines (<1%, n = 1 misoriented division of 106 completed divisions) compared with *tan1* mutants (~37%, n = 48). This finding suggested that D-TAN1-13–YFP *tan1/tan1* represents a partial loss of function mutant because of low expression rather than a telophase-specific defect. In addition, undetectably low D-TAN1–YFP fluorescent intensities at spindles or phragmoplasts together with observed mitotic delays in D-TAN1-13–YFP *tan1/tan1* lines is consistent with a role of TAN1 in altering microtubule dynamics at mitotic structures. Therefore, D-TAN1-13–YFP *tan1/tan1* represented a partial loss-of-function mutant, where significant mitotic delays were observed but division plane defects were infrequent.

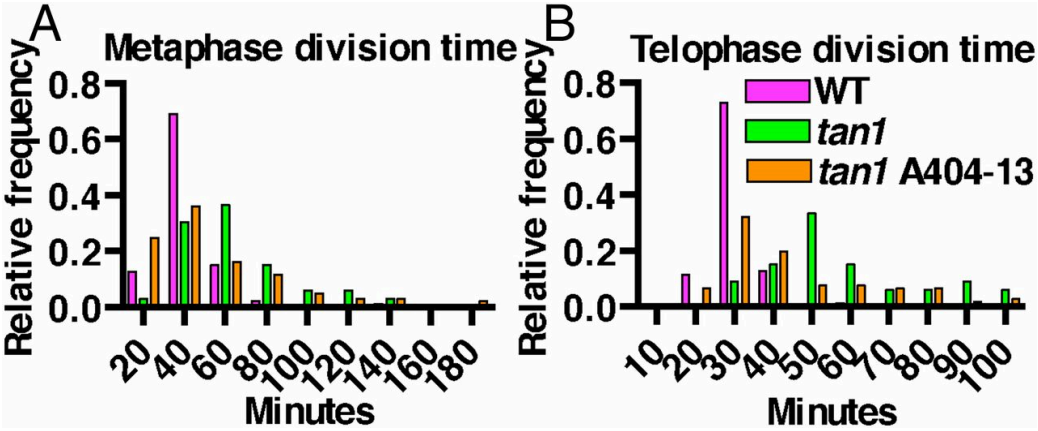

Figure 3.4: Partial rescue during metaphase and telophase of D-TAN1-13–YFP in the *tan1* mutant background. Data for wild-type and *tan1* is the same as presented in Figure 3.2 A and B, graphed alongside the *tan1* D-TAN1-13 data for direct comparison. (A) Metaphase division time for tan1 D-TAN1-13–YFP cells (51 ± 6.4 min, 95% CI, n = 106). Metaphase times are significantly different from wild-type (KS test, P = 0.0027) and from *tan1* (KS test, P = 0.0002). (B) Telophase times (36.3 ± 3 min 95% CI n = 90) for transverse cell divisions. Telophase times are significantly different from wild-type (KS test, P < 0.0001) and from *tan1* (KS test, P = 0.0007).

We predicted that the poorly expressed D-TAN1–YFP partial rescue line would have growth defects intermediate to the *tan1* mutant and wild-type siblings because it had intermediate cell- cycle delays. However, D-TAN1-13–YFP *tan1/tan1* plants grew as well as wild-type siblings. Growth and development of sibling plants was assessed by taking pictures of plants, measuring shoot and root wet weight, and determining length, area and average width of the leaves (Figs. S3.9–S3.13). Completely rescued growth of plants with cell-cycle delays and minor division plane defects suggested that defects in cell-cycle progression and minor division plane orientation were corrected, potentially by expansion or by another compensatory mechanism (Bassel et al., 2014). We measured cell area in the proliferative division zone of the maize blade, but no significant

difference was observed between sibling wild-type and D-TAN1-13–YFP cells, suggesting either that another compensatory mechanism is used or that the cells compensate by expansion in another part of the leaf (Figure S3.14). In some cases, cell-cycle delays do not noticeably alter overall plant (Hemerly et al., 1995) or animal (Neufeld et al., 1998) growth, but other cell-cycle delays alter embryonic or root patterning in *A. thaliana* (Jenik, 2005; Sozzani et al., 2010). More severe cell-cycle delays using overexpression of cyclin-dependent kinase inhibitor, ICK1, demonstrated that cell expansion could partially compensate for mitotic delays. However, slow cell-cycle progression still led to abnormal growth and development (Wang et al., 2000). The small stature of *tan1* mutants suggested that division orientation and proper cell-cycle timing are important aspects of plant growth. The simplest interpretation of the small stature of the *tan1* mutant compared with the normal growth of the partially rescued D-TAN-13–YFP *tan1* line is that proper division orientation is directly required for plant growth. Alternatively, the short stature of the *tan1* mutant might indicate slowed growth in response to altered cell shape. Indeed, cell shape and corresponding mechanical constraints influence growth, even in the absence of cell division (Bassel et al., 2014). Another interpretation is that altered cell-wall placement causes unexpected mechanical strain, which then activates a biochemical response, such as the cell-wall integrity pathway, to slow growth (Voxeur and Höfte, 2016). These hypotheses are not mutually exclusive.

Most division plane orientation mutants likely also have mitotic delays, although this phenotype has only rarely been assessed (Lipka et al., 2014; Kawamura et al., 2006). In addition, many symmetric division plane orientation mutants have defects in both

interphase and mitotic microtubule dynamics, making it impossible to address mitotic and interphase function independently (Camilleri, 2002; Kawamura et al., 2006; Azimzadeh et al., 2008; Wright et al., 2009; Komaki et al., 2010; Spinner et al., 2010; Spinner et al., 2013; Zhang et al., 2016). There are a few mutants that represent intriguing exceptions to highly pleiotropic mutants. One example is the *sabre* mutant, which has misplaced PPBs rather than defective or absent PPBs, leading to defects in establishing the proper division plane orientation in *A. thaliana* (Pietra et al., 2013). Another example is a quintuple *myosinVIII* mutant generated in *Physcomitrella patens*. These mutants display division plane defects in cells that undergo PPB-independent divisions (Wu et al., 2011). The MYOSINVIII protein promotes proper phragmoplast guidance while localizing to the spindle, phragmoplast midzone, and the division site. The proposed model is that MYOSINVIII moves along actin filaments to properly translocate the microtubules in the phragmoplast toward the division site (Wu and Bezanilla, 2014). TAN1 is only present during mitosis, so mutant analysis provides understanding of mitotic specific division plane orientation and cell-cycle progression. This study highlights the importance of correct division plane orientation and timely cell-cycle progression to maintain proper growth.

Materials and Methods

Plants were grown in standard greenhouse conditions. Transgenic maize lines were generated as part of the maize cell genomics project (maize.jcvi.org/cellgenomics/index.php), including YFP variant Citrine fused to α-TUBULIN (YFP–TUBULIN, GRMZM2G153292) and cyan-fluorescent protein fused to β-TUBULIN (CFP–TUBULIN, GRMZM2G164696) (Mohanty et al., 2009). Anding Luo created the TANGLED1 transgene through translational fusion with the YFP variant Citrine (TAN1–YFP, GRMZM2G039113) described in SI Materials and Methods. Construction of D-TAN1–YFP and mD-TAN1–YFP fused wild-type or mutated CYCLIN1B coding sequence from maize GRMZM2G034647 to the N-terminal end of TAN1 is described in SI Materials and Methods.

All time-lapse and quantitative fluorescent imaging was done using a custom-built spinning disk system (Solamere Technology) described in SI Materials and Methods. Time-lapse imaging experiments were performed using standardized imaging conditions. Four-week-old plants were used and leaves were removed until the ligule height was <2 mm. Adaxial symmetrically dividing blade samples were mounted in water, surrounded by vacuum grease on a coverslip, and loaded with another coverslip placed carefully on top of the sample into a Rose chamber (Wadsworth, 2012) and held at constant temperature (21 °C) (Rasmussen, 2016). Z-stacks of cells in late prophase were taken every 5 min for up to 6 h. Only cells that completed a division from prophase until the new cell wall was formed were used to analyze the timing of cell-cycle stages to ensure that the cells used in the analysis were not damaged during sample preparation. Morphology of mitotic structures labeled with YFP–TUBULIN was assessed to infer

mitotic stage. Metaphase timing included first time the spindle was observed until the anaphase spindle was observed. This time-point became the first time-point for anaphase. Anaphase spindles rapidly transitioned to phragmoplasts in telophase. Telophase timing was measured from the first time-point a phragmoplast was observed until the phragmoplast was completely disassembled (Rasmussen, 2016).

For quantification of fluorescence intensities, micrographs were taken of TAN1–YFP, mD-TAN1–YFP, and D-TAN1–YFP lines using standardized imaging conditions. Plants coexpressing CFP–TUBULIN were used to identify each stage of mitosis. Z-stacks were transformed into maximum projections in ImageJ or FIJI (fiji.sc/) using two or more Z slices. Sample movement was corrected using the StackReg Plugin in FIJI. Micrographs for Figure 3.3 A–H and Figure S3.6 C, E, G, and I were taken with a point scanning confocal microscope (SP5, Leica) with HyD detector with Argon 514-nm laser emission 510–601 nm for each mD- or D-TAN1–YFP and 458 with emission 505–510 nm for CFP-TUBULIN using a 40× NA 1.1 water objective. See Table S3.1 for primers used in this study.

Supplementary Materials and Methods

Plant Growth and Genotyping

Maize plants were grown in 10 cm^2 or 7.6 L (2 gallon) pots in standard greenhouse conditions, 16-h light, 8-h dark at the University of Wyoming Agriculture Experiment Station or at University of California, Riverside Agricultural Operations (agops.ucr.edu). Seeds were planted, and grown to two to four leaves and then they were tested the transgenes by applying 4 g/L glufosinate (Finale, Bayer) in 0.1% Tween 20 (Sigma) to leaves. Resistance to glufosinate was assessed after 2–5 d. If genotyping was necessary, DNA was extracted using a TissueLyser (Qiagen) and PCR was performed using KOD Hot Start or Extreme Hot start polymerase (EMD Millipore) using the manufacturer's conditions supplemented with 7% (vol/vol) DMSO. Primers are listed in the Table S3.1. Seed genotyping followed protocol described previously (Gao et al., 2008).

Toluidine Blue O Staining and Analysis.

Toluidine Blue O (TBO, Fisher Scientific) staining was performed on mature leaf number 8 of 3- to 5-wk-old *tan1* mutant and wild-type sibling maize epidermal peels, as previously described (Wright et al., 2009). Briefly, adult leaf 8 leaves were harvested, cut into ∼1-cm2 squares and then fixed in 3.7% (vol/vol) paraformaldehyde for 1 to 3 h, washed, digested with 0.1% Pectolyase (Sigma Aldrich) for 2 h, and washed in water. Using forceps, the epidermis was gently removed and stained in 0.1% TBO in 0.1 M sodium acetate buffer pH 4 for 10 min, then washed in water for two 10-min washes. Color micrographs were taken of adaxial and abaxial adult leaf peels using an Arcturus XT Laser Capture Microdissection Microscope (Arcturus, IIGB Microscopy Facility). Then, four *tan1* mutant and five sibling wild-type micrographs were randomly chosen to

analyze cells. All of the cells in each micrograph were counted, categorized by type, and observed for the presence of multiple nuclei or cell-wall stubs. These micrographs were used to quantify the subsidiary cell division plane defect. Subsidiary cells were identified by their location and pink color. Each subsidiary cell in the micrographs were categorized as normally or abnormally shaped.

Construction of TAN1–YFP, mD-TAN1–YFP, and D-TAN1–YFP.

A full- length, native promoter-driven TAN1–YFP translational fusion was created by A.L. with 2,489 bp native promoters and 1,440 native terminator (Wu et al., 2013). The TAN1 native promoter sequence was obtained by subcloning and sequencing of an EcoRI fragment from ZMMBLc-3L9 (Arizona Genomics Institute). The construction of the CYCLIN1b destruction box TANGLED–YFP fusion (D-TAN1–YFP) used to eliminate the TAN1 protein during anaphase. First, the CYCLIN1B coding sequence from maize GRMZM2G034647 was aligned with the coding sequence of the Arabidopsis thaliana cyclin1b homolog AT5G06150. The homologous N-terminal region containing the D-box used to eliminate the kinesin RUNKEL during anaphase (Krupnova et al., 2009) and Aurora kinase (Van Damme et al., 2011) was identified for maize cyclin1b. The maize Cyclin1b sequence was fused in frame to the N terminus of TAN1–YFP using overlap PCR (Sambrook and Russell, 2001) and ligated into pGEMT (Promega). The DNA sequence was verified by sequencing (University of California, Davis sequencing, http:dnaseq.ucdavis.edu/) and then cloned via restriction endonuclease KpnI (New England Biolabs) digest into the TAN1–YFP in pENTR221 (Gateway, Invitrogen) to create D-TAN1–YFP. LR recombination was performed according to the manufacturer's instructions to insert D-TAN1– YFP into the pAM1006 binary vector (54). Subsequently,

sequence-verified plasmids were transformed into Agrobacterium tumefaciens strain EHA101 (55). For the control, the same sequence used for construction of the D-TAN1-YFP fusion was made, except two critical amino acids were mutated by overlap PCR (Sambrook and Russell, 2001) in the destruction box region of the CYCLIN1b portion to inactivate the ability of the destruction box to bind to CDK (GXXV). The mutated D-TAN1–YFP construct was verified by sequencing and called mD-TAN1–YFP. Transgenic plantlets were generated by Iowa State Plant Transformation Facility in the hybrid HiII background (B73 X A188, PTF; Kan Wang, Iowa State University, Ames, IA) and sent to the University of California, San Diego or University of Wyoming, where they were screened by microscopy or glufosinate resistance for expression of the transgene, and then crossed to *tan1/tan1* mutants or into lines expressing CFP-TUBULIN.

Analysis of TAN1–YFP and mD-TAN1–YFP and D-TAN1–YFP Arbitrary Fluorescence Intensities.

The TAN1–YFP and mD- or D-TAN1– YFP fluorescence intensity was measured with an average area of 0.7 μm^2 at the cortical division site. The recorded values were taken from the highest intensity signal in one Z plane (0.5-μm steps) for each side of the cell cortex. Intensity values of the TAN1–YFP, mD-TAN1–YFP, and D-TAN1–YFP signal in cells during preprophase were recorded when the PPB had condensed to a width of 2 μm or less. In lines expressing D-TAN1–YFP, when cells in telophase did not contain detectable D-TAN1– YFP signal at the cortex, the intensity was measured at the expected site of TAN1–YFP localization based on the trajectory of the phragmoplast. Average arbitrary background fluorescence across samples under standard imaging conditions was

4,650 AU; this value was subtracted from measured values for analysis and figures. Quantification of fluorescence intensities at the division site indicated that D-TAN1–YFP was eliminated during telophase only after the majority of transverse divisions were completed when the phragmoplast > 10 μm (main text, Figure 3.3J, and Figure S3.6 H and J).

Analysis of TAN1-YFP and mD/D-TAN1-YFP Rescue of the *tan1* Mutant.

In addition to observing TAN1–YFP, mD-TAN1–YFP, and D-TAN1–YFP at the division site by microscopy, the function of TAN1–YFP, mD-TAN1–YFP, and D-TAN1–YFP was assessed by backcrossing lines expressing TAN1–YFP or mD-/D-TAN1– YFP into the *tan1* mutant twice. Three independent transformed lines of mD-TAN1–YFP and D-TAN1–YFP were used to assess their ability to rescue the *tan1* mutant phenotype. In this crossing scheme, the first cross produced *tan1*/+ progeny that were then painted with glufosinate to identify plants containing the transgene. Those that contained the transgene (*tan1*/+; TAN1–YFP, mD-TAN1–YFP, or D-TAN1–YFP) were crossed to *tan1/tan1* to create progeny which are 25% *tan1/tan1*; TAN1–YFP mD- TAN1–YFP, or D-TAN1–YFP, 25% *tan1*/+ TAN1–YFP, mD- TAN1–YFP or D-TAN1–YFP, 25% *tan/tan1*, and 25% *tan1*/+. To confirm that TAN1–YFP, mD-TAN1–YFP, and D-TAN1–YFP proteins rescued the mutant phenotype, the glufosinate-resistant plants were genotyped by PCR for the absence of the wild-type *tan1* locus and the presence of the transgene. If the *tan1* locus was wild-type or heterozygous, the primers amplified a small band corresponding to the native *tan1* locus in addition to the 1.2-kb larger mD- or D-TAN1–YFP transgene or 1.7-kb band for TAN1–YFP. However, in *tan1* mutants, a 6.7-kb Cinful-Zeon type

retrotransposon disrupts the *tan1* locus and prevents PCR amplification, allowing unique identification of TAN1–YFP, mD-TAN1–YFP, or D-TAN1–YFP *tan1/tan1* plants.

Plant Measurements.

For TAN1–YFP and all mD-/D-TAN1–YFP, leaf area measurements were made to compare 28-d-old wild- type siblings, those that were *tan1* mutants expressing TAN1–YFP, mD-TAN1–YFP, or D-TAN1–YFP and those that were *tan1* mutants. Leaf area measurements were done by removing the blade of a specified leaf at the ligule, scanning it on a flatbed scanner (Cannon) together with a ruler. The images were imported into FIJI and thresholding performed to extract leaf area measurements. For D-TAN1-13–YFP and wild-type siblings, additional measurements were taken by measuring all of the tissues for weeks 1, 2, and 3 after planting. Plants were weighed immediately after washing debris and soil from roots on a digital scale (Mettler Toledo). Leaf sheath and leaf length was measured from the plants with a ruler or digital calipers. Leaf blades were scanned on a flatbed scanner (Cannon) for area measurements. Statistical analysis was performed using KS test for all measurements through the program PRISM 6 (GraphPad).

Confocal Microscopy.

All time-lapse imaging was performed using a custom-built spinning disk (Solamere Technology) with a Yokagawa W1 spinning disk (Yokagawa), EM-CCD camera (Hamamatsu 9100c), and a Nikon Eclipse TE (Nikon) inverted stand. A 40× water immersion lens (1.15 NA) or 60× water immersion lens (1.2 NA) were used with perfluorcarbon immersion liquid (RIAAA-678, Cargille). The stages is fully motorized and controlled by Micromanager software (www.micromanager.org) with ASI Peizo

(300-μm range) and 3 axis DC servo motor controller. Solid-state lasers (Obis from 40 to 100 mW) and standard emission filters (Chroma Technology) were used. For YFP–TUBULIN, TAN1–YFP, mD-TAN1–YFP, or D-TAN1–YFP, a 514 laser with emission filter 540/30 was used. For CFP–TUBULIN, a 445 laser with emission filter 480/40 was used. For propidium iodide, a 561 laser with emission filter 620/60 was used.

Scanning Electron Microscopy.

Leaves were sequentially removed from 28-d-old *tan1* mutant and wild-type sibling maize plants until a sheath height of ~2 mm was observed. The adaxial blade region just above the ligule toward the margin was freshly dissected and mounted onto a piece of double-sided tape then loaded into the tabletop scanning electron microscope (Hitachi TM-1000). Micrographs were taken using Hitachi software.

Supplementary Figures and Table

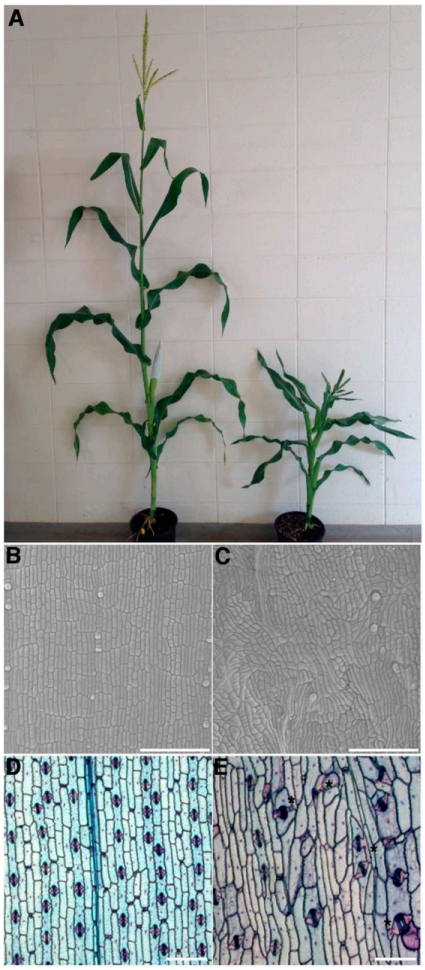

Supplementary Figure 3.1: Wild-type and *tan1* mutant. (A) Photograph of 9-wk-old sibling plants, wild-type plant (Left), and *tan* mutant (Right) grown under standard greenhouse conditions in the A619 inbred background. Scanning electron micrographs were taken from the adaxial leaf blade directly above a 2-mm ligule in (B) nonmutant and (C) sibling *tan* mutant showing disordered cell patterning. TBO staining of abaxial epidermal peels from the mature blade from leaf 8 of (D) nonmutant and (E) sibling *tan* mutant. TBO staining shows that tan1 mutant cells are larger than wild-type sibling cells and that cell divisions are aberrant in both asymmetrically divided and asymmetrically divided (asterisk) cells. (Scale bars, 50 μm.)

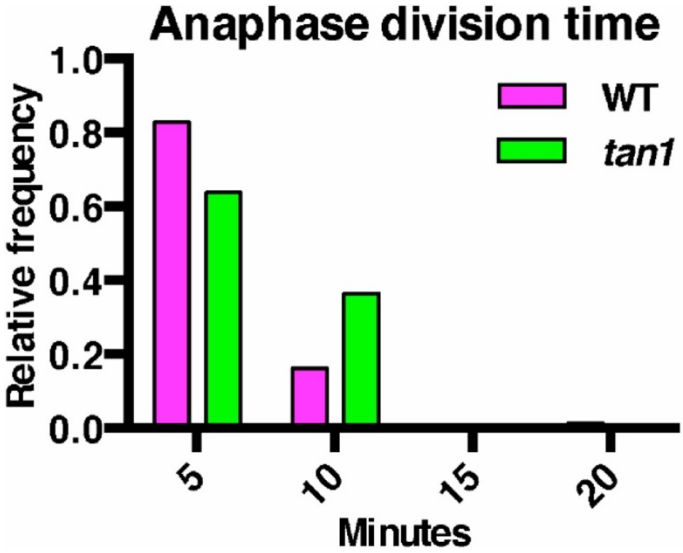

Supplemental Figure 3.2: Anaphase division time of wild-type and *tan1*. Histogram of time cells spent in anaphase measured every 5 min. No statistically significant delays are seen between wild-type (6 min, n = 87) and *tan1* (6.8 min, n = 33) mutants with this time interval (KS test P = 0.34).

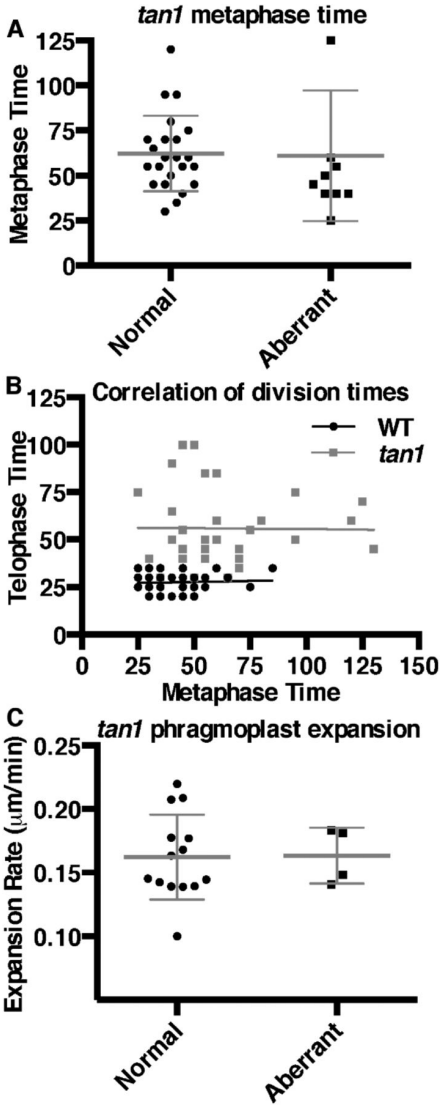

Supplemental Figure 3.3: Correlation of division dynamics. (A) Metaphase division times for *tan1* mutants are not different for correctly oriented division when the new cell wall is in the location predicted by the PPB (62 min, n = 23) or misplaced walls when the new cell wall is not in the location predicted by the PPB (61 min, n = 10) cell. (KS test, P = 0.5761). (B) A longer metaphase division time is not correlated with a longer telophase division time in wild-type (Pearson correlation, P = 0.65) or *tan1* (Pearson correlation, P = 0.944). Outliers (ROUT method, Q2) were removed from wild type, and a nonlinear regression fit is shown. (C) Phragmoplast expansion rates for correctly (0.16 μm/min, n = 14 cells) or misplaced (0.16 μm/min, n = 4 cells) cell walls are not significantly different (KS test, P = 0.9163).

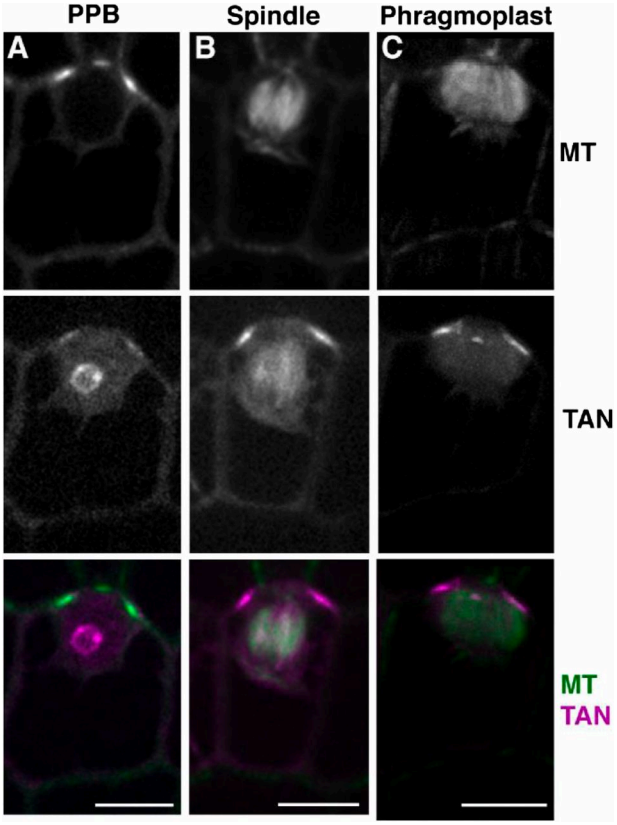

Supplemental Figure 3.4: Localization of TAN1 in asymmetric dividing cells. (A-C) TAN1–YFP and the PPB were colocalized during preprophase/prophase in an asymmetrically dividing cell. (B) During metaphase, the TAN1–YFP signal is still present at the cortical division site and (C) localized at the cortex during telophase. This localization matches what is seen in symmetrically dividing cells. (Scale bars, 10 μm.)

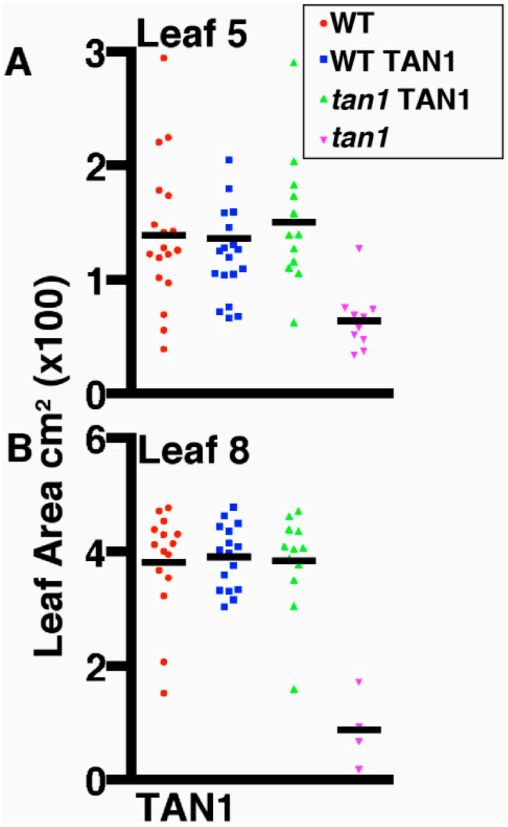

Supplemental Figure 3.5: Leaf 5 and 8 measurements for TAN1–YFP. Maize plants were grown for 28 d: siblings segregating wild-type and tan1 locus with TAN1–YFP were measured to assess rescue. (A) Leaf 5 area measurements are not different between wild-type and *tan1* TAN1 plants (KS test, P = 0.9483). (B) Leaf 8 area measurements between wild-type and *tan1* TAN1–YFP (KS test, P = 0.9912) are not statistically different from each other, indicating a rescue of the *tan1* mutant dwarf phenotype.

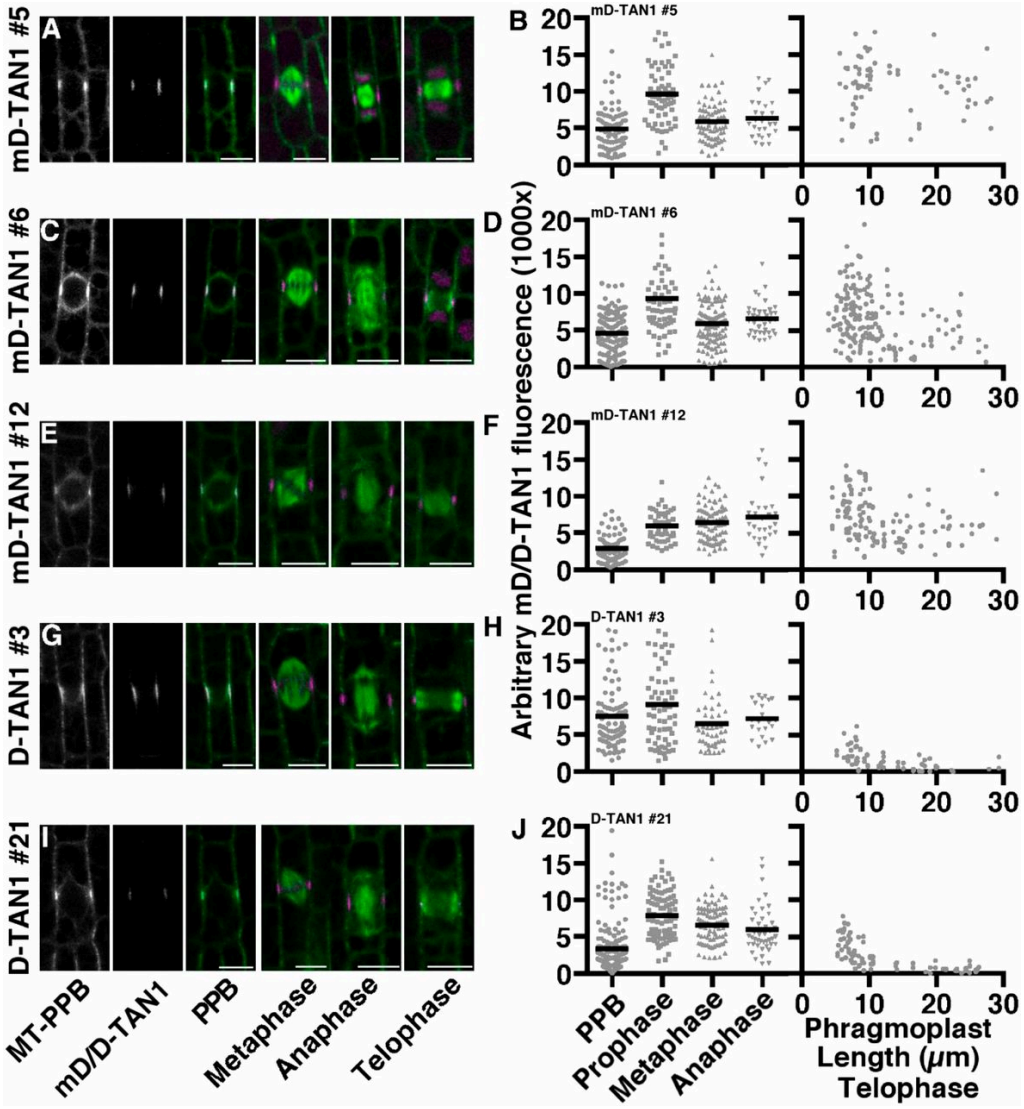

Supplementary Figure 3.6: Localization and expression of mD-/D-TAN1–YFP during mitosis and cytokinesis. (A, C, E, G, and I) Representative images of maize epidermal cells in multiple stages of mitosis expressing CFP–tubulin (green) and mD-TAN1–YFP #5, mD-TAN1–YFP #6, mD-TAN1–YFP #12, D-TAN1–YFP #3, or D-TAN1–YFP #21 (magenta), respectively. Plots for the arbitrary fluorescence intensity values at the CDS for each mD-/D-TAN1–YFP line during individual stages of division are shown in B, D, F, H, and J. Identical imaging conditions were used to measure fluorescence intensity values. Telophase CDS mD-/D-TAN1–YFP intensity values are plotted against phragmoplast length as a proxy for time. (Scale bars, 10 μm.)

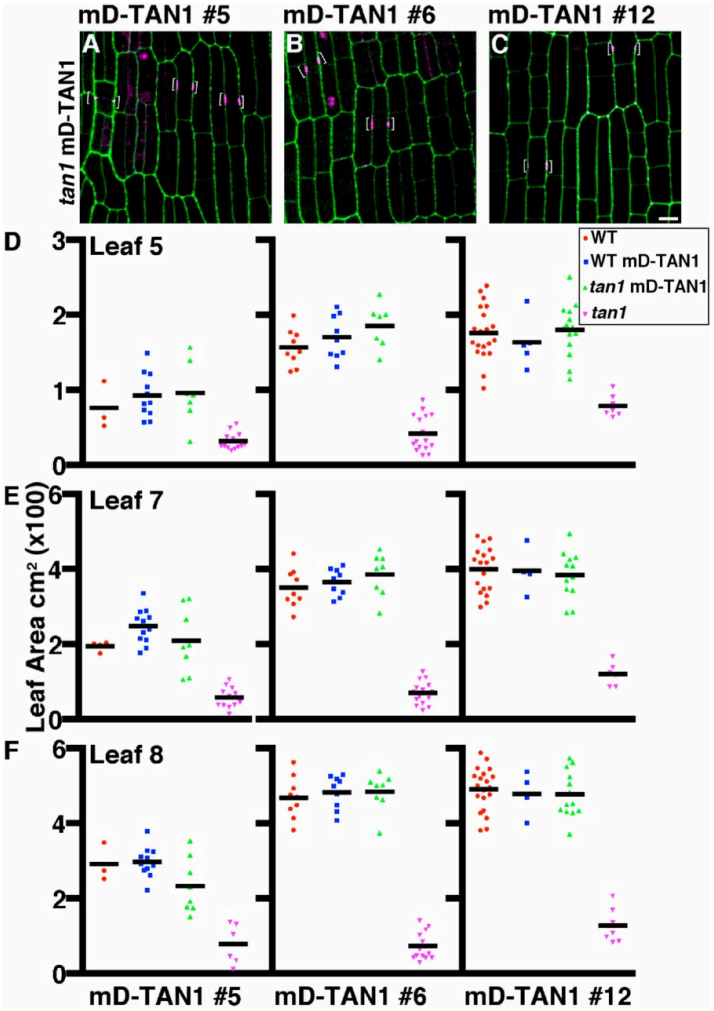

Supplementary Figure 3.7: Rescue of *tan1* mutant phenotype using multiple mD-TAN1–YFP lines. Maize epidermal cells from *tan1* mutants expressing an individual mD-TAN1–YFP are represented in A–C. Cell walls are stained with propidium iodide (green). Brackets indicate the localization of mD-TAN1–YFP (magenta). Maize plants were grown for 28 d: siblings segregating wild-type and *tan1* locus with mD-TAN1–YFP events were measured to assess rescue. Area measurements for each event and genotype are shown for leaf 5 (D), leaf 7 (E), and leaf 8 (F). Measurements for all leaves show that plants which are *tan1* mD-TAN1 are not statistically different from wild-type indicating a rescue of the *tan1* mutant dwarf phenotype (KS test, $P > 0.1732$, for all events). (Scale bar, 10 μm.)

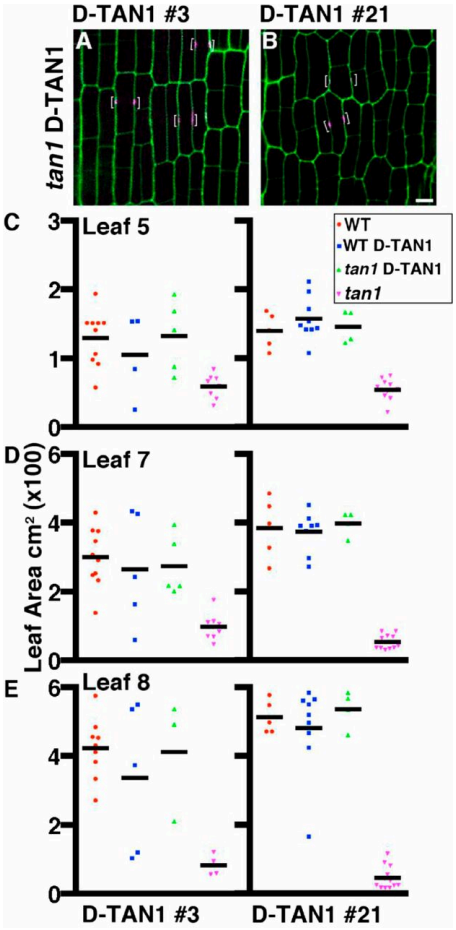

Supplementary Figure 3.8: Rescue of *tan1* mutant phenotype using multiple D-TAN1–YFP lines. (A and B) Maize epidermal cells from *tan1* mutants expressing D-TAN1–YFP events. Cell walls are stained with propidium iodide (green). Brackets indicate the localization of D-TAN1–YFP (magenta). Maize plants were grown for 28 d: siblings segregating the *tan1* locus and D-TAN1–YFP events were measured to assess rescue. Area measurements for each event and genotype are shown for leaf 5 (C), leaf 7 (D), and leaf 8 (E). Measurements for all leaves show that plants which are *tan1* D-TAN1 are not statistically different from wild type, indicating a rescue of the *tan1* mutant dwarf phenotype (KS test, $P > 0.3506$, for all events). (Scale bar, 10 μm.)

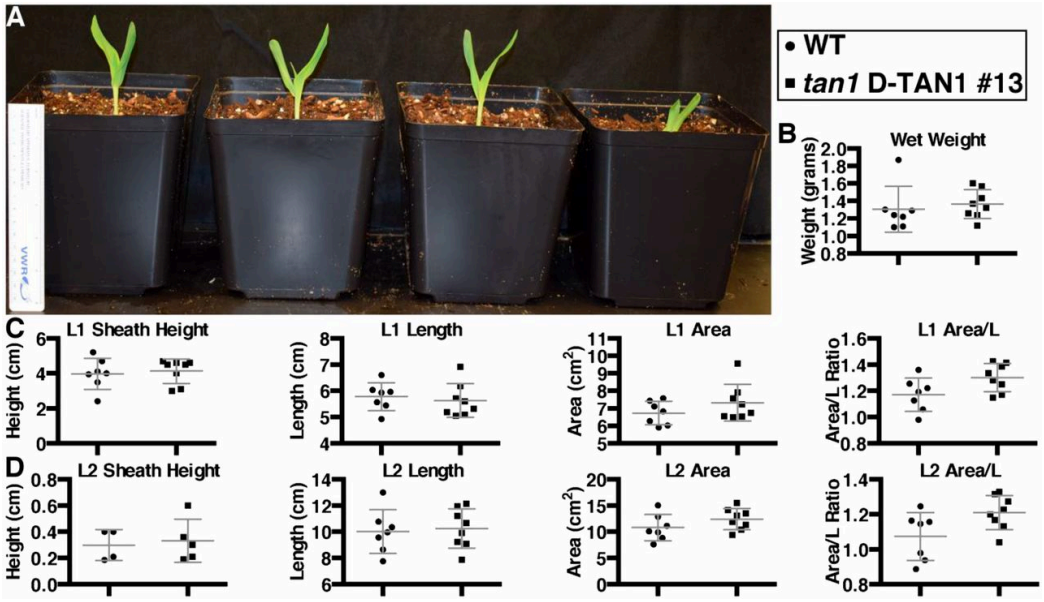

Supplementary Figure 3.9: Rescue of *tan1* mutant phenotype using D-TAN1-13–YFP after 1 wk of growth. (A) Sibling plants (from left to right) wild type, *tan1* D-TAN1-13, wild-type D-TAN1-13, *tan1*. P value presented corresponds to that from KS test. (B) Total wet weight for wild-type and *tan1* D-TAN1-13 is not significantly different (KS test, P = 0.2522). (C) Leaf 1 measurements for sheath height, length, area, and area/length are not different between wild-type and *tan1* D-TAN1-13 (KS test, P > 0.2522). (D) Leaf 2 measurements for sheath height, length, area, and area/length are not different between wild-type and *tan1* D-TAN1-13 (KS test, P > 0.087).

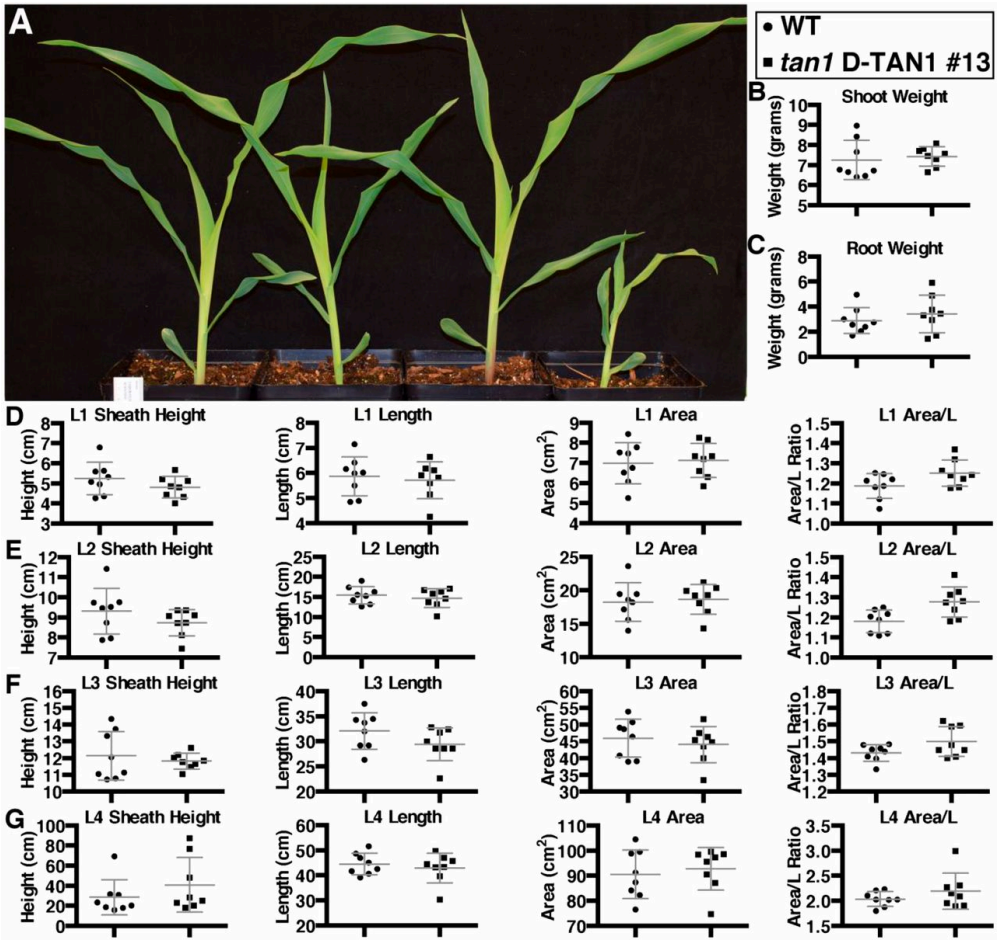

Supplementary Figure 3.10: Rescue of *tan1* mutant phenotype using D-TAN1-13–YFP after 2 wk of growth. (A) Sibling plants (from left to right) WT, *tan1* D-TAN1-13, wild-type D-TAN1-13, *tan1*. (B) Shoot wet weight for wild-type and *tan1* D-TAN1-13 is not significantly different (KS test, P = 0.2827). (C) Root wet weight for wild-type and *tan1* D-TAN1-13 is not significantly different (KS test, P = 0.6601). (D) Leaf 1 measurements for sheath height, length, area, and area/length are not different between wild-type and *tan1* D-TAN1-13 (KS test, P > 0.2827). (E) Leaf 2 measurements for sheath height, length, area, and area/length are not different between wild-type and *tan1* D-TAN1-13 (KS test, P > 0.0870). (F) Leaf 3 measurements for sheath height, length, area, and area/length are not different between wild-type and *tan1* D-TAN1-13 (KS test, P > 0.2199). (G) Leaf 4 measurements for sheath height, length, area, and area/length are not different between wild-type and *tan1* D-TAN1-13 (KS test, P > 0.6601).

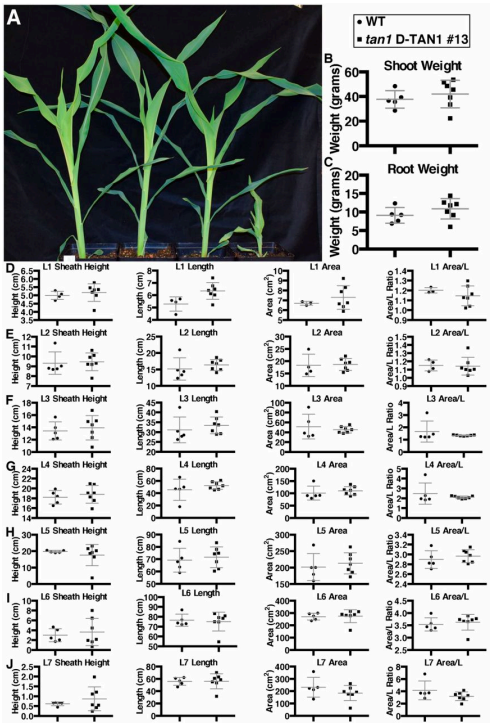

Supplementary Figure 3.11: Rescue of *tan1* mutant phenotype using D-TAN1-13–YFP after 3 wk of growth. (A) Sibling plants (from left to right) wild type, *tan1* D-TAN1-13, wild-type D-TAN1-13, *tan1*. (B) Shoot wet weight for wild-type and *tan1* D-TAN1-13 is not significantly different (KS test, P = 0.5455). (C) Root wet weight for wild-type and *tan1* D-TAN1-13 is not significantly different (KS test, P = 0.3283). (D) Leaf 1 measurements for sheath height, area, and area/length are not different between wild-type and *tan1* D-TAN1-13 (KS test, P > 0.1667); however, length is significantly different (KS test, P = 0.0303). (E) Leaf 2 measurements for sheath height, length, area, and area/length are not different between wild-type and *tan1* D-TAN1-13 (KS test, P > 0.0909). (F) Leaf 3 measurements for sheath height, length, area, and area/length are not different between wild-type and *tan1* D-TAN1-13 (KS test, P > 0.1414). (G) Leaf 4 measurements for sheath height, length, area, and area/length are not different between wild-type and *tan1* D-TAN1-13 (KS test, P > 0.0909). (H) Leaf 5 measurements for sheath height, length, area, and area/length are not different between wild-type and *tan1* D-TAN1-13 (KS test, P > 0.4343). (I) Leaf 6 measurements for sheath height, length, area, and area/length are not different between wild-type and *tan1* D-TAN1-13 (KS test, P > 0.0909). (J) Leaf 7 measurements for sheath height, length, area, and area/length are not different between wild-type and *tan1* D-TAN1-13 (KS test, P > 0.3283).

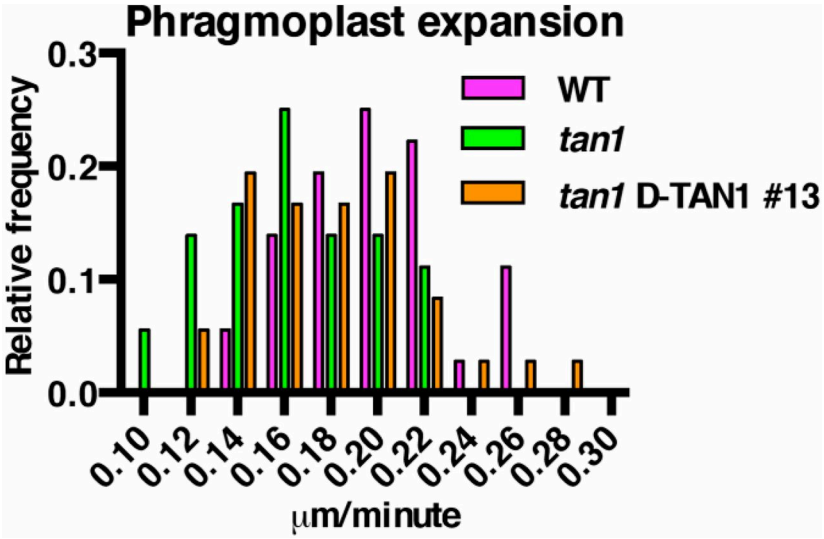

Supplementary Figure 3.12: Phragmoplast expansion rates of wild-type, *tan1*, and *tan1* D-TAN1-13. Phragmoplast expansion rates for wild type and tan1 are presented previously in Figure 2C. Here, they are included with *tan1* D-TAN1-13 values for direct comparison. *tan1* D-TAN1-13 expansion rate is 0.17 ± 0.016 μm/min, 95% CI (n = 18). This rate is significantly different from wild type (KS test, P = 0.0183) but not from *tan1* (KS test, P = 0.5041).

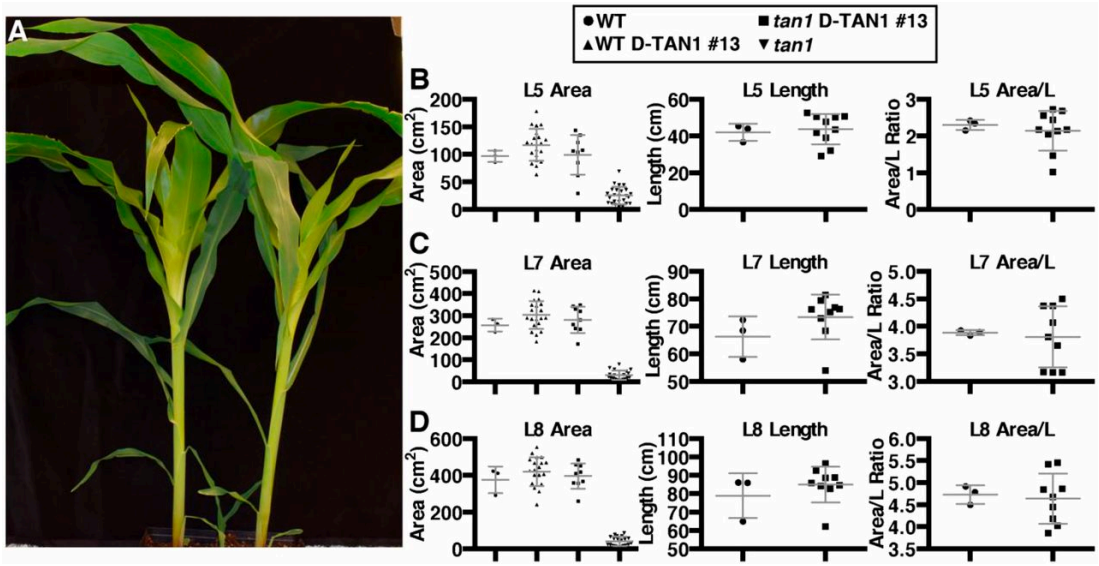

Supplementary Figure 3.13: Rescue of *tan1* mutant phenotype using D-TAN1-13–YFP after 4 wk of growth. (A) Representative image of sibling wild-type and *tan1* D-TAN1-13 28-d-old plants. The plants pictured were not used for the quantification of growth. Leaf areas were measured for wild type, wild-type D-TAN1-13, *tan1* D-TAN1-13, and *tan1*. Length and area/length were measured for wild-type and *tan1* D-TAN1-13. (B) Leaf 5 measurements for area, length, and area/length are not different between wild-type and *tan1* D-TAN1-13 (KS test, $P > 0.4930$). Data for leaf 7 area measurement is presented in Figure 3K. (C) Leaf 7 measurements for area, length, and area/length are not different between wild-type and *tan1* D-TAN1-13 (KS test, $P > 0.3333$). (D) Leaf 8 measurements for area, length, and area/length are not different between wild-type and *tan1* D-TAN1-13 (KS test, $P > 0.7091$).

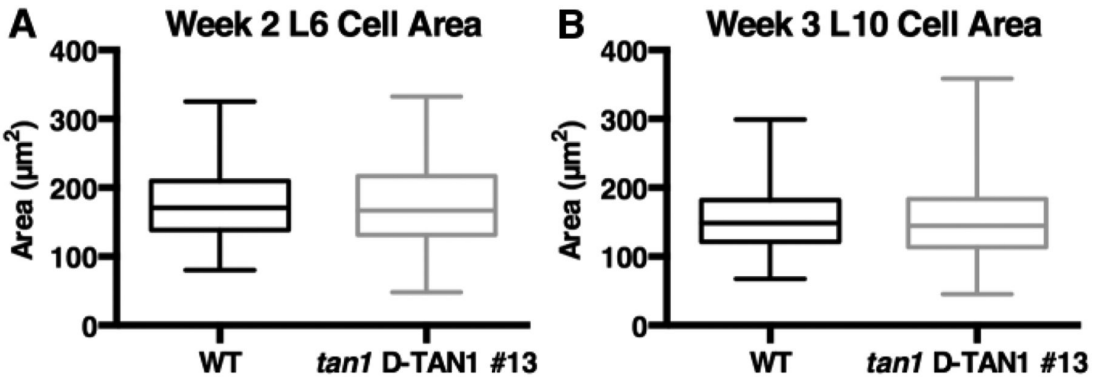

Supplementary Figure 3.14: Cell area measurements in dividing leaf tissue. (A) Cell area measurements for leaf 6 after 2 wk of growth is not significantly different (KS test, P = .3429) between wild-type (n = 401 cells) and *tan1* D-TAN1-13–YFP (n = 265 cells). (B) Cell area measurements for leaf 10 after 3 wk of growth is not different (KS test, P = .3685) between wild-type (n = 282 cells) and *tan1* D-TAN1-13–YFP (n = 192 cells).

Primer name	Gene (GRMZM)	Sequence	Purpose
TANLSP1	2G039113	ACGACCGTTAGCACAGAACC	Differentiate native tan locus from D-box-TAN–YFP
ZmTAN-REV2937	2G039113	CGGCAAGAGTCAGAGTAAGAGACAG	Differentiate native tan locus from D-box-TAN–YFP
TANR13802	2G039113	GCTTGCTTCCAAGTCCAAGTCTC	Differentiate native tan locus from TAN–YFP
ZmTUB-α_RP1	2G153292	GGTTTCGGGTGATCCCTATT	Amplify YFP–TUBULIN
Tub B FP1	2G164696	CGAATTTTCGAATCCTCAGC	Amplify CFP–TUBULIN
BTUBR3187	2G164696	GACAGGCGGGCATAAGATCC	Amplify CFP–TUBULIN

Supplementary Table 3.1: Primers used for this study

Supplementary Video Legends

Supplemental Movie 3.1: Division of a wild-type maize epidermal cell. An example of a wild-type maize epidermal cell dividing using YFP–TUBULIN. The division begins in preprophase and proceeds until the end of telophase. The video is playing at seven frames per second, with each frame representing 5 min. The location of the new cell wall is accurately predicted by the previous position of the PPB. The size was increased for viewing threefold.

Supplemental Movie 3.2: Division of a *tan1* mutant maize epidermal cell. An example of a *tan1* mutant maize epidermal cell dividing using YFP–TUBULIN. The division begins in preprophase and proceeds until the end of telophase. The video is playing at seven frames per second, with each frame representing 5 min. The location of the new cell wall is accurately predicted by the previous position of the PPB. The size was increased for viewing threefold.

Supplemental Movie 3.3: Misoriented division of a *tan1* mutant maize epidermal cell. An example of a *tan1* mutant maize epidermal cell dividing using YFP–TUBULIN. The division begins in preprophase and proceeds until the end of telophase. The video is playing at seven frames per second, with each frame representing 5 min. The location of the new cell wall is not accurately predicted by the previous position of the PPB in this case. The size was increased for viewing threefold

Supplemental Movie 3.4: Misoriented division of *tan1* mutant expressing D-TAN1–YFP #13. *tan1* mutant expressing D-TAN1–YFP and YFP–TUBULIN. The division begins in preprophase and proceeds until the end of telophase. The video is playing at seven frames per second, with each frame representing 5 min. The location of the new cell wall is not accurately predicted by the previous position of the PPB. The size was increased for viewing twofold.

References

Ambrose JC, Cyr R (2008) Mitotic spindle organization by the preprophase band. Mol Plant **1**: 950–60

Azimzadeh J, Nacry P, Christodoulidou A, Drevensek S, Camilleri C, Amiour N, Parcy F, Pastuglia M, Bouchez D (2008) Arabidopsis TONNEAU1 proteins are essential for preprophase band formation and interact with centrin. Plant Cell **20**: 2146–59

Bassel GW, Stamm P, Mosca G, Barbier de Reuille P, Gibbs DJ, Winter R, Janka A, Holdsworth MJ, Smith RS (2014) Mechanical constraints imposed by 3D cellular geometry and arrangement modulate growth patterns in the Arabidopsis embryo. Proc Natl Acad Sci **111**: 8685–8690

Beemster GTS, Fiorani F, Inzé D (2003) Cell cycle: the key to plant growth control? Trends Plant Sci **8**: 154–158

Buschmann H, Chan J, Sanchez-Pulido L, Andrade-Navarro MA, Doonan JH, Lloyd CW (2006) Microtubule-associated AIR9 recognizes the cortical division site at preprophase and cell-plate insertion. Curr Biol **16**: 1938–43

Camilleri C (2002) The Arabidopsis TONNEAU2 Gene Encodes a Putative Novel Protein Phosphatase 2A Regulatory Subunit Essential for the Control of the Cortical Cytoskeleton. PLANT CELL ONLINE **14**: 833–845

Chan J, Calder G, Fox S, Lloyd C (2005) Localization of the microtubule end binding protein EB1 reveals alternative pathways of spindle development in Arabidopsis suspension cells. Plant Cell **17**: 1737–48

Cleary AL, Smith LG (1998) The Tangled1 gene is required for spatial control of cytoskeletal arrays associated with cell division during maize leaf development. Plant Cell **10**: 1875–88

De Smet I, Beeckman T (2011) Asymmetric cell division in land plants and algae: the driving force for differentiation. Nat Rev Mol Cell Biol **12**: 177–188

van Dop M, Liao C-Y, Weijers D (2015) Control of oriented cell division in the Arabidopsis embryo. Curr Opin Plant Biol **23**: 25–30

Facette MR, Smith LG (2012) Division polarity in developing stomata. Curr Opin Plant Biol. doi: 10.1016/j.pbi.2012.09.013

Feng Y, Sentani K, Wiese A, Sands E, Green M, Bommer GT, Cho KR, Fearon ER (2013) Sox9 induction, ectopic Paneth cells, and mitotic spindle axis defects in

mouse colon adenomatous epithelium arising from conditional biallelic Apc inactivation. Am J Pathol **183**: 493–503

Fisher AP, Sozzani R (2016) Uncovering the networks involved in stem cell maintenance and asymmetric cell division in the Arabidopsis root. Curr Opin Plant Biol **29**: 38–43

Gao S, Martinez C, Skinner DJ, Krivanek AF, Crouch JH, Xu Y (2008) Development of a seed DNA-based genotyping system for marker-assisted selection in maize. Mol Breed **22**: 477–494

Han S-K, Torii KU (2016) Lineage-specific stem cells, signals and asymmetries during stomatal development. Dev Camb Engl **143**: 1259–1270

Hemerly A, Engler J de A, Bergounioux C, Van Montagu M, Engler G, Inzé D, Ferreira P (1995) Dominant negative mutants of the Cdc2 kinase uncouple cell division from iterative plant development. EMBO J **14**: 3925–3936

Jenik PD (2005) Interactions between the Cell Cycle and Embryonic Patterning in Arabidopsis Uncovered by a Mutation in DNA Polymerase. PLANT CELL ONLINE **17**: 3362–3377

Jurgens G (2005) Cytokinesis in higher plants. Annu Rev Plant Biol **56**: 281–99

Kajala K, Ramakrishna P, Fisher A, Bergmann DC, De Smet I, Sozzani R, Weijers D, Brady SM (2014) Omics and modelling approaches for understanding regulation of asymmetric cell divisions in arabidopsis and other angiosperm plants. Ann Bot **113**: 1083–1105

Kaplan DR, Hagemann W (1991) The Relationship of Cell and Organism in Vascular Plants. BioScience **41**: 693–703

Kawamura E, Himmelspach R, Rashbrooke MC, Whittington AT, Gale KR, Collings DA, Wasteneys GO (2006) MICROTUBULE ORGANIZATION 1 regulates structure and function of microtubule arrays during mitosis and cytokinesis in the Arabidopsis root. Plant Physiol **140**: 102–14

Komaki S, Abe T, Coutuer S, Inze D, Russinova E, Hashimoto T (2010) Nuclear-localized subtype of end-binding 1 protein regulates spindle organization in Arabidopsis. J Cell Sci **123**: 451–9

Krupnova T, Sasabe M, Ghebreghiorghis L, Gruber CW, Hamada T, Dehmel V, Strompen G, Stierhof YD, Lukowitz W, Kemmerling B, et al (2009) Microtubule-associated kinase-like protein RUNKEL needed [corrected] for cell plate expansion in Arabidopsis cytokinesis. Curr Biol **19**: 518–23

Lipka E, Gadeyne A, Stöckle D, Zimmermann S, De Jaeger G, Ehrhardt DW, Kirik V, Van Damme D, Müller S (2014) The Phragmoplast-Orienting Kinesin-12 Class Proteins Translate the Positional Information of the Preprophase Band to Establish the Cortical Division Zone in Arabidopsis thaliana. Plant Cell **26**: 2617–2632

Mitkovski M, Sylvester AW (2003) Analysis of cell patterns in developing maize leaves: Dark-induced cell expansion restores normal division orientation in the mutant tangled. Int J Plant Sci **164**: 113–124

Mohanty A, Luo A, DeBlasio S, Ling X, Yang Y, Tuthill DE, Williams KE, Hill D, Zadrozny T, Chan A, et al (2009) Advancing cell biology and functional genomics in maize using fluorescent protein-tagged lines. Plant Physiol **149**: 601–605

Murata T, Sano T, Sasabe M, Nonaka S, Higashiyama T, Hasezawa S, Machida Y, Hasebe M (2013) Mechanism of microtubule array expansion in the cytokinetic phragmoplast. Nat Commun. doi: 10.1038/ncomms2967

Neufeld TP, de la Cruz AF, Johnston LA, Edgar BA (1998) Coordination of growth and cell division in the Drosophila wing. Cell **93**: 1183–1193

Pietra S, Gustavsson A, Kiefer C, Kalmbach L, Hörstedt P, Ikeda Y, Stepanova AN, Alonso JM, Grebe M (2013) Arabidopsis SABRE and CLASP interact to stabilize cell division plane orientation and planar polarity. Nat Commun **4**: 2779

Poulton JS, Mu FW, Roberts DM, Peifer M (2013) APC2 and Axin promote mitotic fidelity by facilitating centrosome separation and cytoskeletal regulation. Development **140**: 4226–36

Rasmussen CG (2016) Using Live-Cell Markers in Maize to Analyze Cell Division Orientation and Timing. *In* M-C Caillaud, ed, Plant Cell Div. Springer New York, New York, NY, pp 209–225

Rasmussen CG, Sun B, Smith LG (2011) Tangled localization at the cortical division site of plant cells occurs by several mechanisms. J Cell Sci **124**: 270–9

Rasmussen CG, Wright AJ, Müller S (2013) The role of the cytoskeleton and associated proteins in determination of the plant cell division plane. Plant J Cell Mol Biol **75**: 258–269

Sambrook J, Russell DW (2001) Molecular cloning: a laboratory manual, 3rd ed. Cold Spring Harbor Laboratory Press, Cold Spring Harbor, N.Y

Shao W, Dong J (2016) Polarity in plant asymmetric cell division: Division orientation and cell fate differentiation. Dev Biol. doi: 10.1016/j.ydbio.2016.07.020

Smith LG, Gerttula SM, Han S, Levy J (2001) Tangled1: a microtubule binding protein required for the spatial control of cytokinesis in maize. J Cell Biol **152**: 231–6

Smith LG, Hake S, Sylvester AW (1996) The tangled-1 mutation alters cell division orientations throughout maize leaf development without altering leaf shape. Development **122**: 481–9

Sozzani R, Cui H, Moreno-Risueno MA, Busch W, Van Norman JM, Vernoux T, Brady SM, Dewitte W, Murray J a. H, Benfey PN (2010) Spatiotemporal regulation of cell-cycle genes by SHORTROOT links patterning and growth. Nature **466**: 128–132

Spinner L, Gadeyne A, Belcram K, Goussot M, Moison M, Duroc Y, Eeckhout D, De Winne N, Schaefer E, Van De Slijke E, et al (2013) A protein phosphatase 2A complex spatially controls plant cell division. Nat Commun **4**: 1863

Spinner L, Pastuglia M, Belcram K, Pegoraro M, Goussot M, Bouchez D, Schaefer DG (2010) The function of TONNEAU1 in moss reveals ancient mechanisms of division plane specification and cell elongation in land plants. Development **137**: 2733–42

Van Damme D (2009) Division plane determination during plant somatic cytokinesis. Curr Opin Plant Biol **12**: 745–51

Van Damme D, De Rybel B, Gudesblat G, Demidov D, Grunewald W, De Smet I, Houben A, Beeckman T, Russinova E (2011) Arabidopsis alpha Aurora kinases function in formative cell division plane orientation. Plant Cell **23**: 4013–24

Voxeur A, Höfte H (2016) Cell wall integrity signaling in plants: "To grow or not to grow that's the question." Glycobiology **26**: 950–960

Wadsworth P (2012) Using cultured mammalian cells to study mitosis. Cold Spring Harb Protoc **2012**: 205–212

Walker KL, Müller S, Moss D, Ehrhardt DW, Smith LG (2007) Arabidopsis Tangled Identifies the Division Plane Throughout Mitosis and Cytokinesis. Curr Biol CB **17**: 1827–1836

Wang H, Zhou Y, Gilmer S, Whitwill S, Fowke LC (2000) Expression of the plant cyclin-dependent kinase inhibitor ICK1 affects cell division, plant growth and morphology. Plant J Cell Mol Biol **24**: 613–623

Wright AJ, Gallagher K, Smith LG (2009) discordia1 and alternative discordia1 function redundantly at the cortical division site to promote preprophase band formation and orient division planes in maize. Plant Cell **21**: 234–47

Wu Q, Luo A, Zadrozny T, Sylvester A, Jackson D (2013) Fluorescent protein marker lines in maize: generation and applications. Int J Dev Biol **57**: 535–43

Wu S-Z, Bezanilla M (2014) Myosin VIII associates with microtubule ends and together with actin plays a role in guiding plant cell division. eLife. doi: 10.7554/eLife.03498

Wu SZ, Ritchie JA, Pan AH, Quatrano RS, Bezanilla M (2011) Myosin VIII regulates protonemal patterning and developmental timing in the moss Physcomitrella patens. Mol Plant **4**: 909–21

Yamashita YM, Jones DL, Fuller MT (2003) Orientation of asymmetric stem cell division by the APC tumor suppressor and centrosome. Science **301**: 1547–50

Zhang Y, Iakovidis M, Costa S (2016) Control of patterns of symmetric cell division in the epidermal and cortical tissues of the Arabidopsis root. Development. doi: 10.1242/dev.129502

CHAPTER 4: The microtubule-binding protein TANGLED1 mediates contact-angle-independent microtubule interactions

Abstract:

The microtubule cytoskeleton is involved in multiple developmental processes such as coordinating directional growth, responding to mechanical stimuli as well as executing cell divisions. Microtubule behaviors including growth and catastrophe can be mediated by events such as microtubule interactions with cell edges, other microtubules or microtubule binding proteins. TANGLED1 (TAN1) is a microtubule binding protein which localizes to mitotic microtubule arrays as well as the cortical division site in plants. Here, *in vitro* experiments demonstrate that TAN1 binds to microtubules with high affinity and mediates microtubule interactions in a microtubule crossover angle independent way, leading to both zippering and end-on interactions. *In vivo*, *tan1* mutants display apparent PPB spatial positioning defects. Computational modeling suggests that PPB placement defects are likely a consequence of altered cell shapes and not due to a direct TAN1 function. In telophase we observed cortically localized microtubules which contact the division site outside of the phragmoplast. These microtubules appear to be organized by interactions with the division site. Areas of the division site with higher TAN1 localization limit spatial microtubule growth through end on interactions, acting akin to a "molecular edge". Spaces of the division site with lower TAN1 localization allow microtubules to crossover the division site and subsequently may be bundled. Analysis of these microtubules in the *tan1* mutant suggest that TAN1 may be important

in organizing these microtubules while also aiding to guide the phragmoplast to the division site.

Introduction:

The proper organization of microtubule networks both during interphase and mitosis are important factors in determining proper development at both the cell and organismal level. The dynamic rearrangements of the cytoskeleton promote directional growth for a plant (Panteris et al., 2013; Panteris et al., 2018). During G2, a structure called the preprophase band (PPB) is formed and composed of a ring-shaped arrangement of microtubules, actin and microtubule associated proteins that localize just under the plasma membrane (Pickett-Heaps and Northcote, 1966; Palevitz, 1987). The PPB is an early marker which indicates the location where the future cell wall will be built following mitosis for both symmetric and asymmetric divisions (Rasmussen and Bellinger, 2018; Facette et al., 2019). Additionally, the PPB may orient and organize the metaphase spindle to promote rapid mitotic progression (Chan et al., 2005; Ambrose and Cyr, 2008). As cells enter metaphase, the PPB is completely disassembled, however a handful of proteins colocalize with the PPB and then remain at the division site (Walker et al., 2007; Xu et al., 2008; Lipka et al., 2014; Buschmann et al., 2015; Li et al., 2017; Martinez et al., 2017). During cytokinesis, a structure named the phragmoplast is assembled from microtubule and filamentous actin to move golgi-derived vesicles that form the cell plate and centrifugally expand outwards to the cortex of the cell (Smertenko, 2018; Smertenko et al., 2018). Once the phragmoplast reaches the cortex it is disassembled and the cell plate fuses with the plasma membrane.

Analysis of mutant phenotypes indicate that division site localized proteins often play a critical role in phragmoplast guidance. Double mutants for a set of kinesin-12 paralogs in *Arabidopsis thaliana*, *phragmoplast orienting kinesin 1 (pok1)* and *pok2* display a severe

division plane defect (Müller et al., 2006). POK1 is a direct TANGLED1 (TAN1) interactor and both proteins localized to the cortical division site however TAN1 localization is partially independent of POK1 localization during the formation of the PPB (Müller et al., 2006; Walker et al., 2007; Lipka et al., 2014). After PPB disassembly however, both POK1 and POK2 are necessary for TAN1 maintenance to the cortical division site (Müller et al., 2006; Walker et al., 2007). While POK1 localizes to the cortical division site throughout mitosis, POK2 localizes to both the division site as well mitotic microtubule structures such as the phragmoplast (Lipka et al., 2014; Herrmann et al., 2018). POK2 was shown to be a microtubule plus end directed motor which interact with MAP65-3, a microtubule bundling protein (Chugh et al., 2018; Herrmann et al., 2018). MAP65-3 localizes to the phragmoplast midzone where antiparallel microtubule bundles are found (Ho et al., 2011). The POK2-MAP65-3 interaction was proposed to serve a role in phragmoplast guidance by providing a potential protein-protein interaction connecting the phragmoplast leading edge to the division site (Herrmann et al., 2018).
A closely-related protein, MAP65-4, is localized to the PPB as well as the spindle, phragmoplast and the division site (Li et al., 2017). The *map65-3 map65-4* double mutant in *Arabidopsis thaliana* displays a severe cytokinesis defect (Li et al., 2017). MAP65-4 binds to and bundles microtubules *in vitro* leading to more stable microtubules within the bundle as they were able to grow longer than single microtubules (Fache et al., 2010). This increased microtubule stability within bundles by MAP65-4 was hypothesized to be important for proper assembly of the acentrosomal bipolar mitotic spindle (Fache et al., 2010). The role of microtubule binding and bundling proteins therefore is important for the execution and establishment of properly oriented division planes.

In maize, *tan1* mutants have division plane defects in both symmetric and asymmetric divisions caused by a failure of the phragmoplast to return to the site originally indicated by the PPB (Smith et al., 1996; Martinez et al., 2017). TAN1 protein was shown to localize to the cortical division site throughout mitosis (Walker et al., 2007) as well as mitotic microtubule-based structures using both functional TAN1-YFP *in vivo* (Martinez et al., 2017) and a non-specific TAN1 antibody (Smith et al., 2001). In addition to division plane defects, the *tan1* mutant has mitotic progression delays and reduced plant stature (Smith et al., 1996; Martinez et al., 2017). Mitotic progression delays and phragmoplast guidance defects can be functionally separated using a partially rescued *tan1* mutant expressing TAN1-YFP fused to the CYCLIN B-destruction box motif (Martinez et al., 2017). In this partially rescued line, mitotic delays are observed but division plane defects are rare and TAN1-YFP signal is below detection in the spindle and phragmoplast, but still visibly accumulates at the division site. We hypothesize that TAN1 aids in timely mitotic progression when it localizes to mitotic microtubule structures and functions to maintain division plane orientation when it is localized to the division site. Here we demonstrate that TAN1 mediates microtubule interactions *in vitro* across a wide degree of microtubule contact angles. To assess the *in vivo* function of TAN1, a mathematical model was used to show that TAN1 is unlikely to play a direct role in PPB placement. Instead, we propose that end-on microtubule interactions mediated by TAN1 at the division site organize cortically localized microtubules during telophase which may be important for phragmoplast guidance.

Results:

TAN1 binds to microtubules *in vitro*

TAN1 protein was shown to bind to taxol stabilized microtubules via a blot overlay assay but nothing was known about TAN1 binding affinity for microtubules (Smith et al., 2001). Therefore, recombinantly expressed 6xHIS tagged ZmTAN1 (HIS-TAN1) protein was purified to determine whether it binds microtubules by cosedimentation (Figure 4.1A), followed by determining microtubule binding affinity via quantitative microtubule cosedimentation assays (Figure 4.1B, materials and methods). We observed microtubule-concentration-dependent HIS-TAN1 co-sedimentation and calculated an affinity of 1.27uM [TUBULIN] using 2uM [HIS-TAN1] similar to other microtubule-binding proteins (Figure 4.1B-C, materials and methods) (Tulin et al., 2012; Portran et al., 2013).

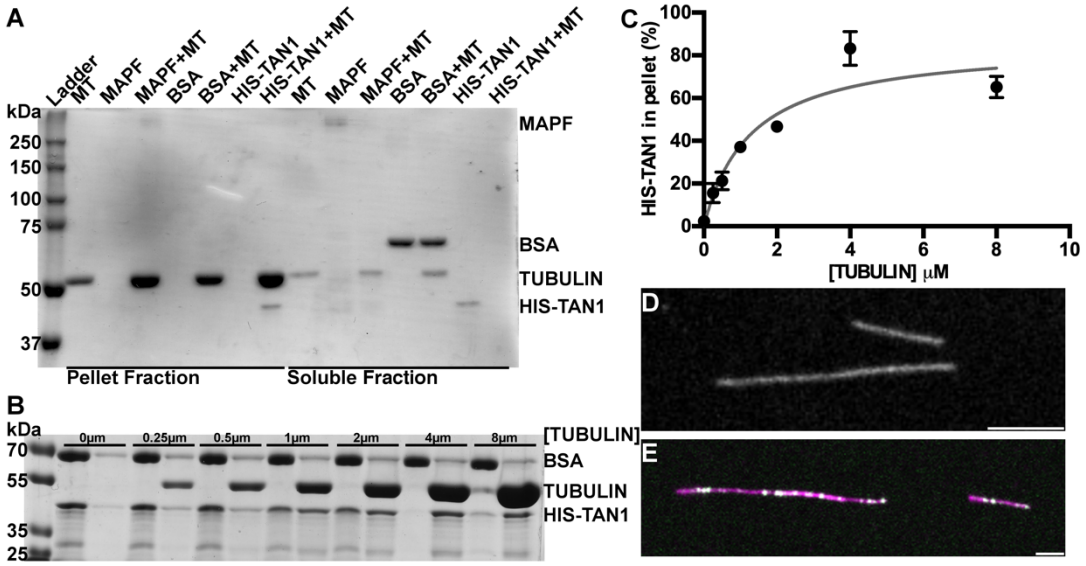

Figure 4.1: Recombinantly expressed TAN1 binds to microtubules. (A) Coomassie stained SDS PAGE results from microtubule cosedimentation with HIS-TAN1, positive (MAPF) and negative (BSA) controls separated into corresponding pellet and soluble fractions. (B) Coomasie stained SDS PAGE results from microtubule cosedimentation assay using 2μM HIS-TAN1 and varying concentrations of tubulin (0-8μM). (C) Michaelis-Menten fit on microtubule cosedimentation data for 2μM HIS-TAN1 at varying concentrations of microtubules determines a binding affinity of 1.27μM +/- 0.3 (S.D) [TUBULIN]. (D) Rhodamine-labeled GMPCPP stabilized microtubules in the absence of TAN1 protein. (E) 0.1μM HIS-TAN1-GFP-Atto488 (green) visualized on rhodamine-labeled GMPCPP stabilized microtubules (magenta). Scale bars are 10μm.

In addition, we determined that both 6x HIS tagged ZmTAN1-GFP (HIS-TAN1-GFP) as well as an Atto488 labeled HIS-TAN1-GFP (HIS-TAN1-GFP-Atto488) interacted with microtubules with a similar binding affinity (materials and methods) (Supplemental Figure 4.1). HIS-TAN1-GFP-Atto488 protein also co-labeled fluorescently labeled microtubules (Figure 4.1D-E). At higher concentrations of HIS-TAN1-Atto488, stabilized microtubules also appeared to be bundled (Figure 4.2A-D). Together, these

data demonstrate that recombinant TAN1 binds stabilized microtubules with a reasonable affinity.

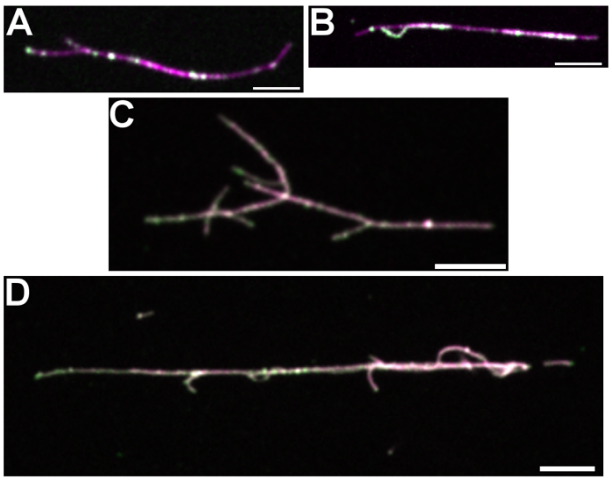

Figure 4.2: HIS-TAN1-GFP-Atto488 appears to bundle stabilized microtubules *in vitro*. (A-D) HIS-TAN1-GFP-Atto488 (green) visualized on rhodamine-labeled GMPCPP stabilized microtubules (magenta). (A-B) 100nM HIS-TAN1-GFP-Atto488 puncta observed along microtubules with some evidence of bundling. (C) 0.5μM HIS-TAN1-GFP-Atto488 localized along microtubules display evidence of bundling. (D) 1μM HIS-TAN1-GFP-Atto488 localized along microtubules display evidence of bundling. Scale bar is 10μm.

In vitro reconstruction of microtubule dynamics with TAN1

Many microtubule-binding proteins directly alter microtubule dynamics *in vivo* and *in vitro* (Tulin et al., 2012; Fan et al., 2018). HIS-TAN1-GFP-Atto488 used in the microtubule colocalization also appeared to induce bundling of microtubules (Figure 4.2A-C) so dynamic *in vitro* microtubule assays were used to test whether TAN1 alters microtubule dynamics and mediates bundling. Using GMPCPP-stabilized microtubule seeds as nucleation sites, 17.5μM 1:25 rhodamine tubulin was used to initiate and assess

microtubule growth and shrinkage with total internal reflection fluorescence (TIRF) microscopy (materials and methods). HIS-TAN1 was used for these experiments due to protein availability instead of the HIS-TAN1-GFP-Atto488. At a concentration of 2μM HIS-TAN1, we observed decreases both in microtubule plus end growth and plus end shrinkage rates. However, no significant effect on microtubule dynamics was observed at lower concentrations of HIS-TAN1 (Table 4.1). HIS-TAN1 addition did not alter the amount of time microtubules spent growing or the frequency of catastrophes, however small but significant differences in time shrinking were observed (Table 4.1). Minus end dynamics were not quantified as there was very little growth observed; additionally, rescue events were not observed with these *in vitro* conditions. These results suggest that TAN1 may play a minor role in microtubule plus end growth rate, shrinkage rate and dynamics.

Plus end dynamics	0µM HIS-TAN1	0.1 µM HIS-TAN1	0.5 µM HIS-TAN1	1µM HIS-TAN1	2µM HIS-TAN1
Growth events (n)	156	180	166	214	196
Growth Rate (µm/sec, mean +/- S.D.)	1.8 +/- 0.4	1.8 +/- 0.3	1.8 +/- 0.3	*1.6 +/- 0.5	***1.5 +/- 0.3
Shrinkage events (n)	109	127	113	153	149
Shrinkage Rate (µm/sec, mean +/- S.D.)	31.5 +/- 15.6	27.7 +/- 10.8	*26.2 +/- 8.8	27.8 +/- 9.7	***24.2 +/- 10.0
Time growing (%)	94.9	93.8	94.5	94.6	95.2
Time shrinking (%)	5.1	**6.2	*5.5	5.4	4.8
Catastrophe Frequency (events/minute)	0.3	0.4	0.4	0.4	0.5

Table 4.1: Summary of microtubule dynamics at different concentrations of HIS-TAN1

Bundling of dynamic microtubules by HIS-TAN1

To induce more crossover events during the dynamic microtubule assay and test for TAN1 mediated microtubule interactions, we used a higher concentration of free tubulin dimers (22.5µM 1:25 rhodamine tubulin) and GMPCPP-stabilized seeds (materials and methods). HIS-TAN1 dependent microtubule interactions occurred when 2µM HIS-TAN1 was used (139 interaction events resulting from 506 crossovers at 2µM HIS-TAN1, Table 4.2). Lower concentrations of HIS-TAN did not promote microtubule interactions. HIS-TAN1 interactions with microtubules were dependent on the angle of microtubule contact. At high contact angles, transient "end-on" microtubule interaction events were observed during microtubule catastrophe. At a crossover site, if one of the microtubules depolymerizes it appears to transiently catch the other microtubule at the crossover point, leading to a pulling effect (n=92/139, 66% of interaction events, angle = 60° +/- 20° average +/- S.D., Figure 4.2A-B). More typical microtubule bundling interactions by zippering occurred when microtubule encounter angles were shallow

(n=47/139 34% of bundling events, angle = 19.6° +/- 7.6° average +/- S.D.). The polarity of zippering events was quantified in cases which bundling did not involve microtubule-seed interactions. They were subsequently classified as parallel (n=13/27, Figure 4.2C) or antiparallel (n=14/27, Figure 4.2D) orientations. Similar frequencies were observed for both. These results suggest that TAN1-microtubule interactions depend on the initial crossover angle between the microtubules, leading to different microtubule behaviors. HIS-TAN1-GFP-Atto488 bundled GMPCPP stabilized microtubules at concentrations as low as 100nM compared to the 2μM concentrations needed in the dynamic assay (Figure 4.1E-I). One possible explanation for the differences between these two experiments was that TAN1 microtubule binding is disrupted by competition from soluble tubulin dimers which are present in the dynamic microtubule assays but absent from stabilized microtubule experiments. Therefore, we tested whether HIS-TAN1-GFP interacted with soluble tubulin dimers using an *in vitro* pull down assay. We observed a direct interaction between HIS-TAN1-GFP and tubulin dimers (Supplemental Figure 4.2). This potential competition between binding soluble tubulin and microtubules may be responsible for the high concentrations of HIS-TAN1 needed to induce crosslinking in dynamic assays.

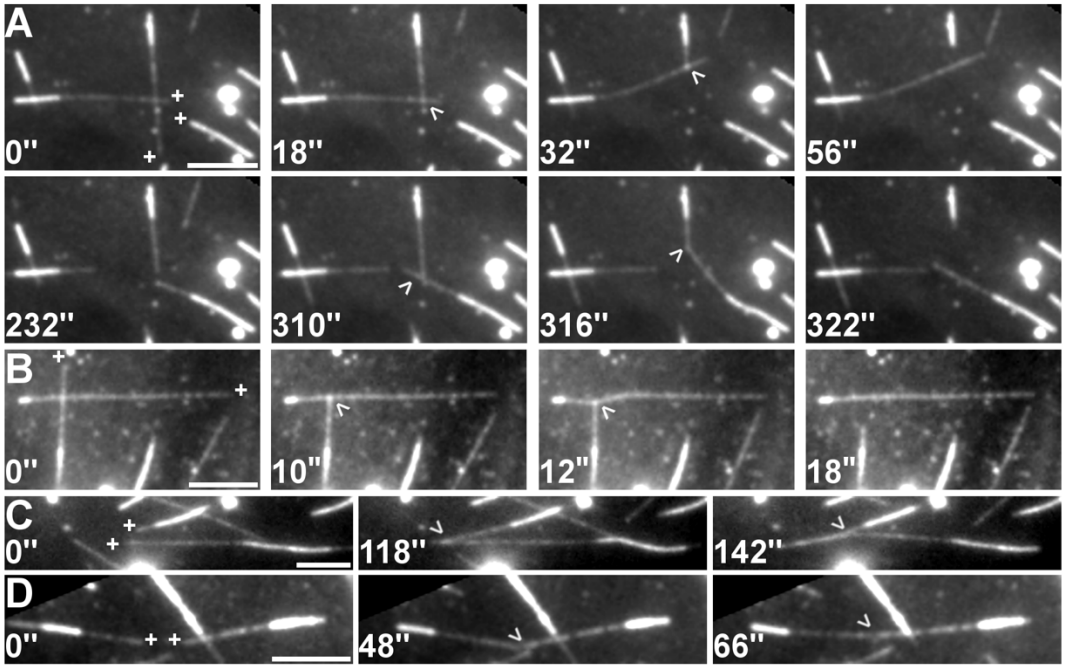

Figure 4.3: HIS-TAN1 crosslinking dynamic microtubules. (A-D) Dynamic rhodamine-microtubules nucleated from GMPCPP stabilized seeds with plus ends of interest indicated by a (+) and the crossover of interest indicated with an arrowhead. Microtubule seeds are identified by their brighter signal compared to the growing microtubule ends. 2μM HIS-TAN1 is present in the assay. (A) Three microtubules are indicated at the start (0"). Two microtubules crossover (18") followed by the depolymerization of one microtubule which is bundled at the crossover point, leading to a pulling of the non-depolymerizing microtubule. At a later time (232") a new crossover is formed followed by a depolymerization event which again pulls at the crossover with the non-depolymerizing microtubule (316"). (B) Two microtubules are indicated at the start (0") which are crossing over a high angle (~90°). During the depolymerization of one microtubule the bundling at the crossover point leads to the deformation of the non-depolymerizing microtubule until the crosslinking is lost. (C) Two microtubules are indicated with their plus ends polymerizing in the same direction. These microtubules encounter each other in a parallel orientation and are zippered together. (D) Two microtubules are indicated with their plus ends growing towards each other. These microtubules are zippered together in an antiparallel orientation. Scale bar is 10μm.

	0μM HIS-TAN1	0.1 μM HIS-TAN1	0.5 μM HIS-TAN1	1μM HIS-TAN1	2μM HIS-TAN1
Crossovers (n)	445	346	334	334	506
Bundling events (n)	2	0	0	3	139
Bundling frequency (%)	0.5	0	0	0.9	27.5

Table 4.2: Summary of microtubule bundling by HIS-TAN1 during dynamic assay

Spatial positioning defects of the PPB in *tan1* mutants revealed through 3D soap-film surface area minimization

Given TAN1 protein localization at the PPB as well as the characterized TAN1 microtubule crosslinking function, we set out to assess the role which TAN1 may play in positioning the PPB. We used a mathematical modeling approach to compare *in vivo* PPB location to predicted symmetric divisions in *tan1* mutant cells (Martinez et al., 2018). Briefly, MorphoGraphX was used to extract WT and *tan1* mutant cell shapes from confocal stacks (Figure 4.3A-B, materials and methods) (Barbier de Reuille et al., 2015). Surface Evolver was used to predict division planes that were compared to *in vivo* PPB location (Figure 4.4A-B) (Brakke, 1992; Martinez et al., 2018). On average PPB offset was higher in *tan1* mutants compared to WT (Figure 4.3C, WT n=16 PPB offset = 0.40μm^2 +/- 0.96, *tan1* n=45 PPB offset = 1.85μm^2 +/- 3.93, average +/- S.D.; p-value = 0.0012 Mann-Whitney) suggesting that TAN1 might be required for proper PPB placement. Alternatively, the PPB placement defects may be a result of abnormalities in cell shapes present in *tan1* mutants.

To specifically test whether TAN1 is critical for PPB placement, we compared cell shape differences to PPB offset measurements. If TAN1 plays a direct role in PPB placement, we expect high PPB offsets in *tan1* mutants across all varieties of cell shapes compared

to WT. First, we measured cell shape "abnormality index", by measuring the deviation from the surface area center and volume center (materials and methods). WT cells had lower and more consistent abnormality index compared to *tan1* mutants (Figure 4.3D, WT n=23 abnormality index = 0.15 +/- 0.09, *tan1* n=50 abnormality index = 0.38 +/- 0.32 p-value = < 0.0001 Mann-Whitney; Average +/- S.D.). These data suggest *tan1* mutants have cells with both normal and abnormal shapes, consistent with our *in vivo* observations. To address whether highly irregular cell shapes influenced PPB placement, we specifically looked for and modeled additional WT cells which displayed altered cell shapes with high abnormality index values. Both WT and *tan1* mutant cells which displayed higher abnormality scores generally had higher PPB offsets (Figure 4.3E). Examples of WT and *tan1* mutant cells are shown with several cell shapes and PPB offsets (Figure 4.3 F-J). These results suggest that the correct placement for a symmetric division in plant cells may be impaired due to cell shape defects, which are common in *tan1* mutants.

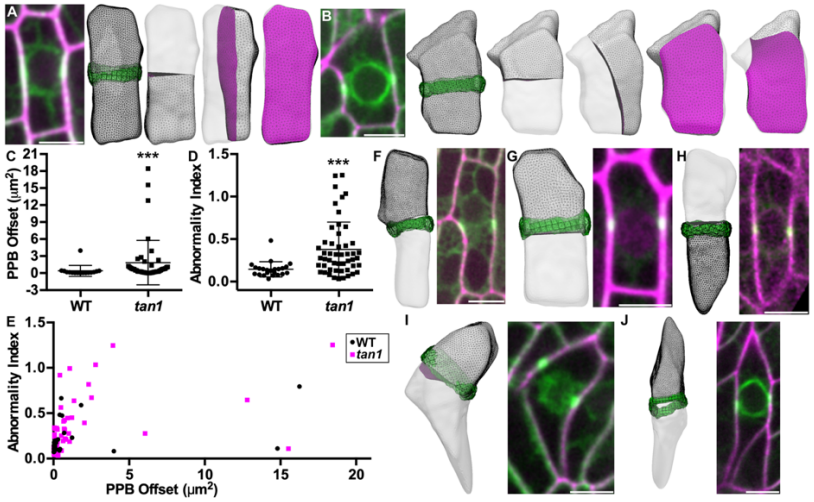

Figure 4.4: Surface area minimization of WT and *tan1* cell shapes reveals PPB offsets in abnormal cell shapes. (A) Micrograph of WT maize leaf epidermal cell expressing YFP-TUBULIN (green) stained with propidium iodide (magenta) next to the 3D cell shape reconstruction smoothed with 30th degree spherical harmonics overlaid with PPB (green) and predicted (left to right) transverse, longitudinal, periclinal division planes (magenta) overlaid. (B) Micrograph of *tan1* maize leaf epidermal cell next to cell shape reconstruction with PPB overlaid and (from left to right) transverse, longitudinal, periclinal and other division planes. (C) PPB offset in *tan1* mutants is significantly higher than WT (WT n=16 PPB offset = 0.40µm^2 +/- 0.96, *tan1* n=45 1.85µm^2 +/- 3.93, average +/- S.D.; p-value = 0.0012 (Mann-Whitney). (D) Abnormality index in *tan1* mutants is significantly higher compared to WT (WT n=23 abnormality index = 0.15 +/- 0.09, *tan1* n=50 abnormality index = 0.38 +/- 0.32 p-value = < 0.0001 Mann-Whitney; Average +/- S.D.) (E) Abnormality index vs PPB offset suggests abnormal cell shapes generally show higher offsets. (F-J) Best-fit predicted divisions overlaid with *in vivo* PPB location next to corresponding micrograph of maize epidermal cells expressing YFP-TUBULIN (green) and either expressing membrane marker PIP2-CFP (H, magenta) or stained with propidium iodide (F-G, I-J, magenta) to outline the cell shape. (F) Example WT cell with abnormality index of 0.59 and PPB offset of 1.82µm^2. (G) Example WT cell with abnormality index of 0.38 and PPB offset of 0.09µm^2. (H) Example *tan1* mutant cell with abnormality index of 0.32 and PPB offset of 0.26µm^2. (I) Example *tan1* mutant cell with abnormality index of 1.25 and PPB offset of 3.92µm^2. (J) Example *tan1* mutant cell with abnormality index of 0.99 and PPB offset of 1.08µm^2. Scale bar is 10µm.

Microtubule interactions with the cortical division site during telophase

One outstanding question is how the phragmoplast moves to the division site, especially in divisions which are tens of microns in length. Proteins such as POK1, POK2 and TAN1 localize to the division site and while their interactions with the phragmoplast and microtubules are not clearly established, they are involved with proper phragmoplast guidance (Cleary and Smith, 1998; Müller et al., 2006; Lipka et al., 2014; Martinez et al., 2017; Herrmann et al., 2018). Observations of astral-like microtubule growth outside of the phragmoplast which appeared to be reaching the cell cortex were instead hypothesized to be responsible for guiding an expanding phragmoplast (Chan et al., 2005). We characterized a dynamic microtubule array seen during telophase which is outside of the canonical phragmoplast body and contacts the division site ahead of the leading edge of the phragmoplast (Figure 4.5A-C). These cortically associated microtubules interact with the division site through end-on interactions at discrete points resulting in microtubule bending or buckling and catastrophe (Figure 4.5D). Along other points of the division site microtubules are able to crossover and if encountered by another microtubule may be bundled together (Figure 4.5E). Some areas of the division site also show high amounts of bundled microtubules ahead of the expanding phragmoplast (Figure 4.5E). These discrete points are likely division site localized microtubule binding proteins which interact with microtubules and appear to spatially restrict microtubule growth or induce microtubule bundling.

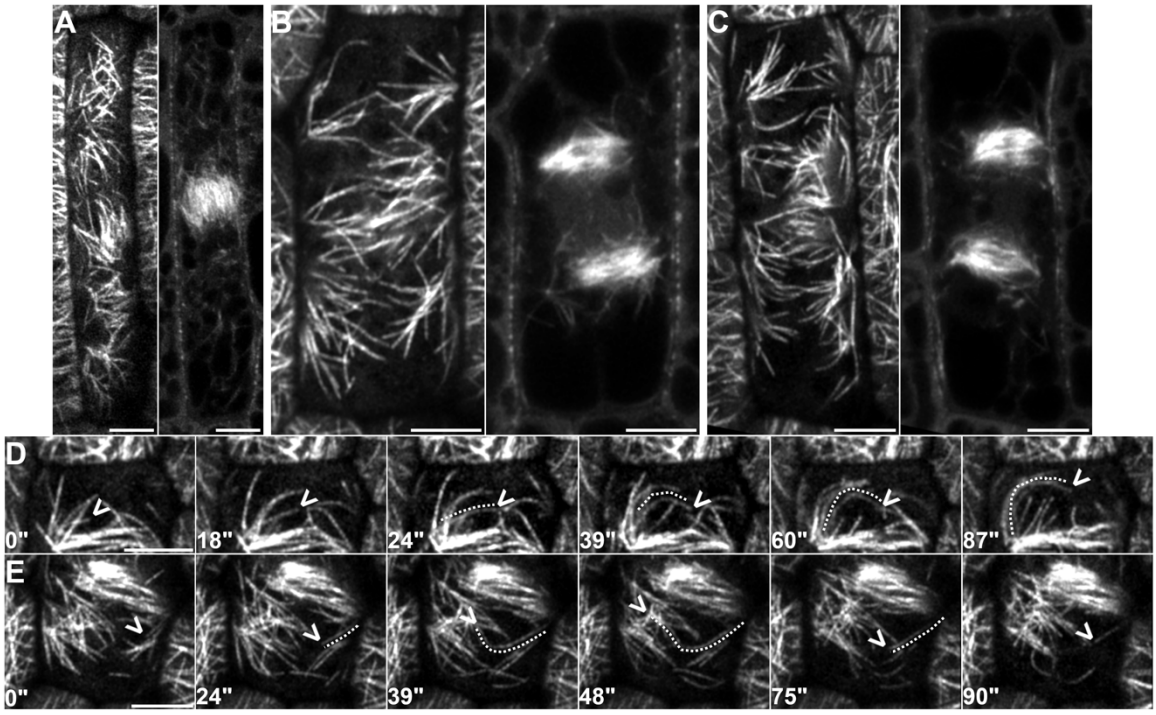

Figure 4.5: Cortically localized microtubule array in telophase contacts the division site. (A-E) Maize leaf epidermal cells expressing YFP-TUBULIN. (A) Transverse cell division showing the cortex of the cell along with an image of the corresponding phragmoplast below the cortex. (B) Longitudinal cell division showing the microtubule array at the cortex as well as the phragmoplast below the cortex. (C) Longitudinal cell division showing the microtubule array at the cortex as well as the phragmoplast below the cortex. (D) Example of microtubule from the cortical associated array which contacts the division site and has its growth spatially restricted as seen by microtubule buckling (39") resulting in no crossover event. (E) Example of microtubule which is able to cross over the division site (24"-39") followed by its depolymerization (75"). Scale bars are 10μm.

Given the intriguing contact angle independent *in vitro* microtubule interactions observed with HIS-TAN1, we hypothesized that TAN1 may be mediating one or both of the microtubule interactions seen at the cortex during telophase. Using maize epidermal cells expressing CFP-TUBULIN and TAN1-YFP we observed that microtubules which

contact areas of the cortex with high levels of TAN1 do not cross over the division site (Figure 4.5A-D). Areas of the division site which have lower amounts of TAN1 are more likely to be crossed over by microtubules followed by the bundling of microtubules in these locations (Figure 4.5E-M). These results suggest that TAN1 at the cortical division site may spatially restrict microtubule growth through high contact angle end on microtubule interactions, acting as a molecular edge at the future site of the new cell wall. An alternate hypothesis is that another division site localized protein colocalized with TAN1 may mediate this activity, however no end-on microtubule interacting proteins in plants have been shown to localize to the division site.

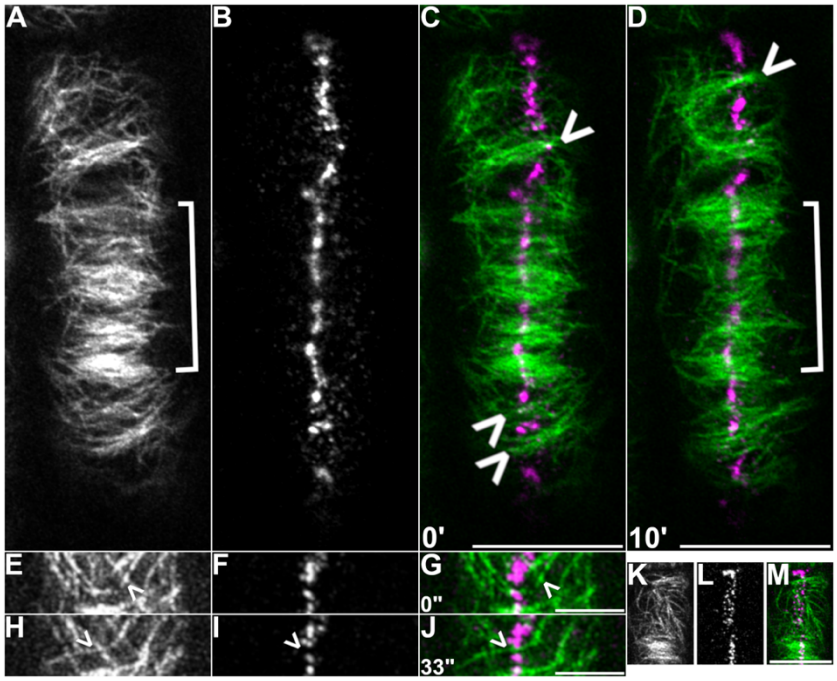

Figure 4.6: Microtubule interactions at the division site. (A) Cortex of maize epidermal cell expressing CFP-TUBULIN during telophase, brackets indicate approximate location of phragmoplast. (B) Cortex of maize epidermal cell shown in (A) expressing YFP-TUBULIN. (C) Merged image of (A) CFP-TUBULIN (green) and (B) TAN1-YFP (magenta) showing evidence of microtubule bundling (arrow heads) in locations of the division site with lower TAN1-YFP accumulation ahead of the phragmoplast. (D) Evidence of additional microtubule bundling (arrowhead) at a new region of the cortex with low TAN1-YFP accumulation at a later time (10'). Bracket shows approximate location of phragmoplast. (E) CFP-TUBULIN and (F) TAN1-YFP at the cortex of a cell in telophase with microtubule bundles ahead of phragmoplast indicated by arrowheads. (G) Merged image of (E) CFP-TUBULIN (green) and (F) TAN1-YFP (magenta). (H) CFP-TUBULIN and (F) TAN1-YFP signal with an arrowhead indicating region at the cortical division zone in between two areas of high TAN1-YFP localization. (J) Merged image of (H) CFP-TUBULIN (green) and (I) TAN1-YFP (magenta) showing a microtubule crossing over the division zone at a later time (33") in between two areas of higher TAN1-YFP localization. (K) CFP-TUBULIN (green) and (L) TAN1-YFP (magenta) merged in (M) depicting the organization of the cortical microtubule array in relationship to sparse TAN1-YFP localization at the cortical division zone. Scale bars (A-D) are 10μm and (E-M) are 5μm.

We characterized the morphology of these cortically localized telophase microtubule arrays in the *tan1* mutant to gain insight into the potential role which TAN1 plays in their organization. While this array broadly displays a symmetric organization across the division site axis in WT (n = 9/9 cells display a complete cortical telophase array) (Figure 4.5A-C), *tan1* arrays are almost completely absent or much more disorganized with only few cells having intact arrays (n = 2/11 cells display a complete cortical telophase array) (Figure 5.7A-C). These results may suggest that TAN1 mediated microtubule end on interactions at the cortical division site are important for the organization of these microtubules.

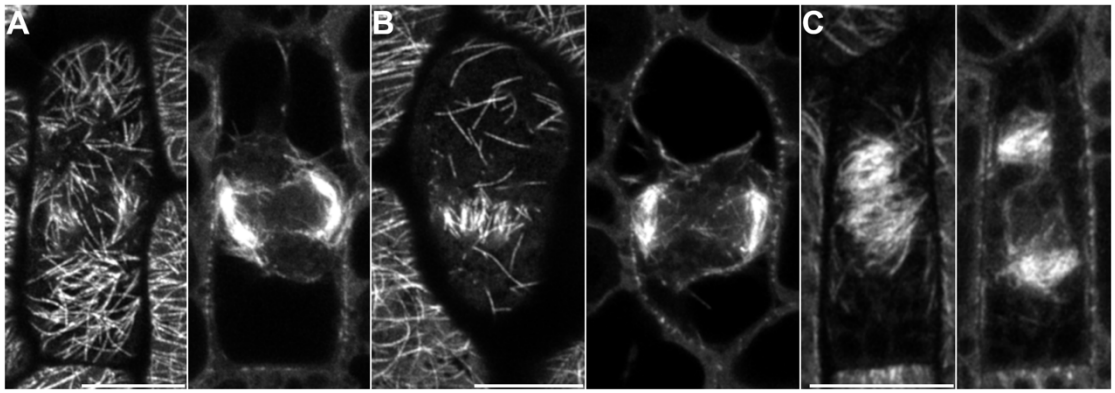

Figure 4.7: Cortically localized array during telophase in the *tan1* mutant. Maize *tan1* mutant epidermal cells expressing YFP-TUBULIN. (A) Transverse cell division showing the cortex of the cell with an intact array along with an image of the corresponding phragmoplast below the cortex. (B) Transverse cell division showing the cortex of a cell with a sparse array along with an image of the corresponding phragmoplast below the cortex. (C) Longitudinal cell division with a sparse array along with an image of the corresponding phragmoplast below the cortex.

Discussion

While TAN1 protein has long been characterized as a microtubule binding protein, its function has remained elusive. *In vitro* analysis of TAN1 has revealed its ability to bind to and bundle microtubules as well as bind to tubulin dimers. *Schizosaccharomyces pombe* CLASP protein (Cls1p) is able to bind to microtubules and tubulin dimers simultaneously in order to rescue microtubules which are undergoing catastrophe (Al-Bassam et al., 2010). Microtubule rescue was not observed in our *in vitro* dynamic assays with HIS-TAN1 so the significance of tubulin dimer binding is currently unknown. HIS-TAN1 used in dynamic microtubule assays did not significantly alter microtubule dynamics or induce bundling until high concentrations (2μM HIS-TAN1) were used. There is a possibility that tubulin dimer binding in the dynamic assay may make the interpretation of concentration dependent interactions between HIS-TAN1 and microtubule dynamics ambiguous. Microtubule interactions mediated by HIS-TAN1 also appear to be microtubule contact angle independent, resulting in end on microtubule crosslinking or zippering across a long stretch of microtubules. Microtubule zippering is a well characterized form of microtubule bundling both *in vitro* and *in vivo* (Dixit, 2004; Tulin et al., 2012) however end on interactions have been observed in occur between motor proteins such as kinesin or dynein and microtubules (Laan et al., 2012b; Laan et al., 2012a). The end on microtubule capture by dynein is important for the spatial positioning of the spindle in animals (Kiyomitsu, 2019). TAN1 is not a motor protein as it lacks any canonical motor domains, however its association with POK1 which localizes to the division site may allow it to be a cargo for the kinesin to regulate its function spatially *in vivo* (Lipka et al., 2014). While POK1 has not been yet characterized *in vitro*,

its sequence similarity to POK2 which is a plus end directed motor that displays processive and diffusive movement may suggest a similar function (Chugh et al., 2018). Careful analysis of TAN1 protein function and *tan1* mutant phenotype have revealed some of the mechanisms which may lead to the division plane orientation defects in the maize *tan1* mutant. Previous results measuring the angle of PPBs in symmetrically dividing cells suggest there is an apparent greater variability in PPB angles in *tan1* mutants compared to WT samples, indicative of a PPB placement defect (Cleary and Smith, 1998; Mir et al., 2018). We determined a modest but significant defect in the average placement of PPBs in *tan1* cells. The defects in PPB placement appear to be a consequence of the high proportion of aberrant cell shapes in the *tan1* mutant because wild-type cells with abnormal shapes also had defects in PPB placement. Additionally, we observed that *tan1* mutants avoid the formation of four-way junctions during pre-prophase just like WT; these avoidances result in higher than expected offsets due to the *in vivo* shift in PPB location (Supplemental Figure 4.3A-C) (Martinez et al., 2018). The majority of division plane defects are caused by the phragmoplast not returning to the site marked by the PPB in the *tan1* mutant (Cleary and Smith, 1998; Martinez et al., 2017). Mitotic delays in the *tan1* mutant may be a consequence of altered microtubule dynamics or microtubule interactions (Martinez et al., 2017). Proper microtubule bundling at metaphase spindle midzone is an important feature for proper spindle assembly (Masoud et al., 2013; Mullen and Wignall, 2017). Many of the spindle microtubules encounter each other at low contact angles, where TAN1 mediated anti-parallel microtubule "zipper-like" bundling may aid in their organization. Low angle microtubule bundling therefore may be important for proper mitotic progression through metaphase.

Cortical localization of TAN1 protein appears to be important for its function in phragmoplast guidance (Martinez et al., 2017; Mir et al., 2018). Models for phragmoplast guidance have previously proposed that leading edge phragmoplast microtubules are caught by proteins at the cortical division site either through specific protein-protein interactions or microtubule-protein interactions (Lipka et al., 2014; Herrmann et al., 2018). Mutant analysis has suggested that altered phragmoplast expansion rates, which may reflect changes in phragmoplast microtubule dynamics are not necessarily responsible for phragmoplast guidance defects (Martinez et al., 2017; Herrmann et al., 2018). While it is well characterized that the leading edge of the phragmoplast is a site of new microtubule nucleation and addition, we observed an additional cortically localized microtubule array which appears during the formation of the phragmoplast and interacts with the division site (Figure 4.5A-C). γ-Tubulin has been observed outside of the phragmoplast body and may serve to nucleate new microtubules outside of the leading edge of the phragmoplast (Murata et al., 2013). Microtubule growth outside of the phragmoplast towards the cell cortex during telophase has also been previously described (Chan et al., 2005). While this microtubule array in telophase was identified in maize anticlinal divisions, it is particularly noticeable in longitudinal divisions which require the phragmoplast to travel a large distance after asymmetrically contacting the periclinal outer and inner cell walls (Figure 4.5B-C). Microtubules which encounter areas of high TAN1 localization do not crossover the division site while areas of lower TAN1 localization allow microtubules to crossover and subsequently be bundled. These potential end on interactions preventing microtubule crossover at the division site result in different behaviors compared to TAN1 microtubule interactions *in vitro*. The end on

interactions *in vitro* mostly lead to the pulling of dynamic microtubules. At the division site TAN1 is presumably retained or possibly anchored through interactions with proteins such as POK1 (Lipka et al., 2014). This association therefore is significantly different from the *in vitro* setup in which microtubules instead are attached to the glass coverslip surface. An *in vitro* setup using TAN1 bound to a surface with directional microtubule growth may be a more suitable system to represent the *in vivo* microtubule interactions and localization of TAN1 at the division site.

The distinct microtubule behaviors observed at the division site also suggest there is complexity of specific protein localization along the division site. Colocalization studies and interactions of division site localized proteins need to be assessed to understand the players which are responsible for the distinct microtubule behaviors. The microtubules at the cortex which are bundled ahead of the phragmoplast leading edge are reminiscent to mini-phragmoplasts which may aid in phragmoplast expansion as preassembled phragmoplast modules are added to the phragmoplast periphery (Otegui and Staehelin, 2000; Lee and Liu, 2013). We hypothesize TAN1 may mediate the spatial restriction of microtubule growth by end on interactions as microtubules approach the division site, acting as a molecular edge to help properly orient microtubules at the division site.

Materials and Methods

HIS-TAN1 and HIS-TAN1-GFP Expression

A codon optimized cDNA encoding the maize HIS-TAN1 and HIS-TAN1-GFP was synthesized followed by the protein expression and purification by Genescript (Genscript Corp Piscataway, New Jersey USA). *E. coli* strain SHuffle was transformed with recombinant plasmid encoding HIS-TAN1. After cell pellets were sonicated and centrifuged, the precipitate was dissolved using urea followed by affinity purification. *E. coli* strain BL21 Star (DE3) was transformed with recombinant plasmid encoding HIS-TAN1-GFP. After cell pellets were sonicated and centrifuged, the precipitate was dissolved using urea followed by affinity purification. Proteins were refolded and sterilized prior to use. HIS-TAN1 and HIS-TAN1-GFP concentrations were checked with a BCA protein assay. Consequently, HIS-TAN1-GFP did not appear to retain its fluorescent capabilities likely due to protein structure denaturation during refolding therefore the protein was tagged with an Atto488 dye for experiments.

Labeling of HIS-TAN1-GFP with Atto488

HIS-TAN1-GFP was conjugated with Atto488-maleimide (Sigma 28562). HIS-TAN1-GFP in BRB80 buffer was reduced with 12.5μM TCEP-HCl (Tris(2-carboxyethyl)phosphine hydrochloride) for 10 minutes followed by a 4 hour incubation with 250μM Atto488 dissolved in DMSO at room temperature. Unreacted excess dye was removed by running sample through a 10DG desalting column (BioRad 732-2010) and concentrated with a 30K MWCO PES concentrator (Thermo 88521). Successful HIS-TAN1-GFP-Atto488 conjugation was confirmed by microtubule co-sedimentation assay

showing fluorescent bands corresponding to a tagged HIS-TAN1-GFP (Supplemental Figure 4.1).

Microtubule co-sedimentation

A microtubule binding assay kit from Cytoskeleton was used to assess HIS-TAN1 microtubule binding along with negative (BSA) and positive (MAPF) controls (Cytoskeleton MK029). For determining affinity of HIS-TAN1 to microtubules, microtubules were polymerized in the presence of 1mM GTP for 2 hours at 37°C followed by the addition of 10μM taxol. HIS-TAN1 and microtubules were incubated for 25 minutes and spun down at 39,000 x *g* at 25°C. HIS-TAN1-GFP and HIS-TAN1-GFP-ATTO488 protein was incubated with microtubules at room temperature for 25 minutes and spun down at 21,000 x *g* at 25°C. Samples were equally loaded onto an SDS page gel, stained with Coomassie and analyzed using ImageJ Gel Analysis tool.

Reconstitution of *in vitro* microtubule dynamics

In vitro microtubule dynamics were conducted according to previous protocols (Dixit and Ross, 2010). Flow chambers were assembled using silanized coverslips and double-sided sticky tape with a chamber volume of ~20μL. A 20% monoclonal anti-tubulin antibody (clone BN-34, Sigma, St. Louis, MO) is used to coat the surface followed by a blocking with 5% pluronic F-127. Rhodamine and biotinylated guanosine 5'=(α,β-methylene)triphosphate (GMPCPP) microtubule seeds are then flowed into the cell. Microtubule growth was initiated using 17.5μM 1:25 rhodamine-labeled bovine tubulin in BRB80 buffer, along with 0.15% methylcellulose, 100mM DTT, an oxygen scavenging system (250μg/mL glucose oxidase, 25μg/mL catalase), 4.5mg/mL glucose, 2mM GTP along with the specified amount of HIS-TAN1 protein. To assess microtubule

bundling 22.5μM 1:25 rhodamine-labeled bovine tubulin was used in the reaction to encourage microtubule growth and crossovers. The samples were excited with a 561-nm (at 4 mW output) diode-pumped solid-state laser (Melles Griot, Albuquerque, NM) to visualize and rhodamine-labeled microtubules using TIRF. Kymographs were used to analyze data.

***In vitro* tubulin dimer pulldown**

10uL of agarose beads bound to anti-GFP (MBL D153-8) were incubated with 1μM HIS-TAN1-GFP or 1μM HIS-GFP (ABM 00033P) and 5μM of TUBULIN (Cytoskeleton T240) in BRB80 buffer with 50mM NaCl, 0.2 mM PMSF, 10mM DTT, 0.05% Tween-20. Samples were incubated for three hours at 4°C and subsequently washed three times using BRB80 supplemented with 50mM NaCl and 0.05% Tween-20. Beads were then transferred to a new tube and washed four more times with BRB-80 supplemented with 50mM NaCl and 0.05% Tween-20. Coomassie stained SDS-PAGE was used for protein visualization.

Predicting Division Planes from Wild-Type and *tan1* Cell Shapes using Surface Evolver

Samples from wild-type and *tan1* mutant maize plants expressing YFP-TUBULIN (α-tubulin fused to the Citrine variant of Yellow Fluorescent Protein) were dissected to the dividing zone on the leaf to identify PPB location (Mohanty et al., 2009). To identify the cell outlines for three dimensional reconstruction, samples were either stained with 0.1mM propidium iodide or PIP2-1-CFP (PLASMA MEMBRANE INTRINSIC PROTEIN2-1 fused to CFP) was used to outline the plasma membranes (Mohanty et al., 2009). Three dimensional cell shape reconstructions were generated using

MorphoGraphX while three dimensional PPB reconstructions were generated using Trainable Weka Segmentation (Barbier de Reuille et al., 2015; Arganda-Carreras et al., 2017). A previous protocol was followed for modeling symmetric divisions by soap-film minimization using Surface Evolver (Brakke, 1992; Martinez et al., 2018). Briefly, cell outlines were smoothed using 30th degree spherical harmonics followed by surface area minimization from 241 starting planes with normals uniformly distributed over a sphere. For PPB offset measurements the midplane of the PPB surface was aligned and compared to the predicted surface. Abnormality index was also determined at this time defined by the ratio of the area surface center and the volume center for the cell. The Surface Evolver pipeline used is hosted on Github (https://github.com/jdhayes/predictive_division/).

Microscopy for *in vitro* and *in vivo* imaging

Rhodamine labeled microtubules and HIS-TAN1-GFP-Atto488 were visualized on custom built inverted Nikon Ti stand with a Yokogawa spinning disk and a motorized stage (ASI Piezo) run with Micromanager software (micromanager.org) and built by Solamere Technology. Solid-state lasers (Obis) and emission filters (Chroma Technology) used excitation 561; emission, 620/60 (for rhodamine-tubulin); and excitation, 488; emission, 525/50 (for HIS-TAN1-GFP-Atto488). Perfluorocarbon immersion liquid (RIAAA-678; Cargille) was used for 60× water-immersion objectives with 1.2 numerical aperture. Maize epidermal cells used for modeling were visualized with the same microscope and objective using an excitation of 561; emission, 620/60 (for propidium iodide) and excitation of 514; emission, 540/30 (for YFP-TUBULIN).

Dynamic rhodamine-labeled microtubules were excited with a 561-nm (at 4 mW output) diode-pumped solid-state laser (Melles Griot, Albuquerque, NM) using a 100X (NA 1.45) objective and TIRF microscopy. Images were acquired with a back-illuminated electron-multiplying CCD camera (Hamamatsu, Bridgewater, NJ, ImageEM) and rhodamine filter sets (582–636 nm emission).

Figure 4.5, 4.6, and 4.7 were imaging using a Zeiss LSM 880 Elyra, Axio Observer and a 100x/1.46 Oil lens (Cargille immersion oil, 16212). TAN1-YFP was excited with 514 while CFP-TUBULIN was excited using 458 and imaged using super resolution airsycan mode with a MBS 458/514 and 420-480 BP + LP 605 filter set. Images were acquired using line by line simultaneous scanning. Airyscan images were processed using default settings using Zen Black software.

Supplemental Figures

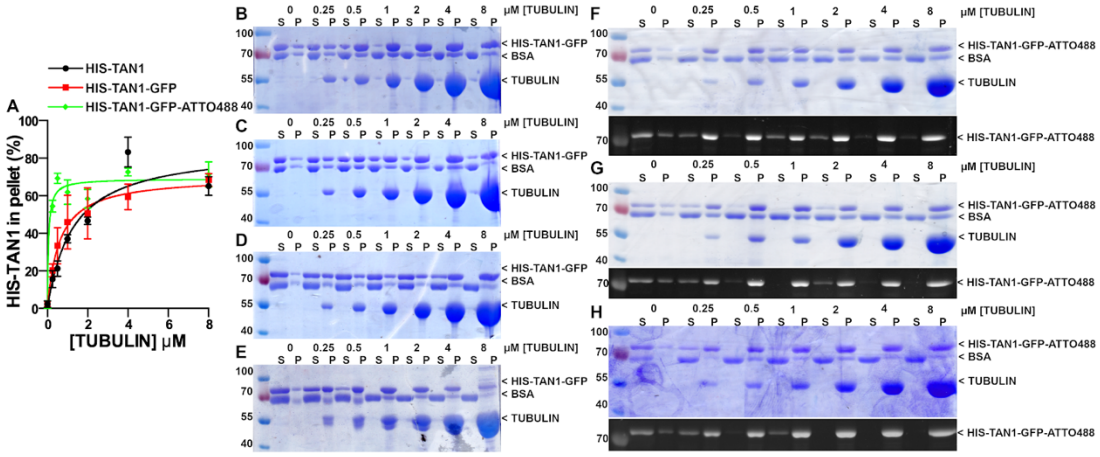

Supplemental Figure 4.1: HIS-TAN1-GFP and HIS-TAN1-GFP-Atto488 binding affinity to taxol stabilized microtubules. (A) Michaelis-Menten fit on binding data for HIS-TAN1 (from Figure 1C), HIS-TAN1-GFP, and HIS-TAN1-GFP-Atto488. Affinity for HIS-TAN1-GFP is 0.59µM +/- 0.25 [TUBULIN] while HIS-TAN1-GFP-Atto488 is 0.06µM +/- 0.03 [TUBULIN] at a concentration of 2µM TAN1 corrected for the average pelleting in samples without microtubules added (average +/- S.D.) (B-C) Coomasie stained SDS PAGE experiment of HIS-TAN1-GFP runs at varying concentrations of tubulin (0-8µM). (D-E) Coomasie stained SDS PAGE experiment of HIS-TAN1-GFP-Atto488 at varying concentrations of tubulin (0-8µM). Below Coomassie stained SDS-PAGE experiment, HIS-TAN1-GFP-Atto488 was excited using ultraviolet light source to show labeling of HIS-TAN1-GFP with the Atto488 dye used in the spin-down assays.

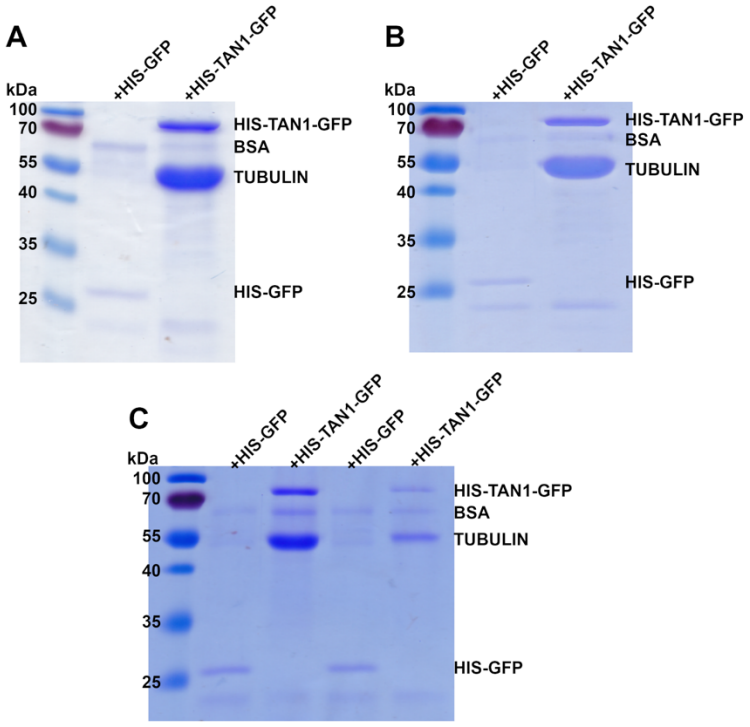

Supplementary Figure 4.2: HIS-TAN1-GFP binds to soluble tubulin. (A-C) Agarose beads fused with an anti-GFP antibody were used to pull down HIS-TAN1-GFP or HIS-GFP in the presence of tubulin dimers. A tubulin band is detected in the presence of 1μM HIS-TAN1-GFP and not detected in a pulldown with 1μM HIS-GFP. Coomasie stained SDS PAGE results from *in vitro* pull down are shown.

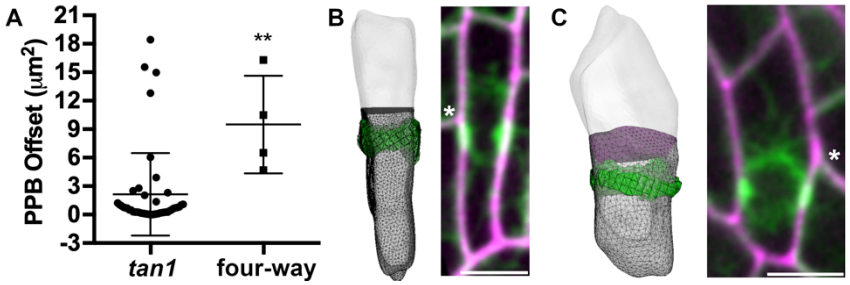

Supplementary Figure 4.3: *tan1* mutants avoid creation of four-way junctions during pre-prophase. (A) PPB offsets are higher in cases where *tan1* mutants avoid the formation of a four-way junction (No four way, n=46, PPB offset = 2.13 +/- 4.3, four-way n = 4, PPB offset = 9.5 +/- 5.1, mean +/- S.D., Mann-Whitney p-value = 0.0021). (B-C) Best-fit predicted divisions overlaid with *in vivo* PPB location next to corresponding micrograph of maize epidermal cells expressing YFP-TUBULIN (green) stained with propidium iodide (magenta) to outline the cell wall. (B) Example *tan1* mutant cell avoiding a neighboring cell wall with abnormality index of 1.12 and PPB offset of 4.7μm^2. (C) Example *tan1* mutant cell avoiding a neighboring cell wall with abnormality index of 0.35 and PPB offset of 16.3μm^2.

References

Al-Bassam J, Kim H, Brouhard G, van Oijen A, Harrison SC, Chang F (2010) CLASP Promotes Microtubule Rescue by Recruiting Tubulin Dimers to the Microtubule. Dev Cell **19**: 245–258

Ambrose JC, Cyr R (2008) Mitotic spindle organization by the preprophase band. Mol Plant **1**: 950–60

Arganda-Carreras I, Kaynig V, Rueden C, Eliceiri KW, Schindelin J, Cardona A, Sebastian Seung H (2017) Trainable Weka Segmentation: a machine learning tool for microscopy pixel classification. Bioinformatics **33**: 2424–2426

Barbier de Reuille P, Routier-Kierzkowska A-L, Kierzkowski D, Bassel GW, Schüpbach T, Tauriello G, Bajpai N, Strauss S, Weber A, Kiss A, et al (2015) MorphoGraphX: A platform for quantifying morphogenesis in 4D. eLife. doi: 10.7554/eLife.05864

Brakke K (1992) The Surface Evolver. Exp Math **1**: 141–165

Buschmann H, Dols J, Kopischke S, Pena EJ, Andrade-Navarro MA, Heinlein M, Szymanski DB, Zachgo S, Doonan JH, Lloyd CW (2015) Arabidopsis KCBP interacts with AIR9 but stays in the cortical division zone throughout mitosis via its MyTH4-FERM domain. J Cell Sci **128**: 2033–2046

Chan J, Calder G, Fox S, Lloyd C (2005) Localization of the microtubule end binding protein EB1 reveals alternative pathways of spindle development in Arabidopsis suspension cells. Plant Cell **17**: 1737–48

Chugh M, Reißner M, Bugiel M, Lipka E, Herrmann A, Roy B, Müller S, Schäffer E (2018) Phragmoplast Orienting Kinesin 2 Is a Weak Motor Switching between Processive and Diffusive Modes. Biophys J **115**: 375–385

Cleary AL, Smith LG (1998) The Tangled1 gene is required for spatial control of cytoskeletal arrays associated with cell division during maize leaf development. Plant Cell **10**: 1875–88

Dixit R (2004) Encounters between Dynamic Cortical Microtubules Promote Ordering of the Cortical Array through Angle-Dependent Modifications of Microtubule Behavior. PLANT CELL ONLINE **16**: 3274–3284

Dixit R, Ross JL (2010) Studying plus-end tracking at single molecule resolution using TIRF microscopy. Methods Cell Biol **95**: 543–554

Facette MR, Rasmussen CG, Van Norman JM (2019) A plane choice: coordinating timing and orientation of cell division during plant development. Curr Opin Plant Biol **47**: 47–55

Fache V, Gaillard J, Van Damme D, Geelen D, Neumann E, Stoppin-Mellet V, Vantard M (2010) Arabidopsis kinetochore fiber-associated MAP65-4 cross-links microtubules and promotes microtubule bundle elongation. Plant Cell **22**: 3804–3815

Fan Y, Burkart GM, Dixit R (2018) The Arabidopsis SPIRAL2 Protein Targets and Stabilizes Microtubule Minus Ends. Curr Biol **28**: 987-994.e3

Herrmann A, Livanos P, Lipka E, Gadeyne A, Hauser M, Van Damme D, Müller S (2018) Dual localized kinesin-12 POK2 plays multiple roles during cell division and interacts with MAP65-3. EMBO Rep e46085

Ho C-MK, Hotta T, Guo F, Roberson RW, Lee Y-RJ, Liu B (2011) Interaction of Antiparallel Microtubules in the Phragmoplast Is Mediated by the Microtubule-Associated Protein MAP65-3 inArabidopsis. Plant Cell **23**: 2909–2923

Kiyomitsu T (2019) The cortical force-generating machinery: how cortical spindle-pulling forces are generated. Curr Opin Cell Biol **60**: 1–8

Laan L, Pavin N, Husson J, Romet-Lemonne G, van Duijn M, López MP, Vale RD, Jülicher F, Reck-Peterson SL, Dogterom M (2012a) Cortical Dynein Controls Microtubule Dynamics to Generate Pulling Forces that Position Microtubule Asters. Cell **148**: 502–514

Laan L, Roth S, Dogterom M (2012b) End-on microtubule-dynein interactions and pulling-based positioning of microtubule organizing centers. Cell Cycle Georget Tex **11**: 3750–3757

Lee Y-RJ, Liu B (2013) The rise and fall of the phragmoplast microtubule array. Curr Opin Plant Biol **16**: 757–763

Li H, Sun B, Sasabe M, Deng X, Machida Y, Lin H, Julie Lee Y-R, Liu B (2017) Arabidopsis MAP65-4 plays a role in phragmoplast microtubule organization and marks the cortical cell division site. New Phytol **215**: 187–201

Lipka E, Gadeyne A, Stöckle D, Zimmermann S, De Jaeger G, Ehrhardt DW, Kirik V, Van Damme D, Müller S (2014) The Phragmoplast-Orienting Kinesin-12 Class Proteins Translate the Positional Information of the Preprophase Band to Establish the Cortical Division Zone in Arabidopsis thaliana. Plant Cell **26**: 2617–2632

Martinez P, Allsman LA, Brakke KA, Hoyt C, Hayes J, Liang H, Neher W, Rui Y, Roberts AM, Moradifam A, et al (2018) Predicting Division Planes of Three-Dimensional Cells by Soap-Film Minimization. Plant Cell **30**: 2255–2266

Martinez P, Luo A, Sylvester A, Rasmussen CG (2017) Proper division plane orientation and mitotic progression together allow normal growth of maize. Proc Natl Acad Sci **114**: 2759–2764

Masoud K, Herzog E, Chabouté M-E, Schmit A-C (2013) Microtubule nucleation and establishment of the mitotic spindle in vascular plant cells. Plant J **75**: 245–257

Mir R, Morris VH, Buschmann H, Rasmussen CG (2018) Division Plane Orientation Defects Revealed by a Synthetic Double Mutant Phenotype. Plant Physiol **176**: 418–431

Mohanty A, Luo A, DeBlasio S, Ling X, Yang Y, Tuthill DE, Williams KE, Hill D, Zadrozny T, Chan A, et al (2009) Advancing cell biology and functional genomics in maize using fluorescent protein-tagged lines. Plant Physiol **149**: 601–605

Mullen TJ, Wignall SM (2017) Interplay between microtubule bundling and sorting factors ensures acentriolar spindle stability during C. elegans oocyte meiosis. PLOS Genet **13**: e1006986

Müller S, Han S, Smith LG (2006) Two Kinesins Are Involved in the Spatial Control of Cytokinesis in Arabidopsis thaliana. Curr Biol **16**: 888–894

Murata T, Sano T, Sasabe M, Nonaka S, Higashiyama T, Hasezawa S, Machida Y, Hasebe M (2013) Mechanism of microtubule array expansion in the cytokinetic phragmoplast. Nat Commun. doi: 10.1038/ncomms2967

Otegui M, Staehelin LA (2000) Syncytial-type cell plates: a novel kind of cell plate involved in endosperm cellularization of Arabidopsis. Plant Cell **12**: 933–947

Palevitz BA (1987) Actin in the preprophase band of Allium cepa. J Cell Biol **104**: 1515–1519

Panteris E, Adamakis I-DS, Daras G, Hatzopoulos P, Rigas S (2013) Differential Responsiveness of Cortical Microtubule Orientation to Suppression of Cell Expansion among the Developmental Zones of Arabidopsis thaliana Root Apex. PLoS ONE **8**: e82442

Panteris E, Diannelidis B-E, Adamakis I-DS (2018) Cortical microtubule orientation in Arabidopsis thaliana root meristematic zone depends on cell division and requires severing by katanin. J Biol Res-Thessalon. doi: 10.1186/s40709-018-0082-6

Pickett-Heaps JD, Northcote DH (1966) Organization of microtubules and endoplasmic reticulum during mitosis and cytokinesis in wheat meristems. J Cell Sci **1**: 109–120

Portran D, Zoccoler M, Gaillard J, Stoppin-Mellet V, Neumann E, Arnal I, Martiel JL, Vantard M (2013) MAP65/Ase1 promote microtubule flexibility. Mol Biol Cell **24**: 1964–1973

Rasmussen CG, Bellinger M (2018) An overview of plant division-plane orientation. New Phytol

Smertenko A (2018) Phragmoplast expansion: the four-stroke engine that powers plant cytokinesis. Curr Opin Plant Biol **46**: 130–137

Smertenko A, Hewitt SL, Jacques CN, Kacprzyk R, Liu Y, Marcec MJ, Moyo L, Ogden A, Oung HM, Schmidt S, et al (2018) Phragmoplast microtubule dynamics – a game of zones. J Cell Sci **131**: jcs203331

Smith LG, Gerttula SM, Han S, Levy J (2001) Tangled1: a microtubule binding protein required for the spatial control of cytokinesis in maize. J Cell Biol **152**: 231–6

Smith LG, Hake S, Sylvester AW (1996) The tangled-1 mutation alters cell division orientations throughout maize leaf development without altering leaf shape. Development **122**: 481–9

Tulin A, McClerklin S, Huang Y, Dixit R (2012) Single-molecule analysis of the microtubule cross-linking protein MAP65-1 reveals a molecular mechanism for contact-angle-dependent microtubule bundling. Biophys J **102**: 802–809

Walker KL, Müller S, Moss D, Ehrhardt DW, Smith LG (2007) Arabidopsis Tangled Identifies the Division Plane Throughout Mitosis and Cytokinesis. Curr Biol CB **17**: 1827–1836

Xu XM, Zhao Q, Rodrigo-Peiris T, Brkljacic J, He CS, Muller S, Meier I (2008) RanGAP1 is a continuous marker of the Arabidopsis cell division plane. Proc Natl Acad Sci **105**: 18637–18642

CHAPTER 5: Discussion and Future Directions

The work presented in this thesis has taken multiple approaches including computational modeling, genetics, *in vivo* imaging, and various *in vitro* techniques to understand how a cell is able to determine a division plane and properly execute the specified division. While most of this work has focused at understanding this process at the cell level, future work will need to focus on broader interactions between cells, changes to tissue morphology resulting from misoriented divisions, as well as to understand more aspects of TAN1 localization and function during mitosis.

Influence of cell shape on division plane orientation

Our modeling approach described was able to accurately determine the position of symmetric divisions given a cell shape by using a soap-film minimization algorithm. Division planes across multiple species and tissue types were accurately determined as well. This analysis revealed some general trends such as specific cell shape archetypes having probabilistic tendencies for certain division types. Taken as a snapshot of a developmental stage, these predictions did not accurately predict the observed ratio of divisions seen. Additionally, while we observed a general trend of cell shapes which may facilitate ligule development in maize, the predicted divisions did not accurately reflect *in vivo* division orientation rates. This suggested that other mechanisms or cues are in place which mediate the non-stochastic behavior of division plane selection.

Our current modeling approach needs to be broadened in order to incorporate information from outside of an individual cell shape. An example can be the integration of four-way junction avoidance into the model. Here specific edges of the cell which are occupied by a tricellular junction can be designated in Surface Evolver to prevent minimization of the surface at this site. This would more accurately reflect the *in vivo* conditions where the cytoskeleton does not allow a PPB to be constructed at three-way junction points. There are limitations given the specificity of the model as designed; one solution can be to analyze the same datasets with several of the models which have been published in order to create a more complete picture of mechanical stress, arrangement of the cytoskeleton, as well as predict division locations based on cell shapes.

Altered tissue morphology in *tan1* mutants

While *tan1* mutants in maize display a large-scale cell patterning defect which is well understood, overall tissue morphology is greatly altered. To specify, while *tan1* leaf shape is proportionally normal, mutants display crepe paper like leaves, resulting in a "wavy" tissue structure compared to a smooth leaf surface in wild-type. This suggests that division plane defects may change the overall mechanics of cell walls across the tissue. Previous results have shown that stress across the tissue can cause rearrangements in the cytoskeleton (Sampathkumar et al., 2014). I hypothesize that these tissue undulations are likely introducing areas of high stress which may impede proper development. The microtubule arrays of *tan1* mutants do not follow predictable organization and were described as usually following local cell morphology instead of aligning mostly perpendicular to the main growth axis (Cleary and Smith, 1998). Much

of the careful analysis done to understand *tan1* mutant growth defects has been performed at the at the cellular level with not much consideration to the tissue context in which these cells reside. Cell wall composition may also be altered as a secondary effect to the non-ideal placement of cell walls, leading to the buckling of the tissue as cells expand. Cell wall composition and mechanics in the *tan1* mutant should be assessed to understand how the plant copes with altered tissue morphology. The impact of misplaced cell positioning defects in the *tan1* mutant can be addressed using treatment with cell wall loosening enzymes, use of cell wall mutants, or physical measurements of cell walls using atomic force microscopy (AFM). These results may reveal how altered division planes may result in non-smooth leaf structure either as a direct or non-direct cause.

TAN1 localization at the cortical division site

How TAN1 and other division site localized proteins are brought to and retained at the division site is an outstanding question. While the PPB seems like a fitting player to recruit TAN1 to the division site through its microtubule binding function, analysis in *Arabidopsis* suggest that TAN1 is able to localize to the division site through multiple mechanisms depending on the stage of the cell cycle (Rasmussen et al., 2011; Mir et al., 2018). This suggest there is microtubule independent TAN1 recruitment to the division site. Additionally, when microtubules of the PPB are disrupted with drug treatments, TAN1 stays localized to the cortical division site (Kosetsu et al., 2017). These results suggest that TAN1 is stably localized to the cortical division site and retained there either through protein-protein interactions or TAN1-membrane interactions. TAN1 is a highly basic protein (isoelectric point ~12) therefore it may have the ability to bind to negatively

charged phospholipids at the membrane. Analysis of membrane structures using electron microscopy during division show topological differences at the cortical division site (Porter, 1960). *In vitro* analysis can be used to determine phospholipid binding as shown for other membrane associated proteins in plants (Lee et al., 2018). If any phospholipid is identified, then its localization during mitosis would need to be assessed. I hypothesize an accumulation of this phospholipid at the division site during mitosis.

In *Arabidopsis*, TAN1 localization to the division site is lost after PPB disassembly in the *Arabidopsis phragmoplast orienting kinesin1/2* (*pok1/pok2)* double mutants (Lipka et al., 2014). POK1 is a TAN1 interacting protein and both colocalize at the division site during pre-prophase and are both retained until cytokinesis (Lipka et al., 2014). In mutants which lack the ability to form PPBs, POK1 is preferentially absent from the division site during pre-prophase, however is accumulated at the cortical division site in later stages of mitosis (Schaefer et al., 2017). POK1 ability to directly bind to microtubules has not been assessed. Understanding how TAN1 and TAN1 interacting proteins are retained at the division site could both reveal important factors which are acting during early division site specification and maintenance.

Phosphorylation status of TAN1 protein

TAN1 is also a phosphoprotein as detected by *in vivo* analysis of the maize phosphoproteome at Serine-63 (Figure 5.1) (Walley et al., 2016). Current *in vitro* analysis of TAN1 function were performed using recombinantly expressed protein from bacterial systems, therefore is most likely not phosphorylated. Microtubule binding proteins show altered activity depending on their phosphorylation status which are necessary for

regulating their function *in vivo*, usually phosphorylation leading to increased dissociation from microtubules (Illenberger et al., 1996; Boruc et al., 2017; Vavrdová et al., 2019).

MVARSPNAKPDRQKAAALAAAAALNPALLRETLKKVDRCMARLQELQYTVAGGAKVVSGVSLsPRSTRGYLRTSLRCKQE
TVRMRGGASAQKRSPSGKFGGGVGGEGAQWRRMSLPAMLLGETVLEIVQASQFARDIVTAAGATNREPPRTPKPAPRTRK
PAAGEPTPLRARRAREKQSHRGGAATRGADAATPPSRSRVRSRIQFKPVSPVAVGRPSVSANRVSPKNRPWAKKAVMFPN
PTFHASTSAATDPCATPSPSKKQKRLYKTRSPVAARQTPHKFLVKSPPSALGSKLRMHGKALPARPAAVSPPPPVKAQAS
PAKTRRCSFSPSRLATRLMSPIKARLSLGRSRDSGVGVGGGPMSGLKQRPGVSLTVRTVSSKISSR

Figure 5.1: Phosphoproteomic analysis reveals TAN1 phosphorylation status *in vivo*. ZmTAN1 protein sequence with phosphopeptide highlighted in yellow and phosphorylated residue in red. Non-modified peptide highlighted in grey. Phosphoproteome data from (Walley et al., 2016).

In vitro phosphorylation assays can be performed on TAN1 followed by microtubule co-sedimentation to measure the effect of phosphorylation on microtubule binding. One caveat however is that the kinase which regulates TAN1 phosphorylation is not currently known. An alternative approach is to create phosphor-dead or phosphor-mimic TAN1 proteins at the identified site followed by microtubule co-sedimentation and bundling assays.

A potential phosphatase complex which may regulate TAN1 phosphorylation status contains the PP2A B" subunits DISCORDIA1/ALTERNATE DISCORIA1 (DCD1/ADD1) in maize (Gallagher and Smith, 1999; Wright et al., 2009). These proteins make interesting candidates as DCD1/ADD1 localize to the PPB and are retained at the cortical division site until the end of metaphase (Wright et al., 2009). Mutants of these

proteins in maize are lethal, however knock down of these genes results in cells which are impaired in their ability to form PPBs, display division plane defects and cell wall stubs (Wright et al., 2009). Given DCD1/ADD1 localization to the cortical division site throughout mitosis, we hypothesize that this PP2A phosphatase complex may help TAN1 protein at the cortex stay unphosphorylated to retain its ability to bind to microtubules. A genetic approach to this question includes looking at TAN1-YFP localization in the maize *dcd1/add1* mutant or knock downs. These knockdown lines also display division plane defects, possibly mediated by loss of TAN1 microtubule binding function at the division site or overall loss of TAN1 from the division site. TAN1 localization can be assessed in *dcd1/add1* mutants through embryo rescue experiments. Additionally, TAN1 phosphorylation abundance can be determined in wild-type and embryo rescued *dcd1/add1* maize mutants to determine if this complex targets TAN1 directly.

Determining TAN1 microtubule binding domain and mode of binding

While it is clear that TAN1 is capable of binding to microtubules, the mode of binding is unknown. TAN1 may bind to microtubules as a monomer, form a dimer and then bind to microtubules, or bind as a monomer and dimerize to induce bundling. Bundling may not only be induced by dimerization as it may be mediated by a single TAN1 protein if multiple microtubule binding sites exist. This analysis is confounded by TAN1 protein sequence which lacks any canonical domains that may suggest function. Additionally, we have no direct evidence that microtubule binding is important for TAN1 function *in vivo*. In *Arabidopsis* several regions of TAN1 have been tested for their functionality using the *tangled1/auxin-induced-in-roots9* (*tan1 air9*) double mutant which displays division

plane defects and can be rescued by expression of full length TAN1 (Mir et al., 2018). Given current results, we know that TAN1 missing region (I) which is lost from the division site following pre-prophase is unable to rescue division plane defects in the *tan1/air9* double mutant (Rasmussen et al., 2011; Mir et al., 2018). TAN1 missing region (II) which localizes during later stages of mitosis is able to rescue the *tan1/air9* double mutant division plane defects (Rasmussen et al., 2011; Mir et al., 2018). This data indirectly suggests that initial TAN1 recruitment to the division site is likely to be PPB (microtubule) dependent mediated by TAN1 region (II) (Rasmussen et al., 2011). In later stages of mitosis localization becomes microtubule independent mediated by TAN1 region (I) (Rasmussen et al., 2011). If we assume that TAN1 microtubule binding is important for phragmoplast guidance during telophase, we can hypothesize that the two domains of TAN1 which mediate distinct localization patterns are both capable of binding to microtubules. To test this hypothesis, TAN1 protein truncations need to be expressed and purified *in vitro* and tested for their ability to bind and bundle microtubules. These truncated TAN1 proteins should also be expressed in a mutant background in order to assess rescue and function *in vivo*. Ideally experiments would be performed in maize to continue the work presented in this thesis, however heterologous expression may be an option as maize TAN1 protein displays similar localization to the division site when expressed in *Arabidopsis thaliana* (Walker et al., 2007). Functionality can be assessed by rescue of the *Arabidopsis tan1/air9* double mutant by the maize TAN1 protein.

TAN1 binding to tubulin dimers

In vitro, TAN1 protein was determined to bind to soluble tubulin dimers. This means that TAN1 can bind to both microtubules as well as its subunit constituents. While *in vitro* microtubule dynamic experiments with TAN1 did show altered microtubule growth and shrinkage rates, the ability for TAN1 to bind to tubulin may change the interpretation of the results depending on TAN1 binding modes to these two substrates. One possibility is that TAN1 can only bind to of the two substrates at any given moment. Alternatively, TAN1 can bind to both microtubules and tubulin dimers at the same time to spatially regulate tubulin concentrations along microtubules. The *in vitro* dynamic assays performed however suggest the second option is not likely as there was no increase in microtubule rescue frequencies in the presence of TAN1; which would be expected for microtubule growth rescue factors (Al-Bassam et al., 2010).

To assess TAN1 binding modes, unlabeled biotin labeled microtubule seeds can bound to a glass coverslip treated with α-biotin antibody and incubated with fluorescently labeled TAN1 protein. Soluble tubulin which is fluorescently labeled with a different dye than TAN1 can then be flowed into the sample. If fluorescent tubulin dimers localize along unlabeled seeds at points of TAN1 binding, then this suggests that TAN1 is able to simultaneously bind to both microtubules and tubulin dimers. A different combination of fluorophores with proteins can be used for this assay such as using biotin-rhodamine microtubule seeds, unlabeled TAN1 protein, and soluble HiLyte488- tubulin. An *in vitro* electron microscopy (EM) approach can also be taken to understand the interaction between TAN1 and tubulin dimers. TAN1 and tubulin dimers can be incubated and

imaged using negative uranyl acetate stain using transmission electron microscopy. This technique can be used to reveal stoichiometry of the interaction as well as some structural information on the protein interactions. Stoichiometry of binding can also be assessed using high performance liquid chromatography (HPLC) to separate out protein complexes and determine their estimated molecular weight. Similar to determining the region of TAN1 which can bind to microtubules, the region responsible for tubulin binding can be derived from the generated protein truncations and functionality can be determined using mutant rescue experiments.

Genetic analysis of TAN1 paralog in maize

A paralog of the maize TAN1 gene was found in the maize genome due to sequence similarity (Schnable et al., 2009). This gene is being referred to as TANGLED2 (TAN2, Zm00001d036047) and is currently uncharacterized, however a study did identify it as residing in a candidate mapping interval for resistance against maize rough dwarf disease (Li et al., 2018). TAN1 and TAN2 share a 66% sequence similarity from amino acids 50-339 (Figure 5.2) (Chojnacki et al., 2017). A reverse genetics approach is being taken to understand the function of this gene and its relation to TAN1. CRISPR-CAS9 system was used for both TAN1 and TAN2 in order to generate novel mutant alleles in both genes. The construct used for gene knockout contains two guide RNAs for each of the genes and was transformed into maize. Single and double mutants can then be generated to study phenotypes associated with each genetic combination.

After initial transformation and regeneration of transgenic maize plants, the T_0 generation was outcrossed to begin screening for mutations and to remove the CRISPR-CAS9

transgene. When maize plants contain the CRISPR-CAS9 and gRNA targeting TAN1 and TAN2 genes, phenotypes wildly varied from normal looking plants to having extremely curled, wrinkled leaves and short stature (Figure 5.3A). After the recovery of homozygous mutants for new *tan1* mutant alleles, maize plants displayed extreme growth defects (only a few cm tall) and division plane defects compared to heterozygous or wild-type siblings (Figure 5.3B-C). These novel homozygous *tan1* mutants display a much more severe phenotype compared to previously described *tan1* mutants in maize, which either reflects a true null phenotype or differences due to variations in the parental genetic inbred backgrounds (Smith et al., 1996; Martinez et al., 2017). Plants which were genotyped as homozygous *tan2* mutants did not display severe growth defects or division plane defects compared to the *tan1* single mutants. Detailed phenotypic analysis of multiple mutant alleles of *tan2* need to be analyzed to understand the possible impact of *tan2* on growth and development, as well as the phenotypes associated with the double mutants.

```
TAN1            MVARSPNAKPDRQKAA-----------------ALAAAAA-----------LNPALLR
TAN2            MPTRRGTAAPERLRCCANADTGHRPHKASRAEHRALGCATASSHRARAGRAPHHEPSWLS
                * :*  .* *:* ...                 **..*:*             :*: *

TAN1            ETLKKVDRCMARLQELQYTVAGGAKV--------------------------VSGVSL
TAN2            WALLICEAVVGPTNPYLFQFICAAPVHYLWSVIERRLLSEQNIYLMKVYNEQIIVSVLKV
                 :*   :  :.  :   : .  .* *                          ** :.:

TAN1            SPRSTRGYLRTSLRCKQETVRMRGGASAQKRSPSGKFGGGVGGEGAQWRRMSLPAMLLGE
TAN2            YNEQIHDLLLTGSQPGATTKGMRGGASAQKRSPSGKFGGIVGGEGAQWRRMSLPAMLLDE
                   . .. * *. .    *  ****************** ******************.*

TAN1            TVLEIVQASQFARDIVTAAGATNREPPRTPKPAPRTRKPAAGEPTPLRARRARE KQSHRG
TAN2            T----VQVSQFARGIVTTAGAMNREPPRTPKPAPRTRKPAAGEPTPLHARRARE KQSHRG
                *    **.*****.***:*** ************************.************

TAN1            GAATRGADAATPPSRSRVRSRIQFKPVSPVAVGRPSVSANRVSPKNRPWAKKAVMFPNPT
TAN2            GTTTRGAGTATPPSRSRVRSRIQFKPVSSVAVSRPSVSANRVSPKNRPWAKKAVMFQNPM
                *::****.:******************.***.********************** **

TAN1            FHASTSAATDPCATPSPSKKQKRLYKTRSPVAARQTPHKFLVKSPPSALGSKLRMHGKAL
TAN2            FHASTSAAIDPCATSSPSKKQKRLYKTRSPVVAQQIPHKFLVK-----------------
                ******** *****.****************.*.* *******

TAN1            PARPAAVSPPPPVKAQASPAKTRRCSFSPSRLATRLMSPIKARLSLGRSRDSGVGVGGGP
TAN2            ------------------------------------VATERARIQSQDARE-------GP
                                                    ::. .**:.   :*:       **

TAN1            MSGLKQRPGVSLTVRTVSSKISSR
TAN2            ARETRRRS----------------
                  ..*.
```

Figure 5.2: TAN1 and TAN2 CLUSTAL multiple sequence alignment. TAN1 protein sequence similarity to TAN2 lies mostly in the central region of the two proteins.

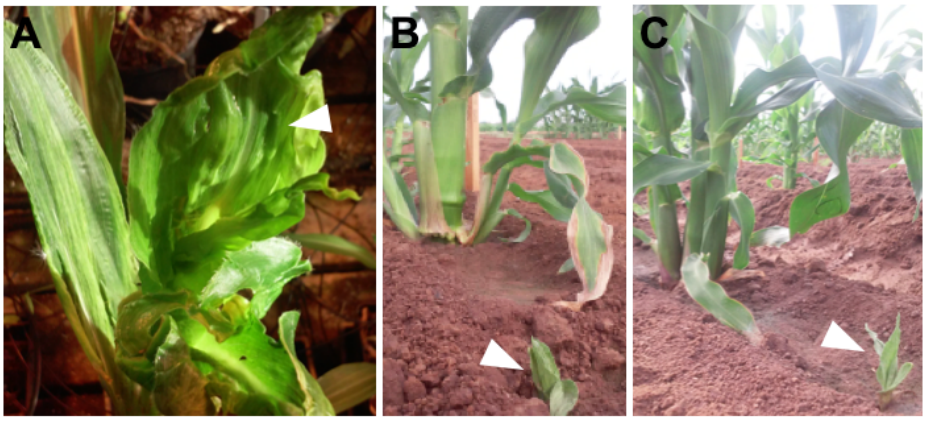

Figure 5.3 Phenotypes associated with generation of novel TAN1 and TAN2 mutant alleles. (A) Maize expressing CRISPR-CAS9 and gRNAs targeting TAN1 and TAN2 shows altered leaf morphology (arrowhead). (B) Maize plant homozygous for new *tan1* mutant allele next to its wild-type sibling. (C) Maize plant homozygous for a different new *tan1* mutant allele next to its wild-type sibling

References

Al-Bassam J, Kim H, Brouhard G, van Oijen A, Harrison SC, Chang F (2010) CLASP Promotes Microtubule Rescue by Recruiting Tubulin Dimers to the Microtubule. Dev Cell **19**: 245–258

Boruc J, Weimer AK, Stoppin-Mellet V, Mylle E, Kosetsu K, Cedeño C, Jaquinod M, Njo M, De Milde L, Tompa P, et al (2017) Phosphorylation of MAP65-1 by Arabidopsis Aurora Kinases Is Required for Efficient Cell Cycle Progression. Plant Physiol **173**: 582–599

Chojnacki S, Cowley A, Lee J, Foix A, Lopez R (2017) Programmatic access to bioinformatics tools from EMBL-EBI update: 2017. Nucleic Acids Res **45**: W550–W553

Cleary AL, Smith LG (1998) The Tangled1 gene is required for spatial control of cytoskeletal arrays associated with cell division during maize leaf development. Plant Cell **10**: 1875–88

Gallagher K, Smith LG (1999) discordia mutations specifically misorient asymmetric cell divisions during development of the maize leaf epidermis. Dev Camb Engl **126**: 4623–4633

Illenberger S, Drewes G, Trinczek B, Biernat J, Meyer HE, Olmsted JB, Mandelkow E-M, Mandelkow E (1996) Phosphorylation of Microtubule-associated Proteins MAP2 and MAP4 by the Protein Kinase p110: PHOSPHORYLATION SITES AND REGULATION OF MICROTUBULE DYNAMICS. J Biol Chem **271**: 10834–10843

Kosetsu K, Murata T, Yamada M, Nishina M, Boruc J, Hasebe M, Van Damme D, Goshima G (2017) Cytoplasmic MTOCs control spindle orientation for asymmetric cell division in plants. Proc Natl Acad Sci **114**: E8847–E8854

Lee BH, Weber ZT, Zourelidou M, Hofmeister BT, Schmitz RJ, Schwechheimer C, Dobritsa AA (2018) Arabidopsis Protein Kinase D6PKL3 Is Involved in the Formation of Distinct Plasma Membrane Aperture Domains on the Pollen Surface. Plant Cell **30**: 2038–2056

Li R, Song W, Wang B, Wang J, Zhang D, Zhang Q, Li X, Wei J, Gao Z (2018) Identification of a locus conferring dominant resistance to maize rough dwarf disease in maize. Sci Rep. doi: 10.1038/s41598-018-21677-3

Lipka E, Gadeyne A, Stöckle D, Zimmermann S, De Jaeger G, Ehrhardt DW, Kirik V, Van Damme D, Müller S (2014) The Phragmoplast-Orienting Kinesin-12 Class Proteins Translate the Positional Information of the Preprophase Band to

Establish the Cortical Division Zone in Arabidopsis thaliana. Plant Cell **26**: 2617–2632

Martinez P, Luo A, Sylvester A, Rasmussen CG (2017) Proper division plane orientation and mitotic progression together allow normal growth of maize. Proc Natl Acad Sci **114**: 2759–2764

Mir R, Morris VH, Buschmann H, Rasmussen CG (2018) Division Plane Orientation Defects Revealed by a Synthetic Double Mutant Phenotype. Plant Physiol **176**: 418–431

Porter KR (1960) Studies on the Endoplasmic Reticulum: IV. Its Form and Distribution during Mitosis in Cells of Onion Root Tip. J Cell Biol **7**: 167–180

Rasmussen CG, Sun B, Smith LG (2011) Tangled localization at the cortical division site of plant cells occurs by several mechanisms. J Cell Sci **124**: 270–9

Sampathkumar A, Krupinski P, Wightman R, Milani P, Berquand A, Boudaoud A, Hamant O, Jönsson H, Meyerowitz EM (2014) Subcellular and supracellular mechanical stress prescribes cytoskeleton behavior in Arabidopsis cotyledon pavement cells. Elife **3**: e01967

Schaefer E, Belcram K, Uyttewaal M, Duroc Y, Goussot M, Legland D, Laruelle E, de Tauzia-Moreau M-L, Pastuglia M, Bouchez D (2017) The preprophase band of microtubules controls the robustness of division orientation in plants. Science **356**: 186–189

Schnable PS, Ware D, Fulton RS, Stein JC, Wei F, Pasternak S, Liang C, Zhang J, Fulton L, Graves TA, et al (2009) The B73 Maize Genome: Complexity, Diversity, and Dynamics. Science **326**: 1112–1115

Smith LG, Hake S, Sylvester AW (1996) The tangled-1 mutation alters cell division orientations throughout maize leaf development without altering leaf shape. Development **122**: 481–9

Vavrdová T, ˇSamaj J, Komis G (2019) Phosphorylation of Plant Microtubule-Associated Proteins During Cell Division. Front Plant Sci. doi: 10.3389/fpls.2019.00238

Walker KL, Müller S, Moss D, Ehrhardt DW, Smith LG (2007) Arabidopsis Tangled Identifies the Division Plane Throughout Mitosis and Cytokinesis. Curr Biol CB **17**: 1827–1836

Walley JW, Sartor RC, Shen Z, Schmitz RJ, Wu KJ, Urich MA, Nery JR, Smith LG, Schnable JC, Ecker JR, et al (2016) Integration of omic networks in a developmental atlas of maize. Science **353**: 814–818

Wright AJ, Gallagher K, Smith LG (2009) discordia1 and alternative discordia1 function redundantly at the cortical division site to promote preprophase band formation and orient division planes in maize. Plant Cell **21**: 234–47

APPENDICES

Primer Name	Polarity	Gene	Maize GDB Code	Sequence
ZmTAN1a-R	Reverse	TANGLED1	Zm00001d038060	GAACATCACCGCCTTCTTT
ZmTAN1a-F	Forward	TANGLED1	Zm00001d038060	TGGCTTCGGTTGGGAACTTG
TAN LSP1	Forward	TANGLED1	Zm00001d038060	ACGACCGTTAGCACAGAACC
ZmTAN REV2937	Reverse	TANGLED1	Zm00001d038060	CGGCAAGAGTCAGAGTAAGAGACAG
py_323R	Reverse	TANGLED1 *tan1-py* allele	N/A	CTGCTTCTTCGTGTGAGACCTTC
TANR13802	Reverse	TANGLED1	Zm00001d038060	GCT TGCTTCCAAGTCCAAGTCTC
TAN1bF	Forward	TANGLED2	Zm00001d36047	AGTCGATCTCACTGGTGGGTAC
TAN1bR	Reverse	TANGLED2	Zm00001d36047	TGGAACATCACCGCCTTCTTG
Os-CAS9-F	Forward	CRISR-CAS9	N/A	GGGTAATGAACTCGCTCTGC
Os-CAS9-R	Reverse	CRISR-CAS9	N/A	TGGCGTCAAGAACTTCCTTTG
ZmTUB-alpha_FP1	Forward	TUBULIN α1	Zm00001d033850	GCAAGGTTTCGATTTCCGTA
ZmTUB-alpha_RP1	Reverse	TUBULIN α1	Zm00001d033850	GGTTTCGGGTGATCCCTAIT
CYFP L1	Forward	TUBULIN β1	Zm00001d027295	AGCGCGATCACATGGTCCT
BTUBR3187	Reverse	TUBULIN β1	Zm00001d027295	GACAGGCGGGGCATAAGATCC
ZmPIP2A_2724F	Forward	PLASMA MEMBRANE INTRINSIC PROTEIN 2	Zm00001d019563	TCGTCTCTGCCTCCAGTTCTATTCG
GFP5Rev	Reverse	N/A	N/A	CTGAACTTGTGGCCGTTTACGTCGC
GFP5FOR	Forward	N/A	N/A	GCGACGTAAACGGCCACAAGTTCAG

Appendix 1: Table of Primers Used in Dissertation